DEVELOPMENT AND MECHANISTIC STUDY OF A PEPTIDE-BASED METHODOLOGY FOR THE PREPARATION OF NANOPARTICLE SUPERSTRUCTURES

By

Leekyoung Hwang

B.S., Ewha Womans University, 2003

M.S., Korea Advanced Institute of Science and Technology, 2005

Submitted to the Graduate Faculty of

the Kenneth P. Dietrich School of Arts and Sciences

in partial fulfillment

of the requirements for the degree of

Doctor of Philosophy

University of Pittsburgh

2012

UNIVERSITY OF PITTSBURGH

FACULTY OF DIETRICH SCHOOL OF ARTS AND SCIENCES

This thesis was presented

By

Leekyoung Hwang

It was defended on

April 17, 2012

and approved by

Tara Y. Meyer, PhD, Professor, Department of Chemistry

Alexander Star, PhD, Associate Professor, Department of Chemistry

Jung-Kun Lee, PhD, Assistant Professor, Department of Mechanical Engineering and Materials
Science

Dissertation Advisor: Nathaniel L. Rosi, PhD, Assistant Professor, Department of Chemistry

Prof. Nathaniel L. Rosi

DEVELOPMENT AND MECHANISTIC STUDY OF A PEPTIDE-BASED METHODOLOGY FOR THE PREPARATION OF NANOPARTICLE SUPERSTRUCTURES

Leekyoung Hwang, PhD

University of Pittsburgh, 2012

The aim of this research is to develop and generalize a peptide-based methodology for inorganic nanoparticle assembly and to understand the underlying mechanism governing the synthesis and assembly process. This research is based on a new methodology to synthesize complex and well-organized nanoparticle superstructures that the Rosi group has developed. This method relies on the use of peptide conjugate molecules to direct both synthesis and the assembly of the nanoparticles. To accomplish goals of this research, new peptide conjugates were designed and synthesized in order to program substantial amounts of information into the peptide conjugate molecules. Their self-assembly has been studied and their ability to direct nanoparticle synthesis and self-assembly has been studied.

The research details how modifications to the peptide sequence can impact the resulting structure formation. Fundamental studies were also performed to understand the mechanistic factors underlying this methodology. The key criteria for preparing highly-ordered nanoparticle superstructures were also investigated using this methodology. Ultimately, this approach will lead to precise control over the shape, composition, and interparticle distance within nanoparticle superstructures.

TABLE OF CONTENTS

LIST OF FIGURES

ACKNOWLEDGEMENTS

I would like to thank my advisor, Prof. Nathaniel Rosi, for providing me with a wonderful chance to work on cutting-edge nanoparticle assembly projects. Throughout my graduate research his enthusiasm for discovering new structures and understanding new phenomena has always encouraged me to augment my abilities and to have confidence in myself. Without his deep knowledge, guidance, and encouragement during the last five years, I would not even have been able to start all of the work that I accomplished. I sincerely thank him for his efforts and for the patience that he has extended to me as I finish my doctoral research.

I would also like to express my deep appreciation for my committee members: to Prof. Tara Meyer for her invaluable advices, mentorships, and support for my research and career; to Prof. Alexander Star for his encouragement and positive feedback throughout this process; and to Prof. Jung-Kun Lee for willingly being one of my committee members.

I would also like to thank my mentor for my research proposal, Prof. Seth Horne, for his great mentorship, encouragement, and support for my proposal and career.

I am very grateful to all of the members of the Rosi Group for their help. I want to thank Dr. Chun-Long Chen, Dr. Jihyun An, and Dr. Kiley White for their help they gave me when I first joined the group; I also want to thank Chengyi Song, Tao Li, Chen Zhang, Alex Spore, Jessica Sammons, Chong Liu, Ryan Ruenroeng, and Andrea Merg for sharing his or her knowledge, happiness, and optimism with me. It is thanks to all of them that I was able to perform my research more actively and more happily.

I would like to express deep appreciation to these people for their help during this journey: Cole Van Ormer (TEM), Dr. Joel Gillespie (MCL), Dr. Susheng Tan (PINSE), Dr. Ericka Huston (teaching coordinator), Dr. Gongpu Zhao (Tomography), Prof. Peijun Zhang, and Dr. Bhaskar Godugu (MALDI). It is thanks to the help of all of these people that I was able to finish my doctoral research.

Finally, I want to express my sincere and loving thanks to my parents and my sister. It would have been impossible for me to finish this work without their support. Sis! Thank you so much for being there for me all these years. I could have never reached this point if you had not been there with me. I am very lucky that we could share our experience and efforts to achieve Ph.D together here. Dad! I know how much faith you have in me. You are my biggest supporter. Mom! You have always supported me and urged me to be strong and independent to get through all of the tough times. Thanks to your great advices and encouragement, I have been able to keep my strength during this journey. Thank you so much for everything that you have done for me and devoted to me. I owe you my eternal gratitude, and I will spend the rest of our time together paying you back day by day.

1.0   INTRODUCTION

1.1   ATOMIC AND MOLECULAR ASSEMBLY

New advanced chemical materials are generated via two synthetic approaches: 1) top-down, and 2) bottom-up approaches.[1] The bottom-up strategy, in particular, is advantageous because various chemical building blocks can be utilized and assembled into complex architectures. [2-4]

Assembly is a process whereby basic molecular units are organized through specific interactions into a complex structure with a regular shape or size.[5] For chemists, the smallest accessible building unit is an atom. An atom has valency. Based on this valency, two or more atoms can form directional covalent bonds with other atoms. The connected atoms generate molecules. Molecules can be organized and assembled using specific molecular interactions (i.e., van der Waals interactions or hydrogen bonding).[6] Assemblies of molecules can exhibit functional complexity that derives from the individual molecular building blocks (**Figure 1**). For example, adenine and thymine, two nucleotides in a DNA molecule, are composed of carbon, oxygen, nitrogen, and hydrogen atoms. The nucleotides form hydrogen bonds to create an A-T base pair. This A-T base pair is one of building blocks in the supramolecular assembly of a double-helical structure.

Chemists can also design and control the assembly of solid-state materials. In such materials, the building blocks may be metals, metal ions, metal clusters, organic molecules, or even biomolecules. Since each of these building blocks exhibit valency that can be controlled, we can find ways of linking these building blocks in a directional fashion. As an example, the Rosi group has shown that adenine molecules and metal ions can be used as basic building units to construct generating adenine-metal macrocycles. These macrocycles are themselves building blocks that assemble through directional hydrogen bonds into a highly-ordered crystalline porous architecture (**Figure 1**).[7-9]

This molecular level assembly allows one to define and characterize the atomic constituents, the spatial orientation of the atoms, and their connectivity in higher-ordered structures. In other words, the placement, arrangement, and distance of the atoms in a molecular structure can be predicted, clearly identified, and analyzed. Therefore, molecules and molecule-metal complex building blocks can be readily designed, prepared, and characterized in order to synthesize higher-level architectures with greater complexity. In summary, it is well-established that the assembly of atoms into molecules and molecules into materials is important, and the development of methodology to control this assembly has captivated chemists for decades.
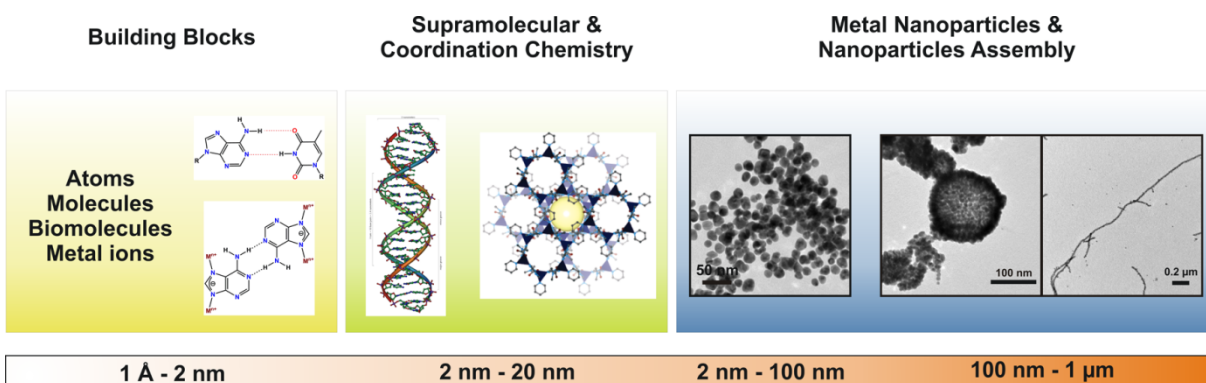
Figure 1. Schematic illustration of building blocks and the hierarchical assembly of these building blocks.

1.2 METAL NANOPARTICLES AND THEIR ASSEMBLY

When thousands of metal atoms are gathered into a single entity, they create a unique form of matter: the metal nanoparticle (NP).[10] Metal NPs are classified by having at least one dimension in the 1-100 nm length scale. The key features of NPs are their small size and high surface areas (**Figure 2**).[11,12] These features lead to many unique optical, electronic, and catalytic properties. The properties of individual nanoparticles are determined by their size, shape, and composition.[10,11,13] Because nanoparticles have particularly active surfaces, they can easily aggregate if their surfaces are not coated with a passivating layer of molecules. These passivating layers may comprise simple organic ligands, such as alkane thiols[14], biomolecules[15,16], or polymers[17]. These layers can also impact the properties of the nanoparticles. Specifically, the surface molecules mediate the interaction of the nanoparticles with each other and with their environment.[18-20]

3
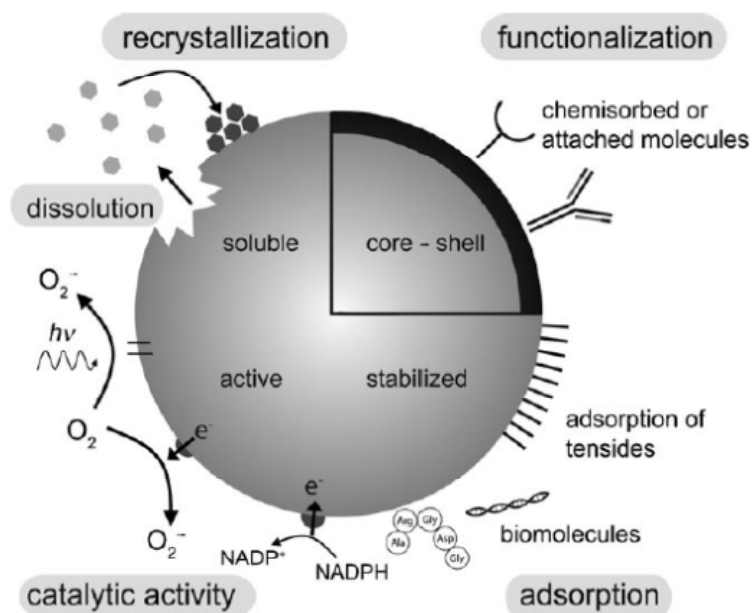
Figure 2. The active surface of nanoparticles (Adapted from ref. 12)

Nanoparticles also exhibit unique assembly-dependent properties that derive not only from the size, shape, and composition of the component nanoparticles but also from the way in which the nanoparticles are assembled with respect to one another. These properties are often called 'ensemble properties' because they are unique to the particular collection of nanoparticles. [4,21-23] The local order of the nanoparticles within the assembly and parameters such as the interparticle distances are very important and can have a large impact on the ensemble properties of the assembly. Based on their interesting individual and ensemble properties, nanoparticles are a particularly attractive building block for constructing new functional materials. In order to control the properties of such materials, we must be able to precisely control the assembly of the constituent building blocks.

Unlike atoms and molecules, spherical isotropic nanoparticles do not possess valency, therefore it is very challenging to control their directional assembly. Just like methods for assembling atoms into molecules (e.g. organic synthesis) and assembling molecules into materials (e.g. polymer synthesis and supramolecular chemistry) have been developed, methodology must be developed for rationally and precisely controlling the assembly of nanoparticles into complex nanoparticle superstructures and nanoparticle-based materials. The need for such methodology is well-recognized. ***The central focus of my dissertation is the development of a new methodology for controlling the assembly of nanoparticles into complex nanoparticle superstructures.*** It should be emphasized that many esteemed research groups have introduced methods for controlling the assembly of nanoparticles.[24] In this chapter, I will introduce and review three general methods for preparing nanoparticle superstructures: colloidal crystallization, template-mediated assembly, and directional assembly of multivalent particles (**Figure 3**). Representative examples of these methods are detailed below. The advantages and drawbacks of each of these methods are discussed.
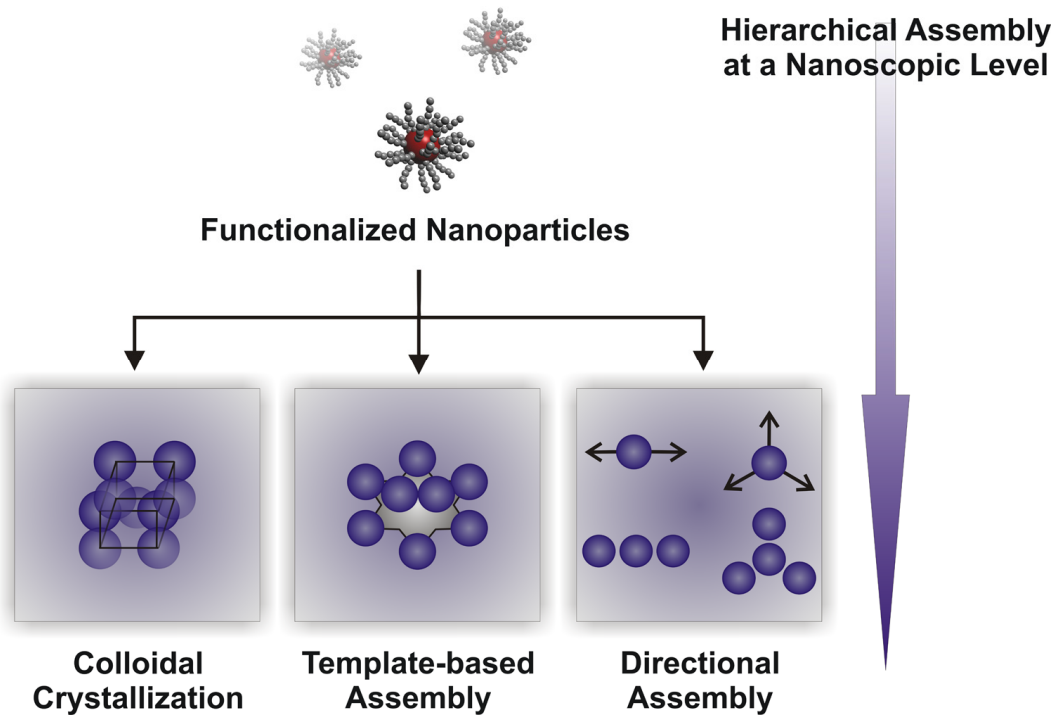
Figure 3. Schematic description of representative assembly methods for preparing nanoparticle superstructures.

1.3   COLLOIDAL CRYSTALLIZATION

Colloidal crystallization is a process for organizing nanoparticles into 2- or 3-D crystalline superlattices that exhibit highly precise local nanoparticle order [25,26]. The driving force for forming colloidal crystals can be spontaneous size segregation [25,27] and electrostatic interaction[28,29] or in some cases DNA base pairing [30] (**Figure 4**).

One advantage of colloidal crystallization is that it offers excellent control over the spatial arrangement of nanoparticles and interparticle distances.[27,28] Additionally, crystalline superlattices with more than one nanoparticle size and composition can be constructed using this method. [29,31] The principle disadvantage of this method, however, is its limited structural scope: while it is useful for preparing 2- and 3-D extended crystals, it is not useful for controlling the directional assembly of nanoparticles into more complex and sophisticated anisotropic superstructures (e.g. nanoparticle chains).
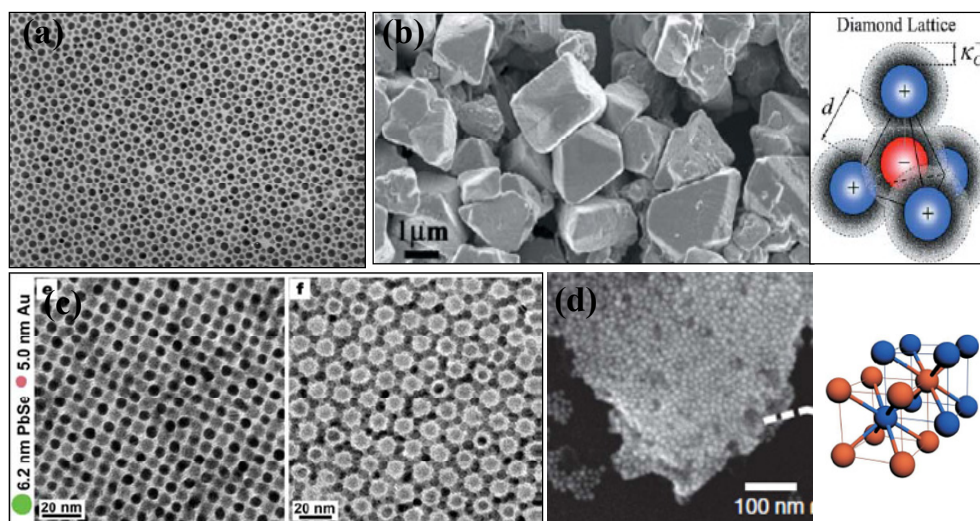
Figure 4. (a) Electron micrographs at 100 nm magnification of ordered Au nanoparticle crystals consisting of particles with two distinct sizes (Adapted from ref. 27); (b) Large-area SEM image of binary crystals consisting of gold and silver particles (Adapted from ref. 28); (c) Binary superlattices of PbSe and Au nanoparticles (Adapted from ref. 29); (d) SEM images of DNA-capped nanoparticles after assembly (Adapted from ref. 30).

1.4   TEMPLATING STRATEGIES

The basic concept of these strategies is to assemble discrete nanoparticles onto template structures. [1,17,32] These methods are excellent for constructing complex nanoparticle superstructures, since structurally-diverse templates can be employed, including microorganisms, polymers, and biomolecules such as nucleic acids, proteins, peptides.[1,6,33-36] In most cases, these methods can be used to assemble nanoparticles of various compositions.   However, most templating strategies require multiple synthetic steps, which can lead to low product yield and significant waste. These steps often can include 1) template synthesis and assembly, 2) template functionalization with suitable molecules for interacting with nanoparticles, 3) nanoparticle synthesis, 4) functionalization of nanoparticles with molecules suitable for interacting with template, and finally 5) mixture of nanoparticles with templates to affect assembly. In most cases, the resulting products have decent long-range nanoparticle order, but poor local nanoparticle order. We emphasize that precise control over local nanoparticle order is critically important for fine-tuning the properties of a nanoparticle superstructure. The template-based approaches most similar to my proposed approach are introduced in this section.

1.4.1   Polymer–template assembly

A polymer can serve as a template for the assembly of nanoparticles. In these cases, intermolecular forces, such as hydrogen bonds, electrostatic interactions, π-π interactions, or van der Waals forces between the polymer and the nanoparticles control the assembly [17,37]. When the polymer is functionalized with small molecules that can interact specifically with functionalized

nanoparticles, it can serve as a template for assembling nanoparticles into more complex superstructures [38]. Rotello and coworkers reported the synthesis of 3-D spherical nanoparticle superstructures by taking advantage of hydrogen bonds between a functionalized polymer template and modified nanoparticles. [20,39]

1.4.2   Nucleic acid–template assembly

Deoxyribonucleic acid (DNA) is a useful molecule for nanoparticle assembly[1,17,32]. Native or modified DNA molecules can act as templates, in which functionalized nanoparticles are arranged into predictable patterns via specific base pairing. DNA molecules of specific base sequences and specific lengths can be synthesized so that not only the overall geometry but also the interparticle distance can be controlled. [40-43]

The field of 'DNA-Origami' has produced many sophisticated DNA-based superstructures that have been exploited as templates for assembling nanoparticles. These templates allow construction of nanoparticle superstructures including small spheres aggregates to 1, 2, and 3-D arrays. [1,17,42-49] For example, a cyclic DNA framework permits construction of dimers, trimers, or cyclic structures (**Figure 5a**). [42,43] Some groups prepared 2-D nanoparticle arrays by utilizing DNA scaffolds as a template (**Figure 5b**) [44,46,47], while others have prepared 1-D chain-like assemblies that serve as templates for 1-D nanoparticle arrays (**Figure 5c-d**) [45,48-50].
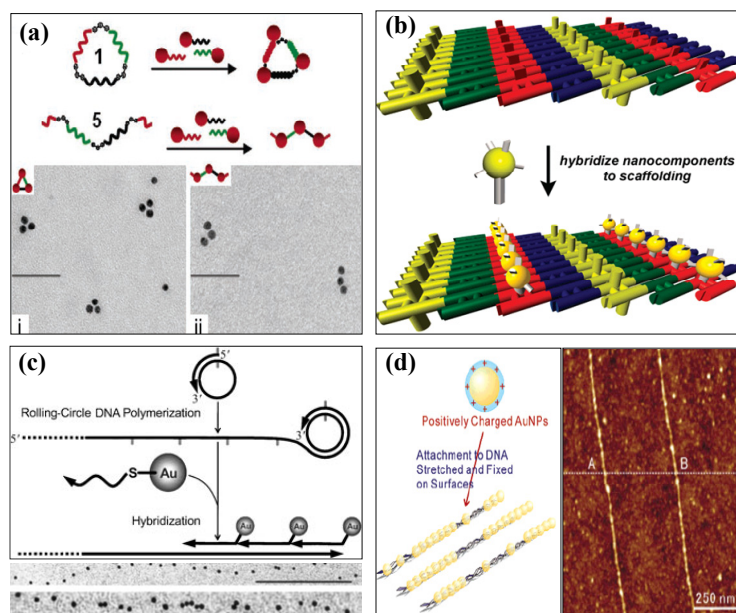
Figure 5. DNA-templated nanoparticle assemblies (a) small aggregates of Au NPs (Adapted from ref. 43); (b) 2-D DNA scaffolds (Adapted from ref. 44); (c) AuNPs DNA chains (Adapted from ref. 45); (d) positively-charged Au NPs attached to negative DNA scaffolds by electrostatic interaction (Adapted from ref. 48)

Even though this approach can be used construct superstructures with complex topologies, it is somewhat limited in the scope of different nanoparticle compositions which can be assembled, because straightforward methods for functionalizing a variety of nanoparticle compositions (e.g. compositions other than Au and Ag) with oligonucleotides have not been developed. In addition, like other templating methods, multiple steps are required for preparing templates and functionalizing nanoparticles, and this preparation demands optimized conditions, such as proper pH, ionic strength, and temperature. [1,41,43,48]

1.4.3   Peptide–based methods

Peptides have unique sequence-specific self-assembly and recognition capabilities that make them attractive molecules for directing the assembly of inorganic nanoparticles.[6,15,51-54] Depending on their sequence, they can self-assemble into a variety of secondary structures, including α-helices and β-sheets [6,55]. Further, peptides can be modified with simple organic molecules that can influence their self-assembly.[51,56-58] Peptides can also adhere to inorganic surfaces; in some cases this interaction is non-specific (e.g. electrostatic) [59] but in other cases, the interaction is highly sequence-specific (e.g. biomineralization peptides)[15,60-64].

In general, there are two different established methods for using peptides to direct nanoparticle assembly. The first method involves the assembly of pre-synthesized nanoparticles onto pre-assembled peptide templates, such as a peptide itself [33,65,66], viral capsids [35], microorganisms [34], and peptides functionalized with a specific organic molecule [67]. This approach suffers from the same limitations of other typical template-based strategies; specifically, while it offers good control over the long-range particle order, the local nanoparticle order in these structures is poor. Moreover, multiple synthetic steps are required.

The second general strategy has primarily been developed by Matsui and coworkers (**Figure 6**).[59] It involves 1) preparation of peptide nanotubes; 2) decoration, via electrostatic interactions, of peptide nanotubes with biomineralization peptides, and 3) nucleation and growth of inorganic nanoparticles onto the biomineralization peptides decorating the nanotubes. The biomineralization peptides provide sites for nanoparticle nucleation and growth onto the template. However, the major problem is that these nucleation sites are randomly distributed onto the

11

template. Therefore, nanoparticle superstructures with poor local nanoparticle order and irregular nanoparticle size are obtained.[68]
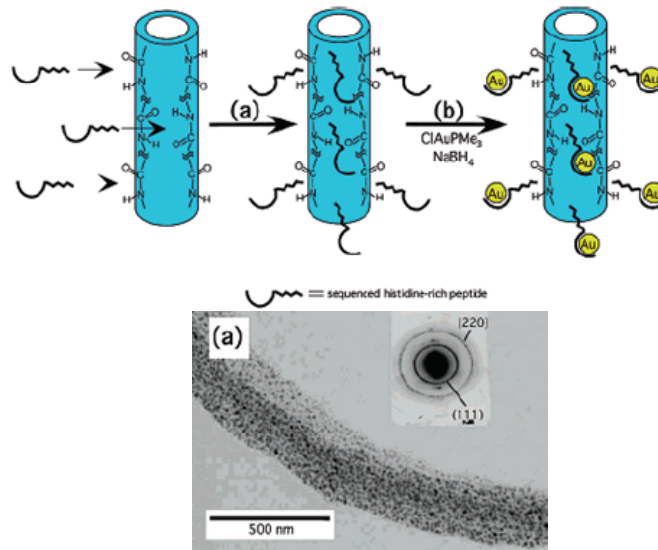
Figure 6. Scheme of Au nanowire fabrication (a) coupling of sequenced histidine-rich peptide at the nanowire, (b) Au nucleation at the histidine sites, and (c) TEM images of the nanowire (Adapted from ref. 59)

These existing peptide-based strategies are useful for obtaining nanoparticle superstructures with complex shapes and various nanoparticle compositions [6,59,66,69,70]; however, they still suffer from the following principle limitations: multiple steps are required for synthesizing and functionalizing templates; there is difficulty in exacting control over interparticle spacing; and nanoparticle size, shape, and spatial distribution is irregular [66-69].

1.5   DIRECTIONAL ASSEMBLY OF MULTIVALENT NANOPARTICLES

Multivalent nanoparticles are produced when a valency of more than two is introduced into the ligand shell of the nanoparticles. Such particles can be used as building blocks for constructing highly-organized superstructures. [71,72] The biggest advantage of this approach is that nanoparticles can be directionally assembled into well-ordered structures with high local nanoparticle order, in much the same fashion that atoms are arranged into molecules.

Alivisatos' group prepared monovalent, divalent, and trivalent DNA-modified particles and used these particles to prepare discrete nanoparticle assemblies (e.g. dimers, trimers, and tetrahedra).[41,73,74] Directional assembly of nanoparticles into short-single chains and clusters with consistent local-order was also reported by taking advantage of divalent and multivalent nanoparticles (**Figure 7a-c**).[71,72,75]
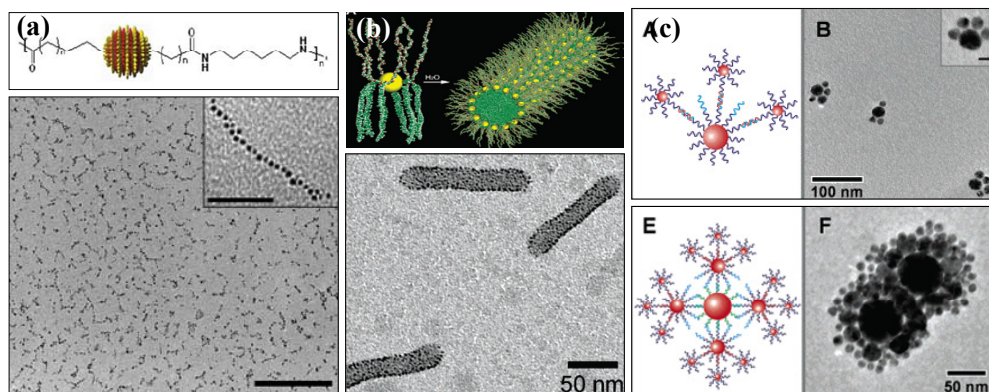
Figure 7. Directional assembly of multivalent nanoparticles into (a) short chains (Adapted from ref. 71); (b) hollow cylinders (Adapted from ref. 75); and (c) cat paw (upper right) and dendrimer-like (lower right) structures (Adapted from ref. 72)

This approach allows construction of nanoparticle assemblies with well-defined shapes and symmetry, and with consistent interparticle distance. However, many synthetic steps are usually required for preparing multivalent nanoparticles. [72,75] Furthermore, preparing particles with valency greater than two has proven to be difficult.

1.6   IMPORTANTAT CRITERIA FOR AN IDEAL NANOPARTICLE ASSEMBLY METHOD

The common goal of existing methods is to assemble nanoparticles into well-organized complex superstructures. In most cases, the existing methods are useful for controlling the long-range order of nanoparticles within superstructures and preparing superstructures with various nanoparticle compositions. However, the development of new methodology is required because the current methods suffer from several disadvantages that limit their practical use. One of the principle disadvantages is the requirement of multiple steps to produce topologically complex nanoparticle superstructures. In addition, current methods are still insufficient for providing both structural diversity and for providing precise control over the local nanoparticle order.

An ideal particle assembly method should: 1) require few synthetic steps, which would minimize waste, and be accomplished under mild, environmentally-benign synthetic conditions (e.g. at room temperature and in aqueous environment); 2) allow for construction of various topologically complex nanoparticle superstructures; 3) allow for precise control over both the long-range and local order of nanoparticles; and 4) allow for precise control of nanoparticle size, composition, and interparticle spacing.   The development of a methodology that satisfies all of these criteria is a considerable challenge. A general methodology that addresses these criteria

would enable researchers to target, design, and construct highly complex nanoparticle superstructures for specific applications in a *logical fashion*. Further, it would lead to the development of new, heretofore undiscovered nanoparticle superstructures and materials that may exhibit useful properties.

1.7 NEW PEPTIDE BASED METHODOLOGY

As introduced in section 1.4.3, peptides have two useful features that can be used to prepare inorganic nanostructures: 1) their self-assembly capabilities [51,58] and 2) their inorganic-recognition capabilities[15,53,60,62-64]. In principle, then, peptide-based methods should allow one to prepare topologically complex structures with various nanoparticle compositions that depend on the chosen inorganic metal binding peptide. While there are many examples of methods that couple these two capabilities, most involve multiple steps and result in assemblies with poor local nanoparticle order [59,67,69]. The reason for this is that researchers have always used two different peptides for performing the self-assembly and particle nucleation tasks: a self-assembling peptide to provide structure and an inorganic metal-binding peptide to direct nanoparticle synthesis. Since the metal binding peptides are randomly distributed on the self-assembled peptide template, randomly distributed nanoparticles result.

To address this problem, the Rosi group has developed a new peptide based methodology to synthesize complex and well-organized nanoparticle superstructures. This method relies on the use of peptide conjugate molecules to direct both the synthesis and the assembly of the nanoparticles. These peptide conjugate molecules serve a dual purpose: the inorganic recognition motif binds specific nanoparticles and plays a role in their synthesis, and the self-

15

assembly motif directs the assembly of the nanoparticles into specific architectures. For example, PEP_{Au} ($AYSSGAPPMPPF^{63}$) has two unique properties: first, it can bind to gold surfaces and mineralize gold cations to form gold nanoparticles[62-64]; and second, the first amino acid residues (AYSS) of PEP_{Au} have a tendency to form β-sheets [76]. When an aliphatic chain C_{12} was covalently tethered on the N-terminus of this peptide, creating C_{12}-PEP_{Au} ($C_{11}H_{23}CO$-PEP_{Au}) conjugates, this peptide conjugate could direct the synthesis and assembly of 1-D left-handed gold nanoparticle double helices with an excellent local order (**Figure 8**) [53].
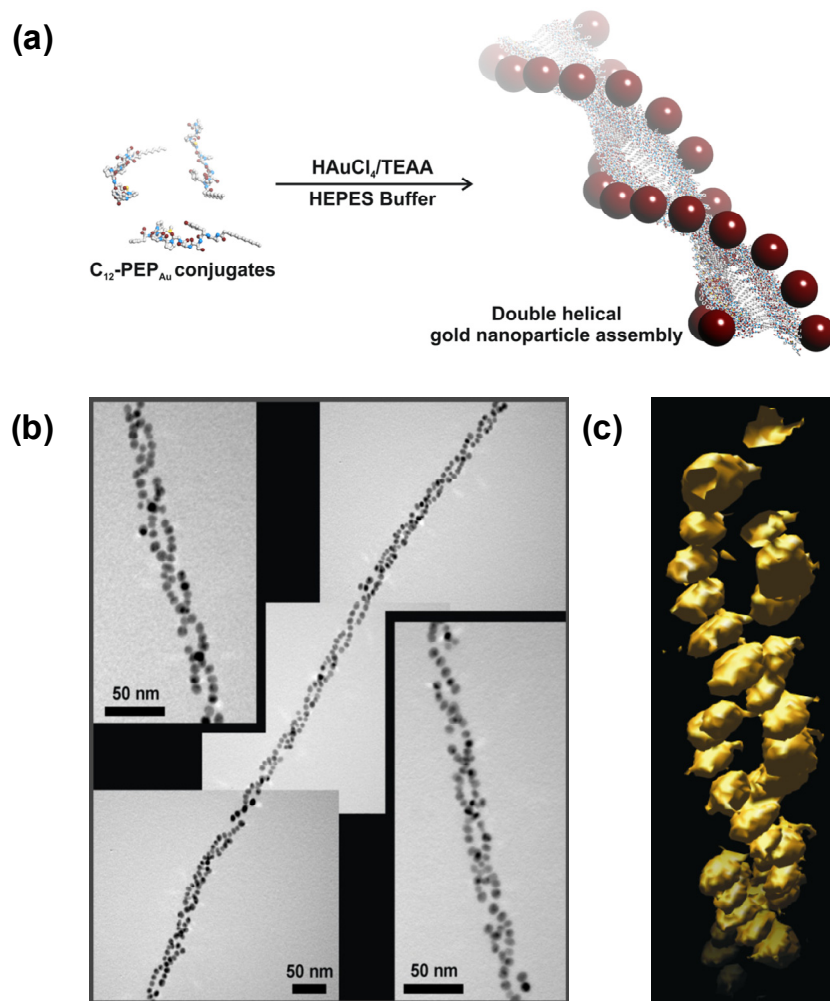
Figure 8. New peptide-based method for left-handed gold nanoparticles double helices: (a) Scheme of the formation of gold nanoparticle double helices; (b) TEM images; (c) Tomographic 3-D reconstruction image (Adapted from ref. 53)

1.8   OBJECTIVES AND OUTLINES

The main objectives of the work in this dissertation are: 1) to further develop the methodology introduced by the Rosi group by expanding its structural scope; and 2) to elucidate the fundamental mechanistic details of this methodology and understand how peptide conjugates direct the synthesis of highly-ordered gold nanoparticle superstructures. Chapter 2 describes the preparation of conjugates that direct the assembly of various spherical nanoparticle assemblies. In particular, this chapter details how modifications to the peptide sequence can impact structure formation (*Small* **2011**, *7*, 1939). Chapter 3 explores the preparation of new linear nanoparticle superstructures and describes how these structures and their preparation lend insight into important mechanistic factors underlying this methodology (*Chemical Communications* **2011**, *47*, 185). Finally, Chapter 4 details fundamental studies aimed at elucidating the mechanism of the methodology and identifying the key criteria for preparing highly-ordered nanoparticle superstructures using this methodology (*manuscript in preparation*).

2.0 SIZE-CONTROLLED PEPTIDE–DIRECTED SYNTHESIS OF HOLLOW SPHERICAL GOLD NANOPARTICLE SUPERSTRUCTURES

2.1 INTRODUCTION

Peptide conjugate molecules comprising programmable self-assembly[77] and inorganic recognition[15,61] motifs have proven to be powerful agents for directing the one-pot synthesis and assembly of structurally-regular and topologically-complex nanoparticle superstructures.[53,78-80] The peptide has a specific amino acid sequence that recognizes and binds to inorganic surfaces. Among the various types of peptides, PEP_{Au} is a peptide that binds to Au [111] surfaces.[81-83] When organic molecules (R) are covalently tethered to the N-terminus of this peptide to create R-PEP_{Au} conjugates, the R group tethered to the peptide can influence the self-assembly behavior of the peptide. The peptide sequence also can be modified to affect its secondary structure, i.e. α-helix or β-sheet. Therefore, the modification of the R group and the peptide sequence allow one to program a lot of information into the peptide conjugate molecules (**Figure 9**).
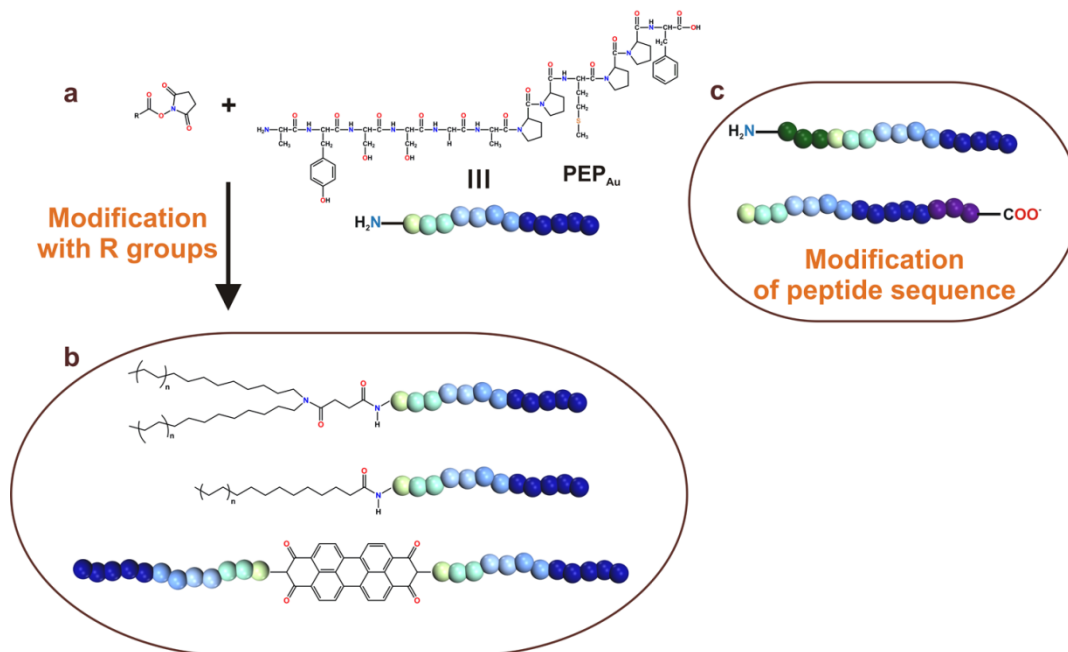
Figure 9. Schematic detailing the preparation of various peptide conjugates. (a) a reaction scheme summarizing the synthesis of a peptide conjugate molecule; (b) modification of organic tether (R) groups; (c) modification of peptide termini.

We recently introduced the conceptual basis of utilizing this class of molecules for nanoparticle synthesis and assembly and demonstrated that particular members of this class could be used to prepare 1-D nanoparticle superstructures,[78,80] including gold nanoparticle double helices[53] and discrete sub-100 nm spherical gold nanoparticle superstructures.[79] In this previous work, we showed that small changes to the organic component of the peptide conjugate can lead to entirely different nanoparticle superstructures. For example, we found that C_{12}-PEP_{Au} directs the formation of gold nanoparticle double helices[53] while C_6-A_2-PEP_{Au} ($C_5H_{11}CO$-

A$_2$-PEP$_{Au}$; A = alanine) directs the formation of 'hollow' spherical gold nanoparticle assemblies (i.e. a spherical shell of gold nanoparticles).[79]

The properties of a nanoparticle superstructure can depend intrinsically on the size and shape of the superstructure and the organization of the nanoparticles within the superstructure.[2,4] One of our main interests is to explore the versatility of our methodology in order to construct new complex nanoparticle assemblies. Here, we explore how modifications to the peptide sequence can impact the structure of a nanoparticle assembly. Specifically, we demonstrate that small modifications to the sequence at the N-terminus of the peptide portion of the conjugate allow one adjust the size of spherical gold nanoparticle superstructures and ultimately enable the direct one-pot preparation of sub-50 nm spherical superstructures. Such structures may potentially exhibit useful optical and catalytic properties and possibly may serve as capsules or delivery agents.[2,4,21-23,84-94] This result proved one particularly useful feature of this methodology: small changes to the composition and sequence of the peptide conjugate can dramatically impact the structure of the resulting nanoparticle assembly.

2.2   EXPERIMENTAL SECTION

2.2.1   Materials

All solvents and chemicals were obtained from commercial sources and used without further purification. 0.1 M HEPES (4-(2-hydroxyethyl)-piperazineethanesulfonic acid) buffer was made by directly diluting 1.0 M HEPES buffer (pH = 7.3 ± 0.1; Fisher Scientific) with water

(NANOpure, Barnstead Diamond^{TM} System.; 18.2 MΩ). All peptides were synthesized and purified by New England Peptide (NEP).

2.2.2 Methods

Reverse-phase high pressure liquid chromatography (HPLC) was performed at ambient temperature with an Agilent 1200 liquid chromatographic system equipped with diode array and multiple wavelength detectors using a Grace Vydac protein C4 column (214TP1010, 1.0 cm × 25 cm). Matrix-assisted laser desorption ionization time-of-flight (MALDI-TOF) mass spectra were obtained on an Applied Biosystem Voyager System 6174 MALDI-TOF mass spectrometer using an α-cyano-4-hydroxy cinnamic acid (CHCA) matrix. Samples for atomic force microscopy (AFM) were prepared on freshly peeled MICA substrates that were treated with a 1% solution of 3-aminopropyl trimethoxysilane.[95] Tapping-mode AFM was performed on a Veeco Dimension VSPM. Transmission electron microscopy (TEM) samples were prepared by pipetting one drop of solution onto a 3-mm-diameter copper grid with carbon film; 2% aqueous phosphotungstic acid or uranyl acetate was used for negative staining. TEM was conducted on a JEOL 200CX instrument operated at 200kV and images were collected using a Gatan CCD image system. The projection images from electron tomography studies were recorded with a Gatan 4K × 4K charge-coupled device (CCD) camera mounted on a Tecnai F20 electron microscope (FEI Corporation, Hillsboro, Oreg.) equipped with a field emission gun (FEG) operating at 200 kV. For electron tomography, a series of images were recorded at room temperature with the Gatan 4K × 4K CCD camera at a nominal magnification of 50,000 by tilting the specimen from -70 $^{\text{o}}$C to 70 $^{\text{o}}$C in increments of 1$^{\text{o}}$. Images were recorded at an underfocus value around 2 μm along

the tilt axis. A back-projection algorithm, as implemented in the IMOD reconstruction package, was used to convert the information present in the series of tilted projection images into three-dimensional density maps.[96] The surface rendering was generated using the Chimera software.[97]

2.2.3 Preparation of N-hydroxyl-succinimide ester
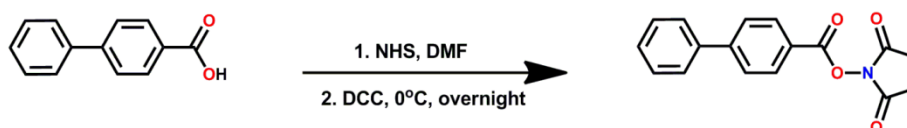
4-phenylbenzoic acid (500.0 mg, 2.52 mmol) and N-hydroxysuccinimide (290.2 mg, 2.52 mmol) were dissolved in 15 ml anhydrous dimethylformamide (DMF) in an argon atmosphere. The solution was stirred for 5 min at room temperature and then cooled to 0 °C in an ice bath. After addition of dicyclohexyl carbodiimide (DCC) (562.1 mg, 2.72 mmol) at 0 °C, the solution was stirred overnight at room temperature. The reaction mixture was processed by removing the precipitate via filtration. The solvent was removed under reduced pressure and the crystalline residue recrystallized from isopropanol to yield the N-hydroxyl-succinimide ester (585.9 mg, 1.984 mmol, 79 %). ^{1}H NMR (300 MHz, CDCl$_3$): δ 8.23-8.20 (dd, 2H, $J = 5.1$ Hz, $J = 6.3$ Hz), 7.75-7.72 (dd, 2H, $J = 4.8$ Hz, $J = 6.6$ Hz), 7.65-7.62 (m, 2H), 7.496-7.454 (m, 3H), 2.92 (s, 4H) (**Figure A1**).

2.2.4   Preparation of peptide conjugates
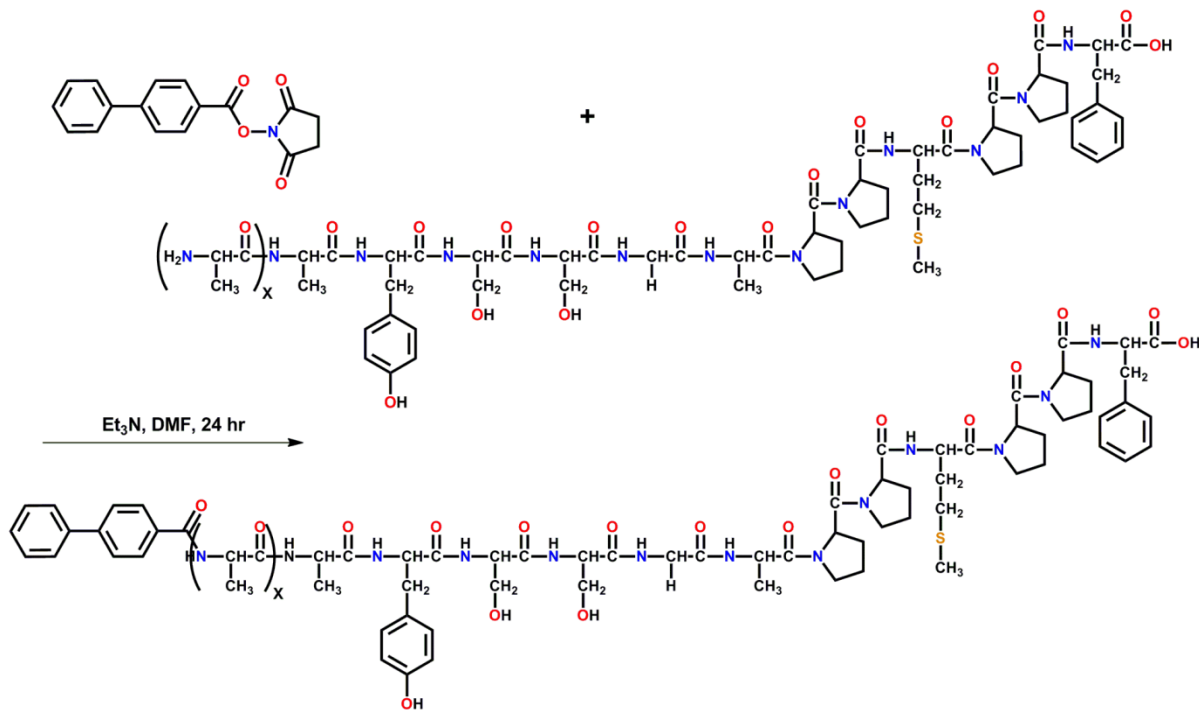
A_x-PEP_{Au} (X = 0-3; PEP_{Au} = AYSSGAPPMPPF) were synthesized and purified by New England

Peptide. BP-A_x-PEP_{Au} were synthesized and purified using established methods.[53] Briefly,

biphenyl N-Hydroxyl succinimide ester (1.69×10^{-6} mol) dissolved in dimethylformamide (DMF;

50 µL) was mixed with A_x-PEP_{Au} (x=2, 8.797×10^{-7} mol; x=3, 7.874×10^{-7} mol) in DMF (70

µL). Triethylamine (1 µL) was added to this solution, and the resulting solution was stirred (24 h)

at room temperature. Once completed, the reaction was diluted with a 1:1 mixture of water and

acetonitrile (1000 µL). This solution was purified by reverse-phase HPLC using a linear gradient

of 0.05% formic acid in CH_3CN and 0.1% formic acid in water (**Figure A2**). The concentration

of the purified peptide conjugates was determined using the molar extinction coefficient of

tyrosine (1280 $M^{-1}cm^{-1}$) at 280 nm. Once HPLC purification was completed, the eluted product

was lyophilized. A sample of the lyophilized product was deposited onto a α-cyano-4-hydroxy

cinnamic acid (CHCA) matrix and its mass was determined using matrix-assisted laser desorption ionization time-of-flight mass spectrometry (MALDI-TOF MS) (**Figure A3**).

2.2.5   Synthesis of gold nanoparticle superstructures

Lyophilized BP-A$_2$-PEP$_{Au}$ (1.36 × 10^{-7} mol) or BP-A$_3$-PEP$_{Au}$ (2.60 × 10^{-7} mol) peptide conjugate was completely dissolved in 0.1M HEPES buffer (0.5 ml; pH=7.3±0.1; Fisher Scientific) in a plastic vial. This solution was allowed to incubate at room temperature (30 min). Thereafter, a freshly prepared solution of 0.1M chloroauric acid (HAuCl$_4$) in 1.0 M triethylammonium acetate (TEAA; pH = 7.0) buffer (2 μl) was added to the peptide conjugate solution. The resulting mixture was vortexed for a few seconds as soon as the HAuCl$_4$ solution was added and then left undisturbed at room temperature (24 h or 48 h).

2.3   RESULTS AND DISCUSSION

Our strategy takes advantages of peptides which have both self-assembly capabilities and inorganic recognition capabilities. As mentioned in the Introduction (section 2.1), we are utilizing AYSSGAPPMPPF (PEP$_{Au}$), which can bind to gold surfaces.[15,61,63] We hypothesize that we can rationally modify PEP$_{Au}$ and prepare peptide conjugates that can direct the synthesis and self-assembly of nanoparticles into various superstructures.

In this work, we have utilized PEP$_{Au}$ and a modified version of PEP$_{Au}$, A$_x$-PEP$_{Au}$ (A$_x$-AYSSGAPPMPPF; x = 0-3). Using these peptides, we prepared several peptide conjugates by appending a biphenyl molecule to PEP$_{Au}$ and the modified A$_x$-PEP$_{Au}$ as an organic tether

molecule (R). **Figure 10** illustrates the different peptide conjugates with a slightly modified peptide sequence were prepared. Alanine is a slightly hydrophobic amino acid, with its methyl side chain. Biphenyl is a rigid hydrophobic tail. Collectively, this series peptide conjugates provide a basis set of molecules that can be used to study how small changes to the hydrophobicity of the conjugate can impact assembly.
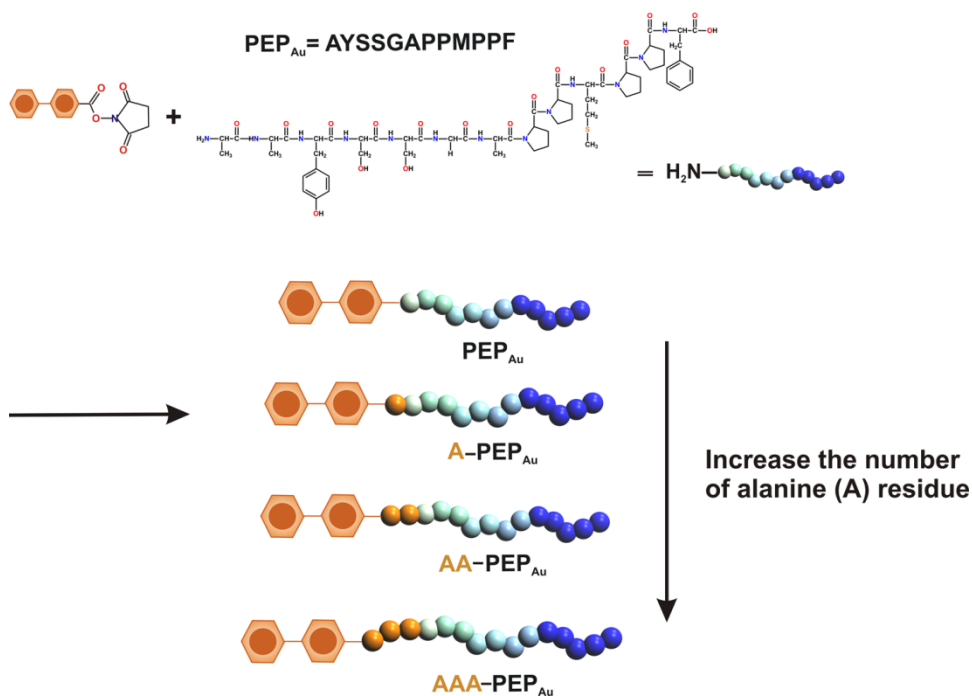
Figure 10. Schematic description of preparation of modified peptide conjugates with a different peptide sequence using a biphenyl appendage.

2.3.1　Self-assembly behavior of peptide conjugates

We began this work by first studying the self-assembly properties of BP-A_x-PEP$_{Au}$ ($C_{12}H_9$CO-A_x-AYSSGAPPMPPF; x = 0-3) in HEPES buffer (0.1 M, pH 7.3±0.1; HEPES = 4-(2-hydroxyethyl)-piperazineethanesulfonic acid) both *before* and *after* the addition of a gold solution (0.1 M HAuCl$_4$ in 1.0 M TEAA; TEAA = triethylammonium acetate).[98,99] Under both assembly conditions, neither BP-PEP$_{Au}$ nor BP-A-PEP$_{Au}$ assembled into well-organized structures. That is, these conjugates did not yield either well-defined 'soft' peptide conjugate assemblies or 'hard' nanoparticle superstructures. We reason that the N-terminal region was not sufficiently hydrophobic to promote assembly under these conditions.

We added an additional hydrophobic alanine residue to produce BP-A_2-PEP$_{Au.}$ When we studied its assembly behavior in HEPES buffer prior to adding a gold solution, no assembly was observed based on analysis of AFM and TEM images. However, we observed the assembly of BP-A_2-PEP$_{Au}$, especially in the presence of the gold salt solution. Specifically, in a mixture of HEPES and HAuCl$_4$/TEAA, BP-A_2-PEP$_{Au}$ assembles into large spherical structures, as revealed by transmission electron microscopy (TEM) (**Figure 11**). The size distribution (~60 nm - ~240 nm; **Figure 11c**) of the large spherical structures suggests a vesicular architecture.[38] We note that these structures are similar to those formed via the self-assembly of C_6-A_2-PEP$_{Au}$.[79]
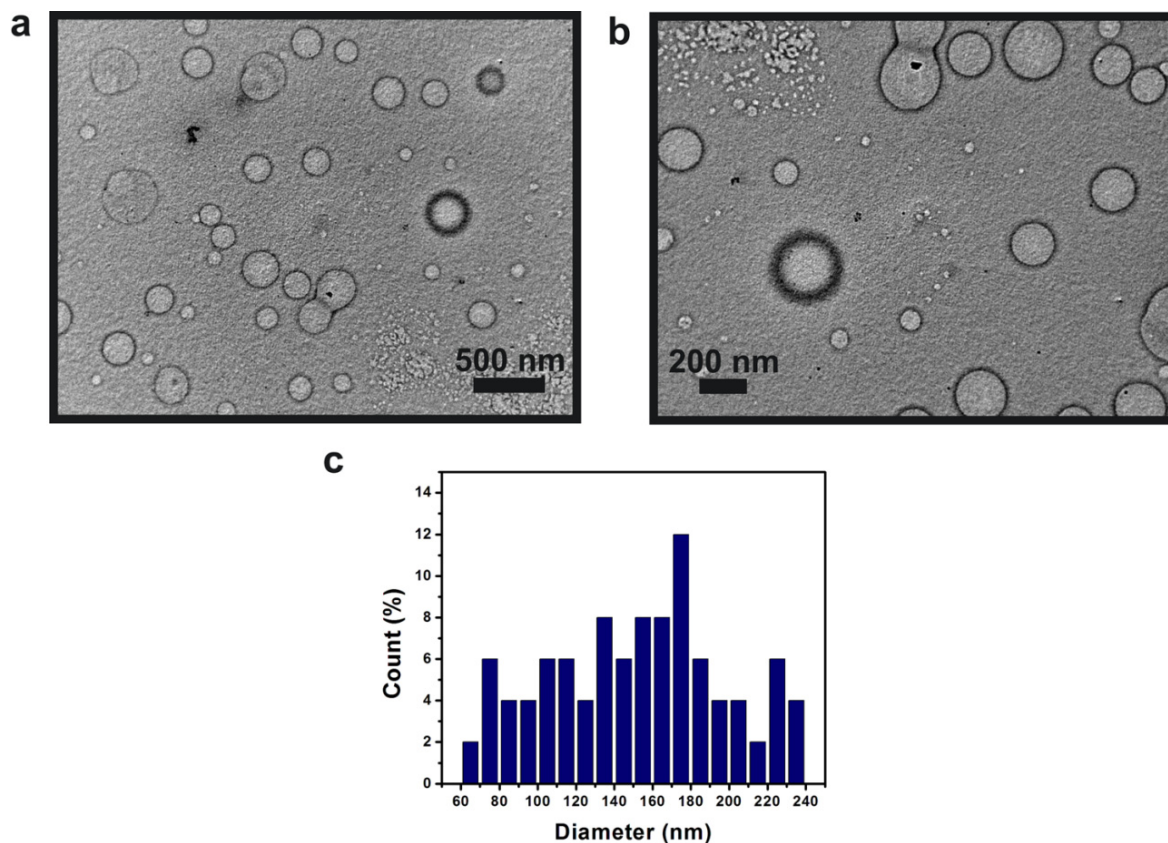
Figure 11. TEM images (a–b) of self-assembled BP-A$_2$-PEP$_{Au}$ stained with 2% aqueous uranyl acetate. The samples used for these images were produced in the following way: 1) BP-A$_2$-PEP$_{Au}$ was incubated for 30 min in HEPES buffer and 2) HAuCl$_4$ solution was added to the BP-A$_2$-PEP$_{Au}$ solution and the resulting mixture was allowed to incubate for 30 min. The diameter of the structures (c) ranged from ~60 nm to ~240 nm.

AFM height and phase images also provided information of the spherical structures (**Figure 12**). First, the spheres formed in a mixture of HEPES and HAuCl$_4$/TEAA solution showed a diameter of ~110-130 nm. Based on the range of a diameters observed via TEM (**Figure 11c**), the diameter of the spheres was still within this range, even though AFM does not provide accurate width/diameter measurement. Second, the yield of the spheres increased as the

incubation time in the gold solution increased. Last, the structures displayed a height of ~7 nm, which suggested a collapsed vesicular structure. The estimated length of a peptide conjugate monomer is ~ 2.5-3. Two BP-A$_2$-PEP$_{Au}$ units that interact through their hydrophobic biphenyl tails will be a basic unit to form a bilayer of a vesicular structure. The expected width of the unit is ~4-5 nm. The height of ~7 nm revealed in AFM is consistent with a tetralayer structure (i.e. a vesicle within a vesicle) when two of the units are stacked together (~8-10 nm).
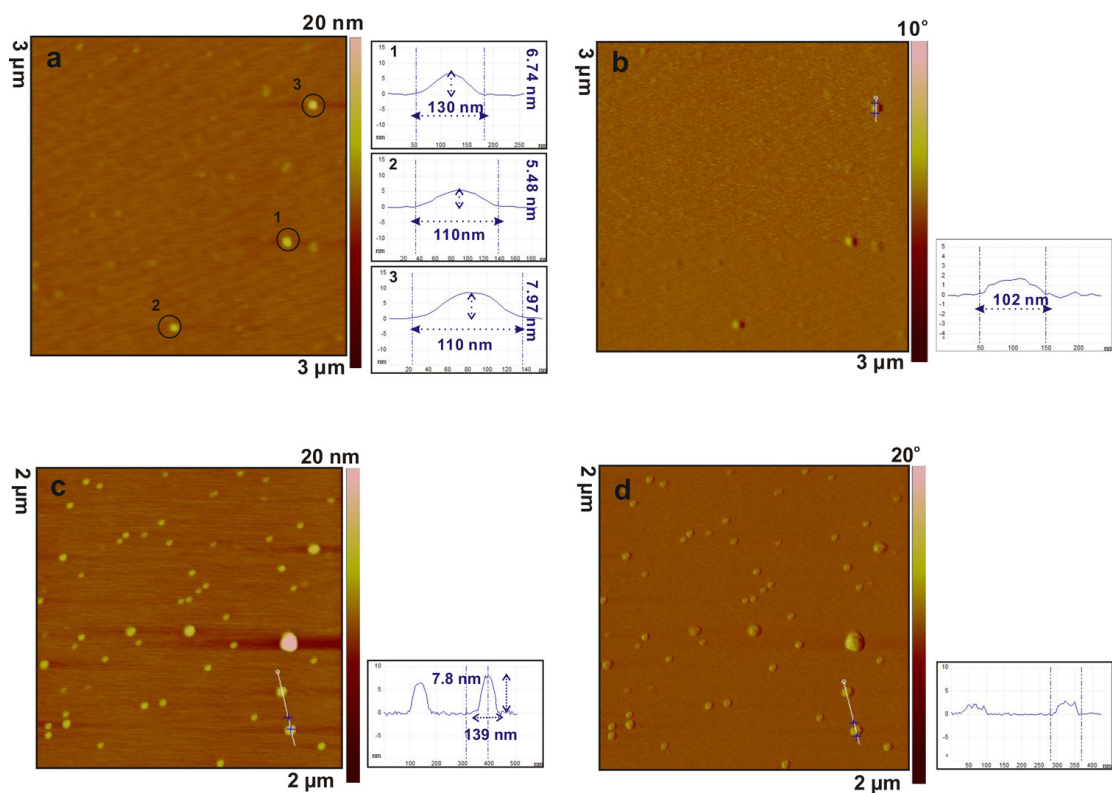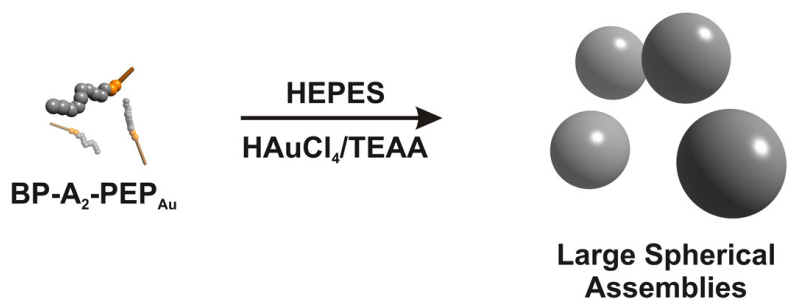
Figure 12. AFM height (a and c) and phase (b and d) of BP-A$_2$-PEP$_{Au}$ self-assembled structures in the presence of a gold source. The samples used for these images were produced in the following way: 1) BP-A$_2$-PEP$_{Au}$ was incubated for 30 min in HEPES buffer and 2) HAuCl$_4$ solution was added to the BP-A$_2$-PEP$_{Au}$ solutions and the resulting mixture was allowed to incubate for 10 min (a and b) and 30min (c and d), respectively.

At this point, we decided to explore whether further modification of the peptide sequence would impact the structure of the resultant nanoparticle assembly. It is well-established that increasing the length of the hydrophobic component of a surfactant molecule can promote a transition from vesicular architectures to tubular micelles or discrete spherical micelles.[38] We reasoned that small spherical micelles would be an ideal underlying template for producing sub-50 nm hollow spherical nanoparticle superstructures. While sub-50 nm clusters of nanoparticles have been prepared,[23,100,101] we are not aware of any sub-50 nm hollow nanoparticle superstructures which have been prepared in a logical single-step process. In our basic conjugate, $BP-A_x-PEP_{Au}$, we can systematically increase the hydrophobic character of the N-terminus by adding additional alanine residues.[102] We therefore prepared $BP-A_3-PEP_{Au}$ and studied its self-assembly. $BP-A_3-PEP_{Au}$ assembled into well-defined spherical structures (**Figure 13a**) after incubating for three days in HEPES buffer, as observed by atomic force microscopy (AFM) (**Figure 13**).

Upon adding $HAuCl_4$/TEAA to a solution of $BP-A_3-PEP_{Au}$ in HEPES, we again observed, after 5 min, the formation of small spherical structures (**Figure 14a**). Based on their size (4.51 ± 0.5 nm), we hypothesize that these spherical structures could be micelles.[38] After prolonged incubation in the HEPES/$HAuCl_4$/TEAA mixture, these spherical structures begin to coalesce (after 10 min; **Figure 14b**), ultimately yielding fibers (after 6 h; **Figure 14c**) whose diameters (4.46 ± 0.6 nm) are suggestive of tubular micelles.[38]
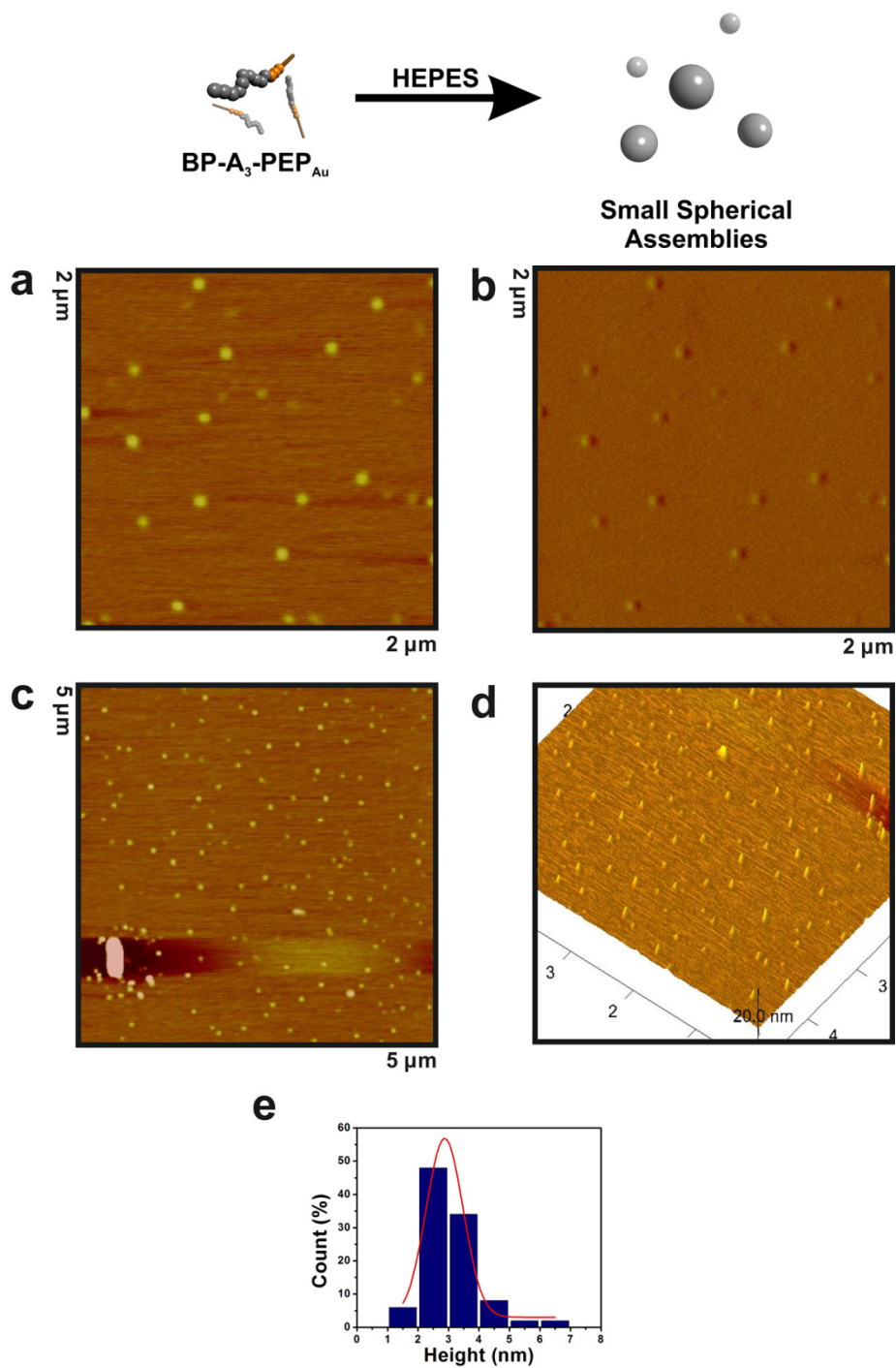
Figure 13. AFM height (a and c), phase (b), and 3-D (d) images of BP-A$_3$-PEP$_{Au}$ self-assembled structures formed 3 days after incubation in HEPES buffer. (e) Height distribution of BP-A$_3$-PEP$_{Au}$ structures (height = 2.87 ± 0.6 nm; based on 50 counts from AFM images).

32
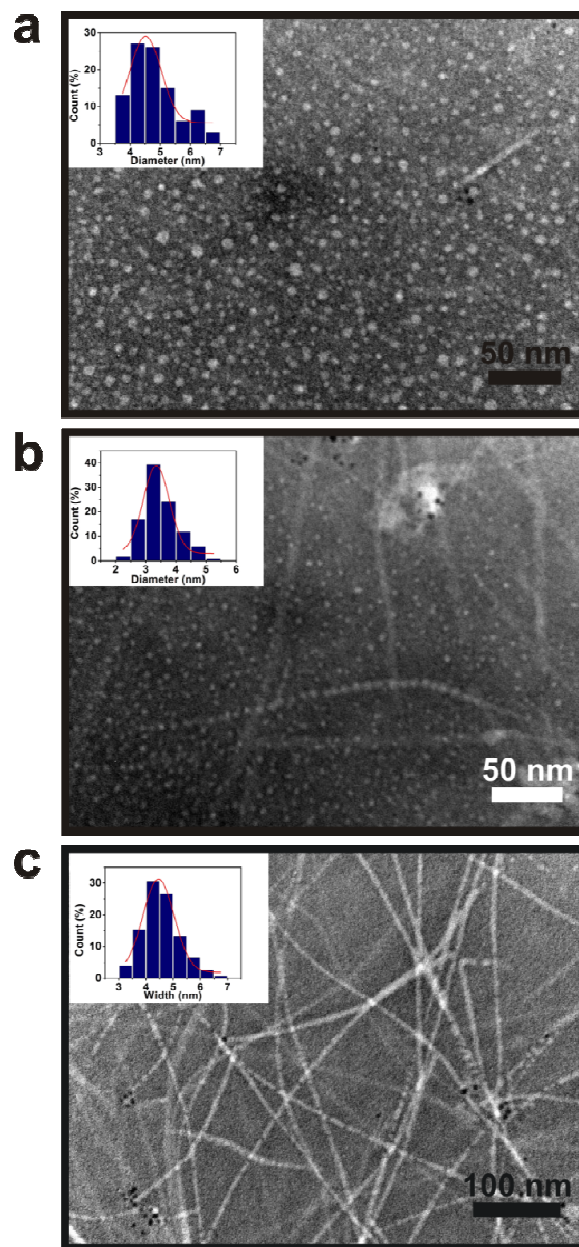
Figure 14. TEM images (a–c) of BP-A$_3$-PEP$_{Au}$ assemblies stained with 2% aqueous phosphotungstic acid. The samples used for these images were produced in the following way: 1) BP-A$_3$-PEP$_{Au}$ was incubated for 30 min in HEPES buffer and 2) HAuCl$_4$/TEAA solution was added to the BP-A$_3$-PEP$_{Au}$ solution and the resulting mixture was allowed to incubate for (a) 5 min, (b) 10 min, (c) 6 hrs. Diameter distribution of spheres (a and b) and width distribution of

fibers (c) were obtained from the TEM images: (a) 4.51 ± 0.5 nm, based on 100 counts; (b) 3.35

± 0.4 nm, based on 120 counts; (c) 4.46 ± 0.6 nm, based on 150 counts. The images show that

micellar gold nanoparticle assemblies are exclusively synthesized.

2.3.2   Assembly of gold nanoparticle superstructures

 After BP-A_2-PEP$_{Au}$ was allowed to incubate (~48 hrs) in the mixture of HEPES and HAuCl$_4$/TEAA,

large spherical nanoparticle superstructures (**Figure 15 and Figure 18a-b**) comprising monodisperse gold

nanoparticles (6.71 ± 1.4 nm; **Figure 16b**) formed. In general, these structures are similar to those

produced using C_6-A_2-PEP$_{Au}$,[79] but they are significantly larger (~60 nm - ~270 nm; **Figure 16a**) because

the vesicular structures that serve as their underlying template are larger than those produced using C_6-A_2-

PEP$_{Au}$. Samples of the spherical gold nanoparticle superstructures exhibited a broad absorbance with a

maximum at 656 nm (**Figure 17**), which, expectedly, is significantly red-shifted from that of the

constituent nanoparticles (~517 nm).[103] We attribute the broad absorbance to the large size distribution of

the superstructures and the presence of large aggregates of superstructures (**Figure 15b**).

We used electron tomography to better understand the 3D architecture of the

superstructures. Tilted images collected at 1° tilt intervals from –70 ^{o}C to +70 ^{o}C were combined

computationally to generate a 3D electron density map (tomogram). The sample tomographic

slices (**Figure 18c and e**) and the surface rendered 3D tomogram (**Figure 18d and f**) revealed

hollow interiors (devoid of nanoparticles) surrounded by a multi-layer of gold nanoparticles.

Moreover, it suggested that the underlying template provided by BP-A_2-PEP$_{Au}$ is a vesicular

architecture (**Figure 18**).
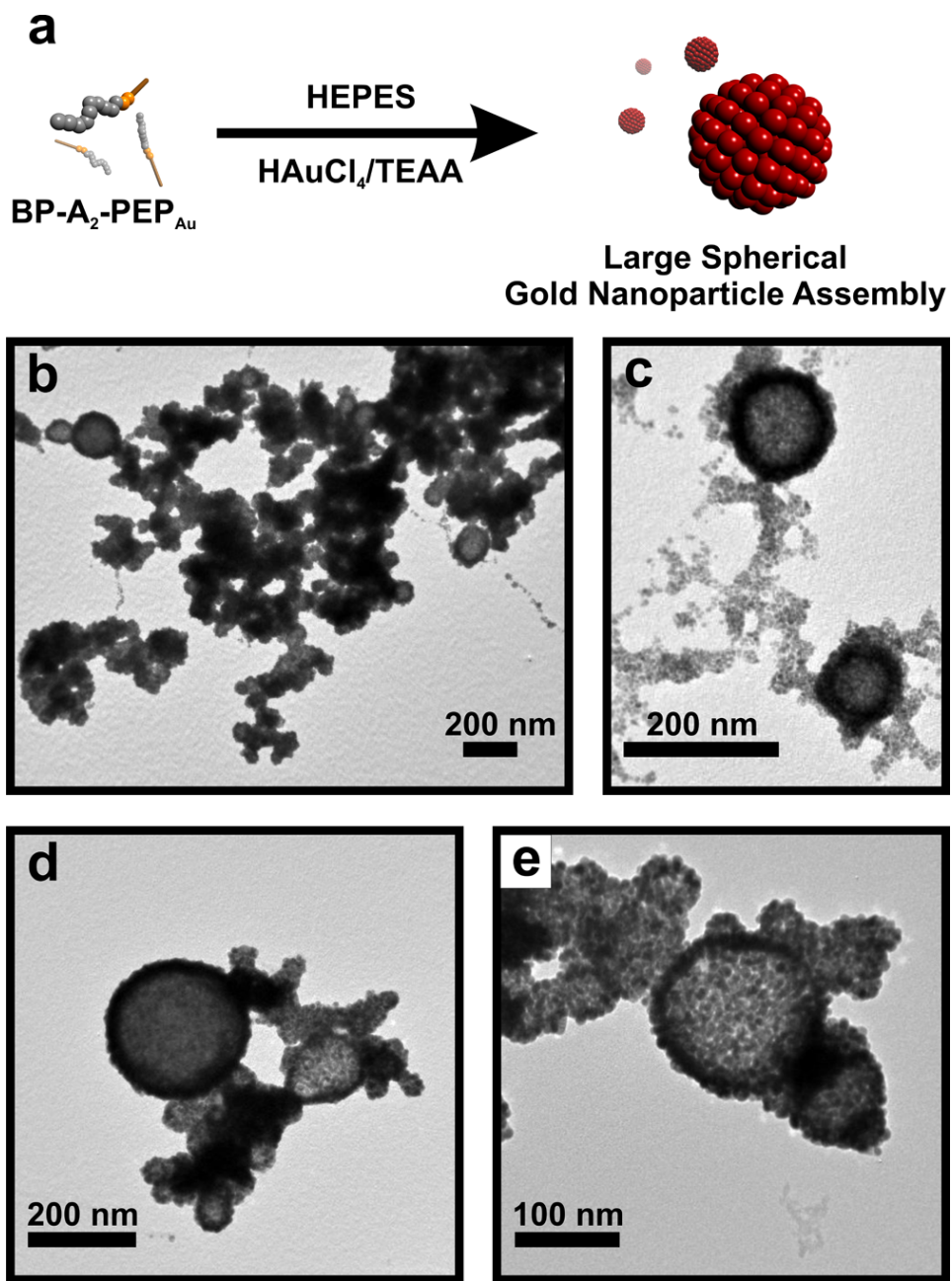
Figure 15. (a) Schematic illustration of the synthesis of large hollow spherical gold nanoparticle superstructures. (b-e) TEM images of the superstructures.
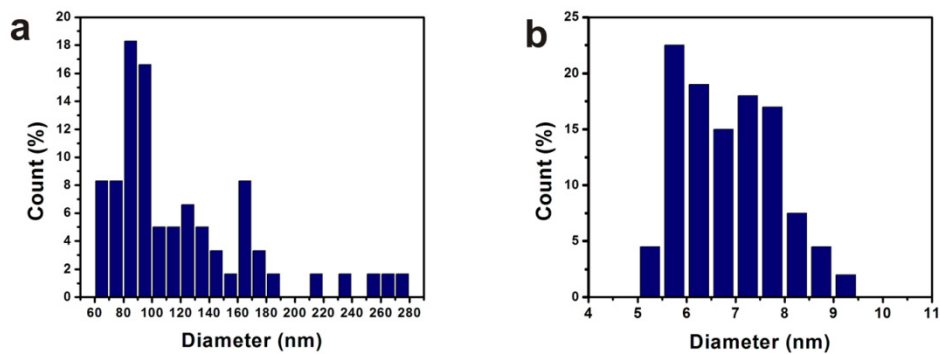
Figure 16. (a) Diameters of the superstructures ranged from ~60 nm to ~270 nm. (b) Size distribution of gold nanoparticles comprising the superstructures (6.71 ± 1.4 nm; based on 200 counts)
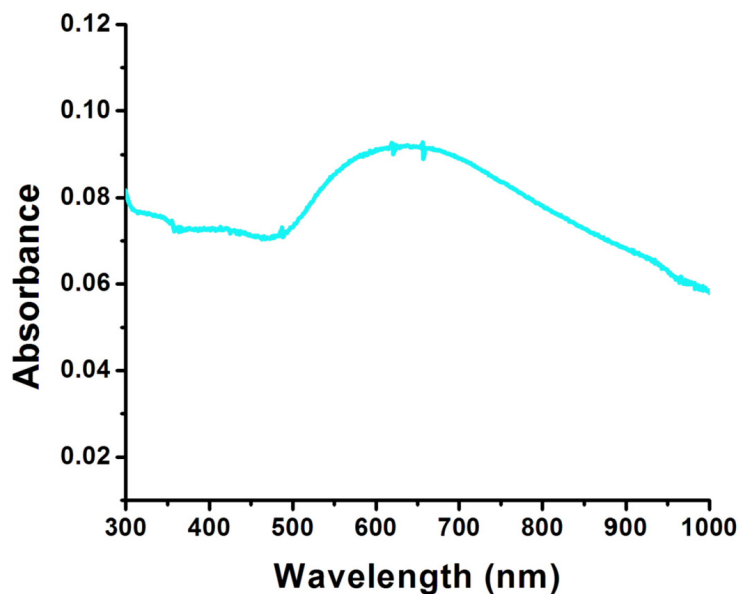
Figure 17. UV-Vis spectrum of the large spherical gold nanoparticle superstructures formed using BP-A$_2$-PEP$_{Au}$. The spectrum was collected in HEPES solution. The absorbance maximun is observed at 656 nm.
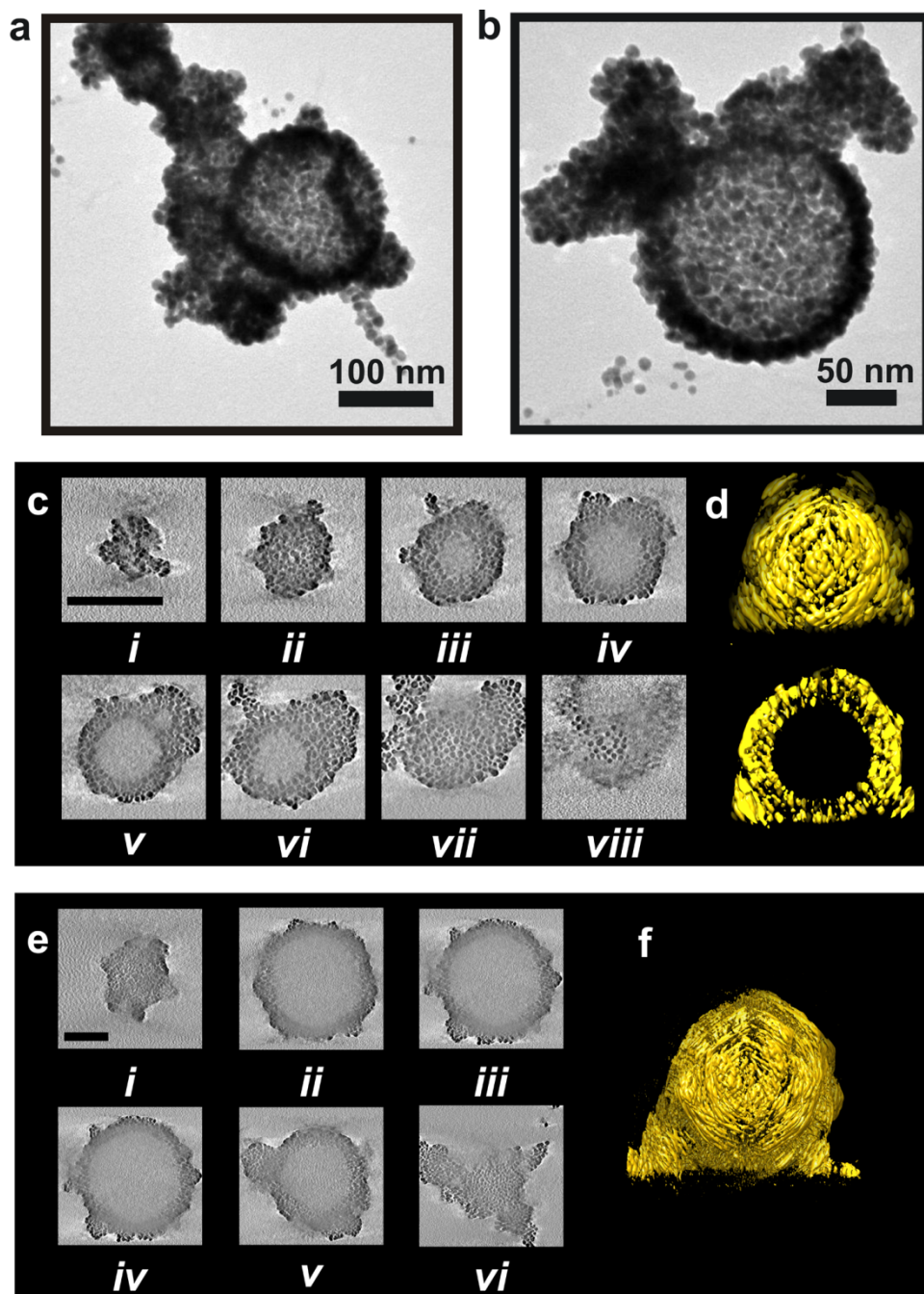
Figure 18. (a, b) Additional TEM images of spherical gold nanoparticle superstructures; (c, e) X-Y computational slices (i-viii) of the 3D tomographic volume containing the nanoparticle assembly (scale bar = 100nm) (d, f) 3D surface rendering of the tomographic volume.

After BP-A$_3$-PEP$_{Au}$ was allowed to incubate for 2 days in the mixture of HEPES and HAuCl$_4$/TEAA, we observed exclusively the formation of sub-50 nm spherical gold nanoparticle superstructures (**Figure 19**). These structures have uniform size (diameter = 29.43 ± 4.6 nm; **Figure 20a**), consist of monodisperse nanoparticles (6.15 ± 1.2 nm; **Figure 20b**), and exhibit a sharp absorption band at 540 nm (**Figure 21**), which is consistent with their size and relatively narrow size distribution. We used electron tomography to better understand the three-dimensional architecture of the superstructures. Tilted images collected at 1° tilt intervals from -70° to 70° were combined computationally to generate a three-dimensional electron density map (tomogram). The sample tomographic slices and the surface rendered 3-D tomogram (**Figure 22**) reveals that the structures are roughly spherical and that their cores are hollow (devoid of nanoparticles).
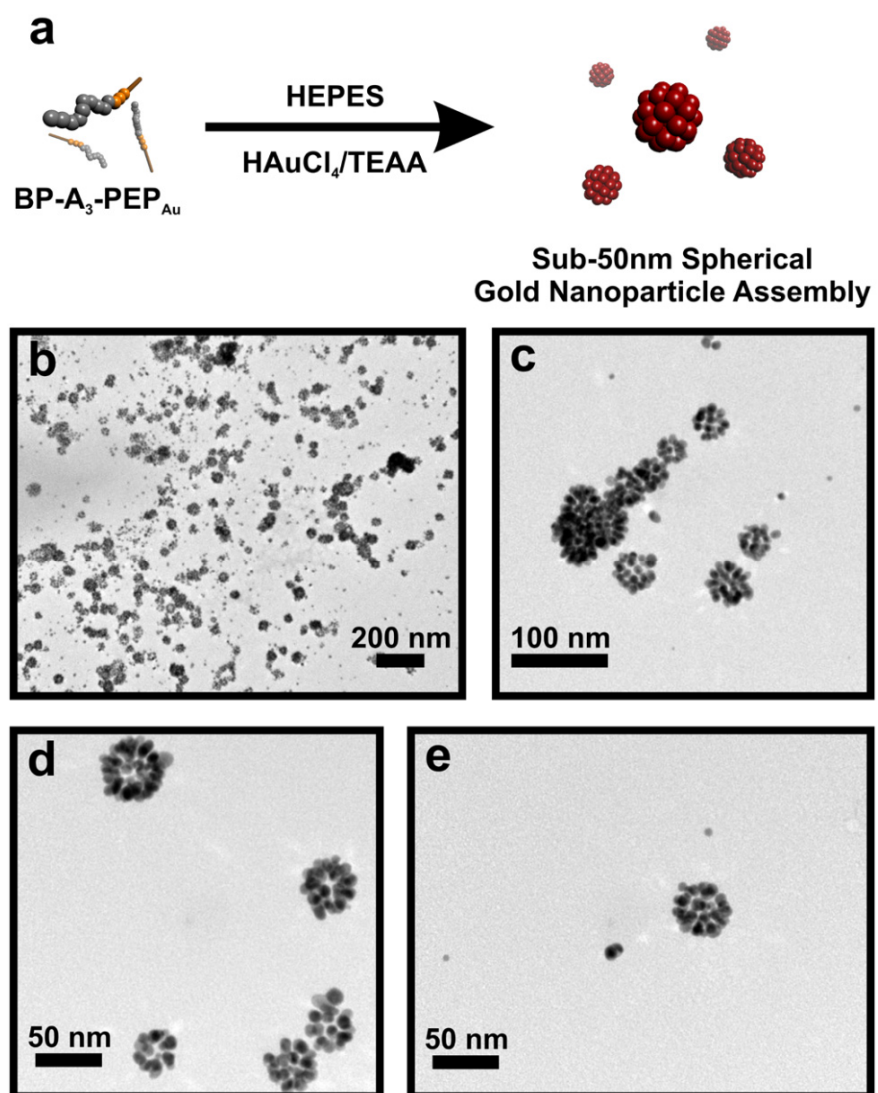
Figure 19. (a) Schematic illustration of the synthesis of sub-50 nm hollow spherical gold

nanoparticle superstructures. (b-e) TEM images of the superstructures.
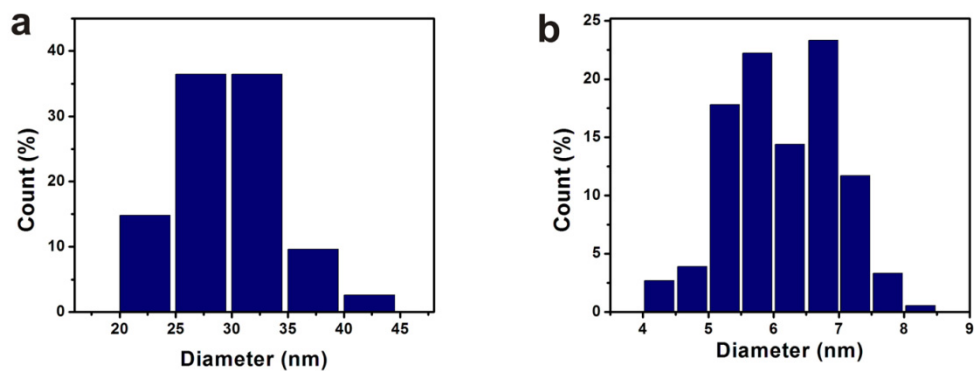
Figure 20. (a) Diameter distribution of superstructures (29.43 ± 4.6 nm; based on 115 counts). (b) Size distribution of gold nanoparticles comprising the superstructures (6.15 ± 1.2 nm; based on 180 counts)
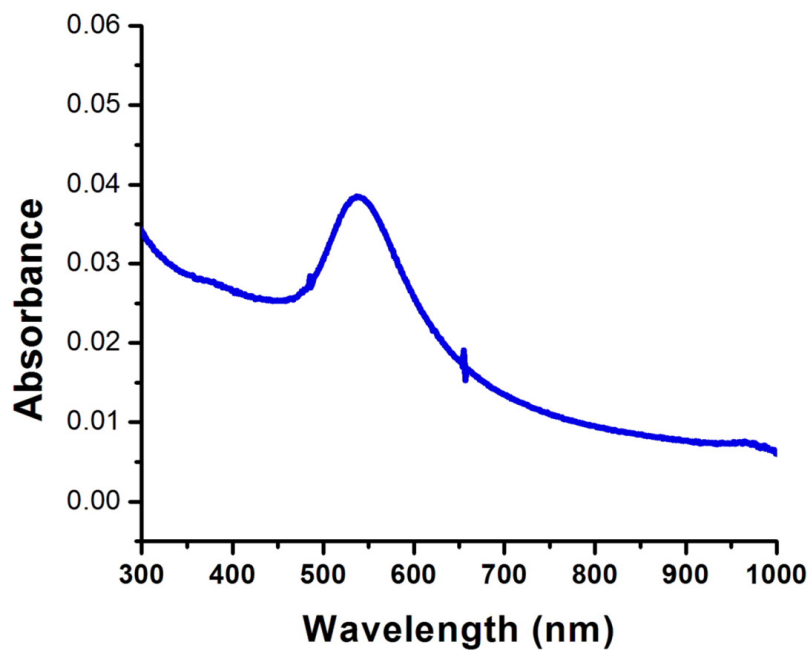
Figure 21. UV-Vis spectrum of the sub-50 nm spherical gold nanoparticle superstructures formed using BP-A$_3$-PEP$_{Au}$. The spectrum was collected in HEPES solution. The absorbance maximun is observed at 540 nm.
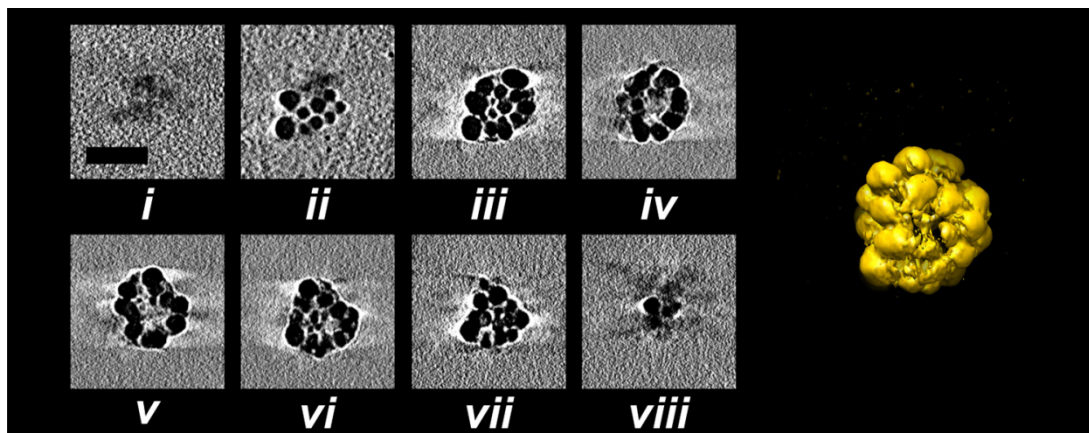
Figure 22. X-Y computational slices (i-viii) of the 3D tomographic volume containing the nanoparticle assembly (scale bar = 30 nm) and 3D surface rendering of the tomographic volume.

Interestingly, no linear nanoparticle superstructures were observed, even though tubular micelles, which could also potentially serve as templates for nanoparticle assembly, were also present (**Figure 23a**). We speculate that the spherical nanoparticle assemblies may be the exclusive product because spherical micelles are the primary structures present upon the addition of the gold salt solution. Therefore, the gold nanoparticles would first grow on the spherical micelles, resulting in the sub-50 nm spherical nanoparticle superstructure products. The tubular micelles which appear after prolonged incubation (*vide supra*) must then form from spherical micelles which are not decorated by gold nanoparticles. Interestingly, when a second aliquot of the $HAuCl_4$/TEAA solution was added six hours after adding the first aliquot, a mixture of both spherical and linear nanoparticle superstructures resulted (**Figure 23b-d**). We can reason that the first dose of gold salt led to the formation of the spherical nanoparticle superstructures while the second dose allowed formation of the linear structures. Thus, one can either produce

41

exclusively spherical nanoparticle superstructures or a mixture of spherical and linear superstructures depending on the gold salt dosing regimen.
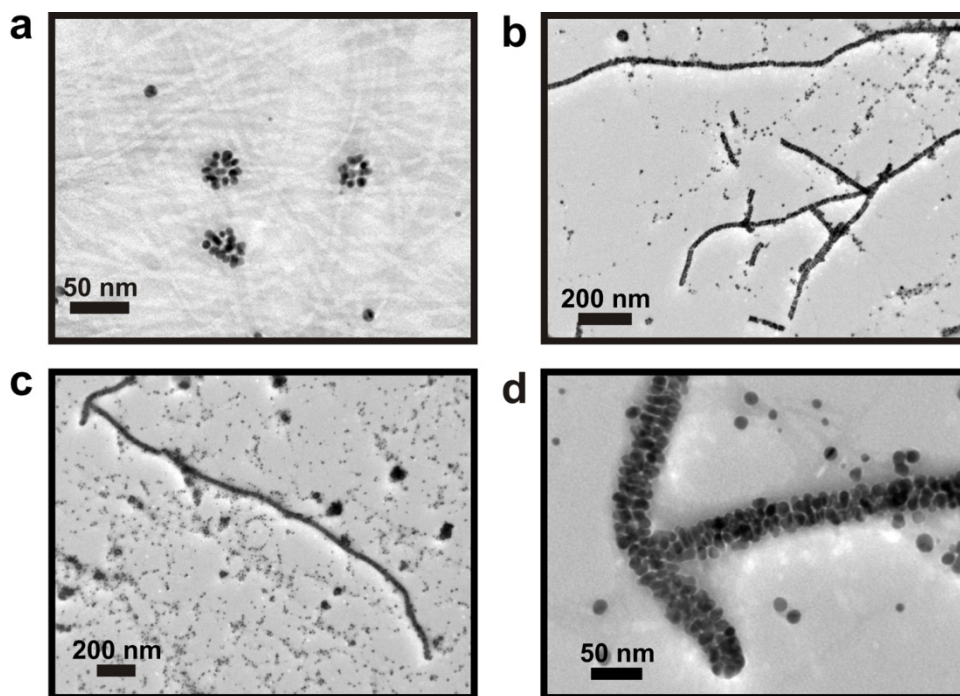
Figure 23. TEM images of (a) spherical and (b–d) linear gold nanoparticle superstructures. The sample used for the image (a) was produced 20 hrs after adding a first aliquot of the HAuCl$_4$/TEAA solution to a BP-A$_3$-PEP$_{Au}$ solution in HEPES. The samples used for the images (b–d) were produced in the following way: 1) BP-A$_3$-PEP$_{Au}$ was incubated for 30 min in HEPES buffer and 2) HAuCl$_4$/TEAA solution was added to the BP-A$_3$-PEP$_{Au}$ solution and the resulting mixture was allowed to incubate for 6 hrs, and 3) a second aliquot of the HAuCl$_4$/TEAA solution was added to the mixture and then allowed to incubate for (b) 16 hrs and (c–d) 20 hrs.

2.3.3   Geometric changes from small spheres to large spheres

When amphiphile molecules assemble in a solution, their structure can be predicted using the packing parameter ($P= v/a_0 l_c$), where v is the hydrophobic volume, a_0 is surface area of polar head group, and l_c is the length of the amphiphile.[38] Our first hypothesis was that the length of the peptide amphiphile (l_c) could be increased by adding additional alanine residues at the N-terminus of the peptide sequence. However, addition of a single amino acid ($< \sim 1$ nm)[104] did not appreciably affect the length of the peptide amphiphile.

The pI of PEP_{Au} is 5.57[105], which indicates that the overall charge of $BP-A_2-PEP_{Au}$ and $BP-A_3-PEP_{Au}$ is slightly negative in HEPES buffer (pH 7). Peptide amphiphile molecules are well known to self-assemble at a high ionic concentration or under elelctroneutral conditions as a way of overcoming the electrostatic repulsion.[106] The polar head group of C-terminus of the peptide amphiphile (COO^-) prevented the assembly of $BP-A_2-PEP_{Au}$ into a structure in HEPES buffer in the absence of a gold source, whereas $BP-A_3-PEP_{Au}$ showed an ability of to assemble slowly (as seen in **Figure 13**). When a gold source is added into a solution, the $BP-A_2-PEP_{Au}$ and $BP-A_3-PEP_{Au}$ conjugates both rapidly assemble into large and small spheres respectively. We propose a possible explanation for the observed structural difference between $BP-A_2-PEP_{Au}$ and $BP-A_3-PEP_{Au}$ assembled structures, even though the mechanism is not clearly understood.

Our proposed explanation involves the increased flexibility of the peptide chain upon addition of alanine residues. We expect that v and l_c of the two peptide conjugates will be similar. The key difference we believe is the flexibility of the peptide amphiphile; that is, one additional alanine residue of $BP-A_3-PEP_{Au}$ can provide additional flexibility to the peptide amphiphile chain in the solution. This will result in larger probability of undergoing significant motion (i.e.,

rotation of a tail) around C-terminus head group when the molecules move around in solution. This larger motion can lead to an increase in the cone angles of the C-terminus head group. Therefore, the relative volume ratio between v and a_0 increases, with formation of small spheres preferable to large spheres (**Figure 24**).[107]
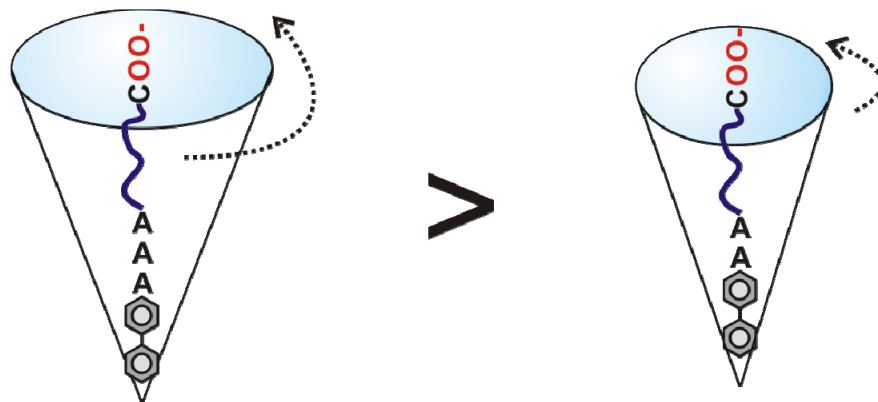
• **Flexibility of peptide amphiphile**
• **Rotation mode of a head group**
• **Cone angle of a head group**

Figure 24. Proposed schematic description of the morphology change between BP-A$_3$-PEP$_{Au}$ and BP-A$_2$-PEP$_{Au}$.

2.4   CONCLUSION

We have shown that peptide conjugate methodology for synthesizing and assembling nanoparticle superstructures can be used to prepare two different kinds of spherical structures. Importantly, we have demonstrated that small modifications to the peptide sequence, in this case addition of a single alanine residue, can significantly impact the diameter of the resulting spherical nanoparticle superstructure. In addition, we have shown that small procedural modifications, such as a second addition of gold salt, can affect nanoparticle superstructure distribution. These results point toward the versatility of this methodology and the rich structural diversity that can easily be achieved when this methodology is employed in a logical and thoughtful manner.

3.0 PREPARATION OF 1–D NANOPARTICLE SUPERSTRUCTURES WITH TAILORABLE THICKNESS USING GOLD–BINDING PEPTIDE CONJUGATES

A portion of this work, written in collaboration with Chulong Chen and Nathaniel L. Rosi*, was published in *Chem. Commun.,* **2011**, *47*, 185-187.

3.1 INTRODUCTION

In Chapter 2, we have demonstrated that small modifications to the peptide sequence, especially in the addition of a single alanine residue, can dramatically impact the diameter of the resulting spherical nanoparticle superstructure. Next, we rationally modified the peptide sequence of PEP_{Au} by adding a 'AYSS' segment, preparing AYSS-PEP_{Au} (AYSSAYSSGAPPMPPF), in which additional amino acid residues (AYSS) were added to facilitate β-sheet formation, resulting in promotion of self-assembly.[76] In the previous work, we found that C_{12}-PEP_{Au} self-assembles very slowly into fibers in the absence of gold salt in HEPES buffer under a short incubation (i.e. 30min). It is important to note that the overall charge of our peptide conjugates is slightly negative because its pI is 5.57 in HEPES (pH7) buffer.[105] We reason that the overall negatively charged peptide conjugates result in repelling each other due to electronic repulsion.

In this chapter, we aimed to explore (1) how the additional hydrophilic segment 'AYSS' of the peptide sequence influences on the nanoparticle superstructures and (2) how structural modifications to the peptide conjugate molecule impact the synthesis and assembly process (**Figure 25**).
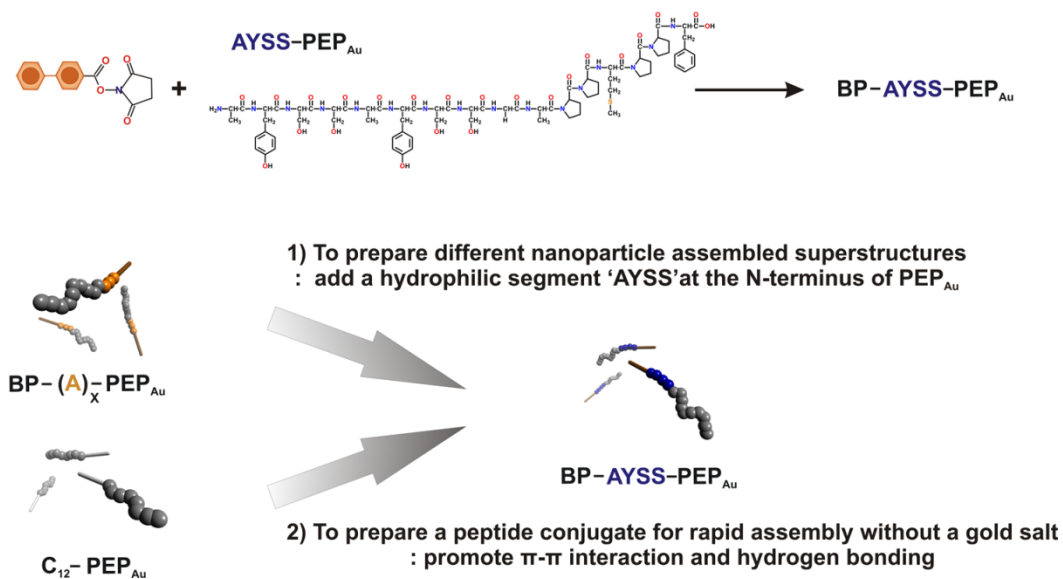
Figure 25. Strategy for preparation of a different peptide conjugate, BP-AYSS-PEP$_{Au}$. There are two purposes to synthesize a BP-AYSS-PEP$_{Au}$ peptide conjugate molecule.

Ensembles of inorganic nanoparticles exhibit unique assembly-dependent physical properties which depend largely on the local order of the nanoparticles.[2,4,21,84,108] To control these properties, short oligopeptides have emerged as promising molecules for directing nanoparticle assembly.[61,109-111] However, many peptide-based assembly methods yield

nanoparticle superstructures with poor local nanoparticle order.[110] We specifically showed that C_{12}-PEP$_{Au}$, a gold-binding peptide[63] (PEP$_{Au}$ = AYSSGAPPMPPF) modified at its N-terminus with an aliphatic 12-carbon chain, could be used to expeditiously prepare 1-D double-helical nanoparticle assemblies in a single preparative step with unprecedented structural complexity and excellent local nanoparticle order.[53]

Several observations from our previous studies using C_{12}-PEP$_{Au}$ serve as important precedent for the studies reported herein. In those studies, 1-D double-helical nanoparticle superstructures were produced upon addition of a gold salt to a solution of C_{12}-PEP$_{Au}$ in HEPES buffer. We found that addition of the gold salt significantly promotes C_{12}-PEP$_{Au}$ self-assembly into nanofibers, while C_{12}-PEP$_{Au}$ conjugates showed very slow assembly ability in HEPES buffer in the absence of the gold salt. This indirectly indicates that dispersed, non-assembled peptide conjugates are required at the initial stages of reaction. Collectively, these observations suggested that nanofiber self-assembly and nanoparticle synthesis are coupled into a simultaneous process. We note that this one-step process is markedly different from typical peptide-based nanoparticle assembly methods which consist of two or more independent preparative steps, including i) peptide self-assembly into a template and ii) either nucleation of nanoparticles or assembly of pre-synthesized nanoparticles onto the template.[61,109-111] We hypothesize that this unique one-step synthetic process is critical for the formation of well-ordered nanoparticle superstructures.

This unique one-step synthetic approach and the integrity and structural complexity of the nanoparticle superstructures it produces prompted us to explore how structural modifications to the peptide conjugate molecule impact the synthesis and assembly process. We reasoned that these studies would provide insight into the mechanism of nanoparticle

assembly and illuminate specific factors which distinguish this methodology from other peptide-based nanostructure assembly methods. In this chapter, we specifically investigate both how the identity of the organic moiety appended to the PEP$_{Au}$ terminus and how amino acid additions to the PEP$_{Au}$ sequence impact the formation of nanoparticle superstructures.

3.2 EXPERIMENTAL SECTION

3.2.1 Materials

All solvents and chemicals were obtained from commercial sources and used without further purification. 0.1M HEPES (4-(2-hydroxyethyl)-piperazineethanesulfonic acid) buffer was made by directly diluting 1.0M HEPES buffer (pH=7.3±0.1; Fisher Scientific) with water (NANOpure, Barnstead Diamond^{TM} System.; 18.2 MΩ). PEP$_{Au}$ (AYSSGAPPMPPF) and AYSS-PEP$_{Au}$ (AYSSAYSSGAPPMPPF) were synthesized and purified by New England Peptide (NEP).

3.2.2 Methods

Reverse-phase high pressure liquid chromatography (HPLC) was performed at ambient temperature with an Agilent 1200 liquid chromatographic system equipped with diode array and multiple wavelength detectors using a Grace Vydac protein C4 column (214TP1010, 1.0 cm × 25 cm). Matrix-assisted laser desorption ionization time-of-flight (MALDI-TOF) mass spectra were obtained on an Applied Biosystem Voyager System 6174 MALDI-TOF mass spectrometer using α-cyano-4-hydroxy cinnamic acid (CHCA) as the matrix. Samples for atomic force microscopy

(AFM) were prepared on freshly peeled MICA substrates that were treated with a 1% solution of 3-aminopropyl trimethoxysilane.[95] Tapping-mode AFM was performed on a Veeco Dimension VSPM. Transmission fourier transform infrared (FT-IR) spectroscopy measurements were recorded on a Nicole Avatar 360 FT-IR spectrometer in the range of $4000 cm^{-1}$ to $500 cm^{-1}$ at about $1 cm^{-1}$ resolution by using smart single bounce horizontal attenuated total reflection (HATR). Transmission electron microscopy (TEM) samples were prepared by pipetting one drop of solution onto a 3-mm-diameter copper grid with carbon film; 2% aqueous phosphotungstic acid was used for negative staining. TEM was conducted on a JEOL 200CX instrument operated at 200kV and images were collected using a Gatan CCD image system. Scanning transmission electron microscopy (STEM) was used in TEM mode. STEM was conducted on a JEOL 2000-FX instrument operated at 200 kV and images were collected using a Gatan CCD camera with digital micrograph software program.

3.2.3   Preparation of peptide conjugates

Either PEP_{Au} (AYSSGAPPMPPF: 1.23 mg, 1.0×10^{-3} mmol) or $AYSS-PEP_{Au}$ (AYSSAYSSGAPPMPPF (1.3 mg, 8.0×10^{-4} mmol) was dissolved in 0.1 ml anhydrous DMF. 0.1M N-hydroxyl-succinimide ester in DMF (60 µl, 1.2×10^{-3} mmol) and 1µl triethylamine were added to the peptide solution. 1day after stirring at room temperature, the reaction mixture was separated by reversed-phase HPLC eluting with a linear gradient of 0.05% formic acid in CH_3CN and 0.1% formic acid in nanopure water (5/95 to 95/5 over 32 min for $BP-PEP_{Au}$ and 5/95 to 95/5 over 35 min for $BP-AYSS-PEP_{Au}$) (**Figure A4**). The concentrations of the peptide conjugates were determined spectrophotometrically in water/acetonitrile (1:1) using a molar

extinction coefficient of tyrosine (1280 $M^{-1}cm^{-1}$) at 280 nm. A sample of the lyophilized product was deposited onto a α-cyano-4-hydroxy cinnamic acid (CHCA) matrix and its mass was determined using MALDI-TOF MS (**Figure A5**).

3.2.4   Preparation of gold nanoparticle superstructures

Lyophilized BP-PEP$_{Au}$ peptide conjugate (7.13×10^{-8} mol) or BP-AYSS-PEP$_{Au}$ peptide conjugate (7.73×10^{-8} mol) was completely dissolved in 0.5 ml of 0.1M HEPES buffer in a plastic vial. This solution was allowed to incubate at room temperature for 30 min (note: for BP-AYSS-PEP$_{Au}$, a second solution was allowed to incubate for 6 d at room temperature). Thereafter, 2 μl of a freshly prepared solution of 0.1M chloroauric acid (HAuCl$_4$) in 1.0 M triethylammonium acetate (TEAA) buffer was added to the peptide conjugate solution. The mixture was vortexed for a few seconds as soon as the HAuCl$_4$ solution was added and then left undisturbed at room temperature.

3.3   RESULTS AND DISCUSSION

We prepared a different peptide conjugate that, unlike C$_{12}$-PEP$_{Au}$, self-assembles rapidly in the absence of gold salt; we expected that such a peptide conjugate would direct nanoparticle assembly via a different mechanism than C$_{12}$-PEP$_{Au}$. First, we studied the self-assembly of BP-PEP$_{Au}$ in HEPES buffer (pH = 7.3). However, neither transmission electron microscopy (TEM) nor tapping-mode atomic force microscopy (AFM) indicated formation of self-assembled BP-PEP$_{Au}$ structures. Our previous studies of C$_{12}$-PEP$_{Au}$ self-assembly[53] suggested that the amino

acids at the N-terminus of PEP$_{Au}$, in particular AYSS,[76] played a key role in directing the assembly of nanofibers. We therefore decided to modify the N-terminus of PEP$_{Au}$ by adding additional amino acids that would promote self-assembly. Accordingly, we prepared BP-AYSS-PEP$_{Au}$ (C$_{12}$H$_9$CO-AYSSAYSSGAPPMPPF).

The peptide conjugates were dissolved completely in 0.1M HEPES buffer (pH 7.3) at room temperature. This was an optimized condition that allowed for the self-assembly of the peptide conjugates. Furthermore, we allowed the BP-AYSS-PEP$_{Au}$ conjugates to incubate for different times (i.e. 2.5-6 days) in HEPES buffer prior to adding gold salt to probe the range of structures which can be assembled using BP-AYSS-PEPAu self-assembled fibers.

FT-IR spectroscopy was used to investigate the peptide secondary structure. Peptide conjugates were suspended in CH$_3$CN. An amide I peak at 1622.73-1636.70 cm^{-1} and an N-H stretching peak at 3272.79 cm^{-1} suggested possible β-sheet formation (**Figure 26**).[58,76] However, the CH$_3$CN used for preparing the FT-IR sample was different from the reaction solvent, aqueous HEPES buffer. To determine if the IR peaks (1636.70 cm^{-1} or 3272.79 cm^{-1}) came from β-sheet structures of the peptide conjugate, we prepared a negatively stained TEM sample suspended in CH$_3$CN, which revealed a fiber formation (**Figure 27**). From the above results, it was concluded that the principle peaks informing the presence of β-sheets came from the fibers assembled using a BP-AYSS-PEP$_{Au}$. Furthermore, the existence of 1622.73-1636.70 cm^{-1} and 1541.37 cm^{-1}, which are representative of an amide I and an amide II stretching band, suggested the formation of parallel β-sheets [112].
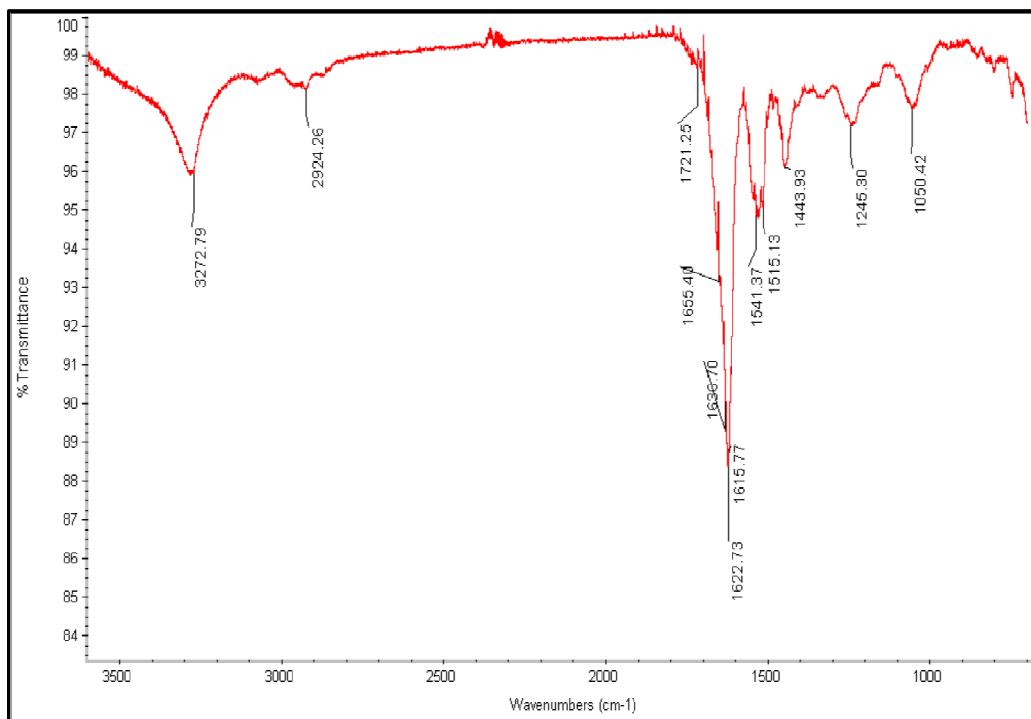
Figure 26. FT-IR spectrum of a thin film of BP-AYSS-PEP$_{Au}$ fibers; the peak at 1721.25 cm^{-1} is representative of the C=O stretching mode for the carboxylic acid at the C-terminus of PEP$_{Au}$. The each peak at 1622.73-1636.70 cm^{-1} and at 3272.79 cm^{-1} is characteristic of an amide I and an N-H stretching band respectively.
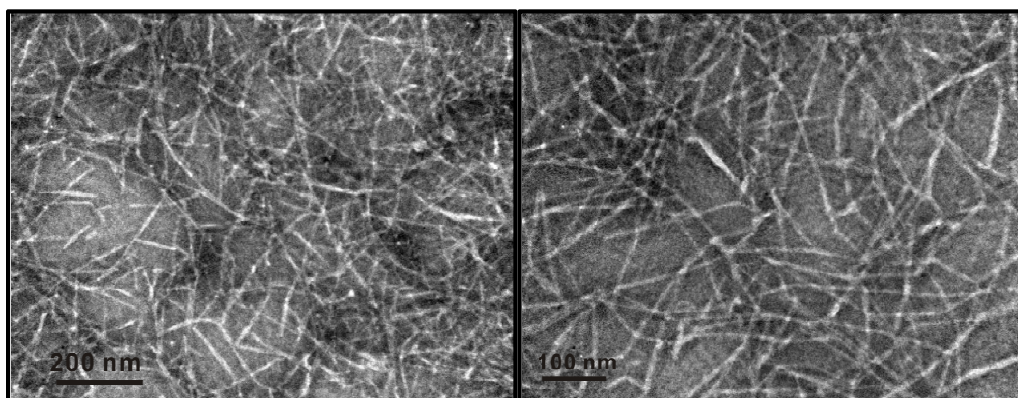
Figure 27. TEM images of assembled fibers by BP-AYSS-PEP$_{Au}$ in CH$_3$CN.

Specifically, AFM was used to determine the time scale for fiber formation. *This process is important to understand, because ultimately the time scale of gold nanoparticle nucleation and peptide conjugate assembly should be similar to enable simultaneous synthesis and assembly.* When BP-AYSS-PEP$_{Au}$ conjugates were incubated in HEPES buffer, the peptide conjugates rapidly self-assembled (within 30 min) to yield short 1-D fibers (**Figure 28a and Figure 29a-b**) with regular width (5.2 ± 0.8 nm; **Figure 31a-b**). AFM imaging was consistent with the results from TEM. However, when the peptide solution was incubated for 6 days in HEPES buffer, BP-AYSS-PEP$_{Au}$ self-assembled longer fibers begin to align and stack together, as revealed in AFM and TEM images (**Figure 28b-d and Figure 29c-f**). BP-AYSS-PEP$_{Au}$ assembles into fibers much more rapidly than C$_{12}$-PEP$_{Au}$. We speculate that the rapid self-assembly of BP-AYSS-PEP$_{Au}$ into fibers precluded dispersion of individual BP-AYSS-PEP$_{Au}$ conjugates in HEPES buffer.
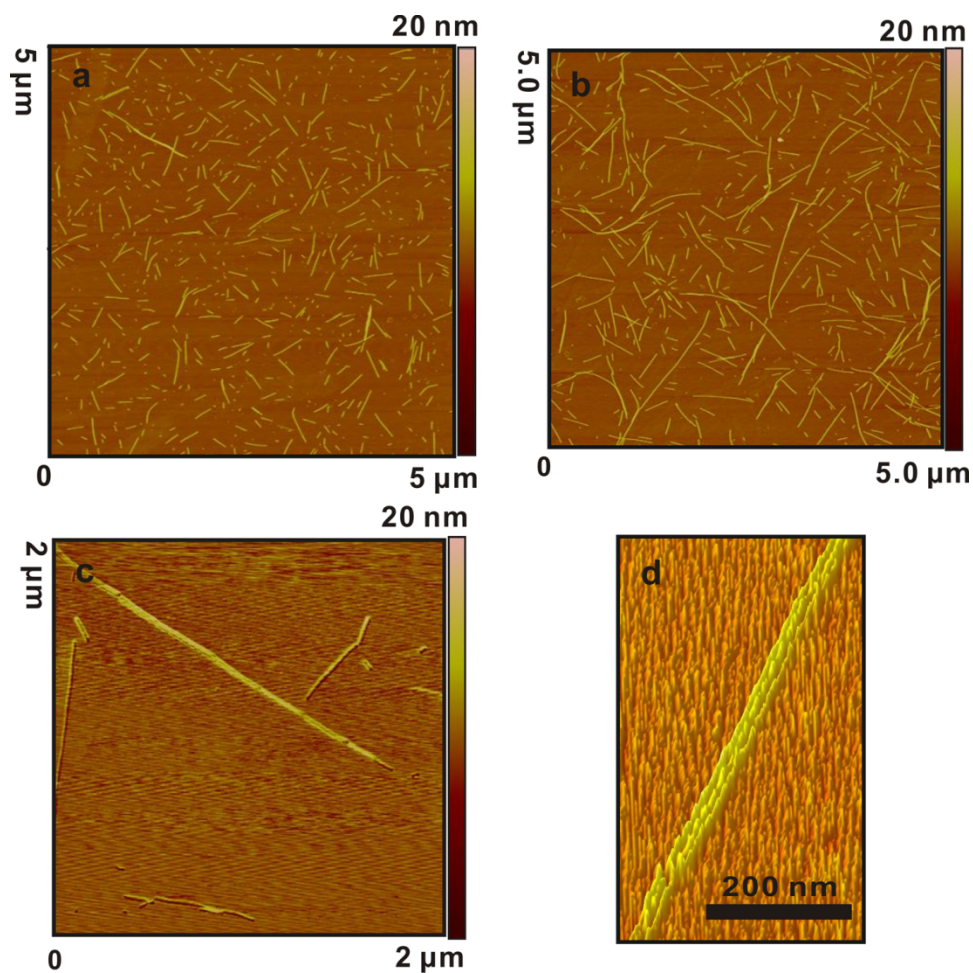
Figure 28. AFM images of fibers by BP-AYSS-PEP$_{Au}$ (7.73×10^{-8} mol) under two different conditions in 0.1M HEPES buffer: (a) 30 min after incubation in HEPES buffer without a gold solution. Thirty minutes after incubation in HEPES buffer, it showed rapid fiber formation; (b), (c) 6 days after incubation in HEPES buffer prior to adding the gold solution; the gold solution; (d) 3-D zoom-in images of a stacked fiber of (c).
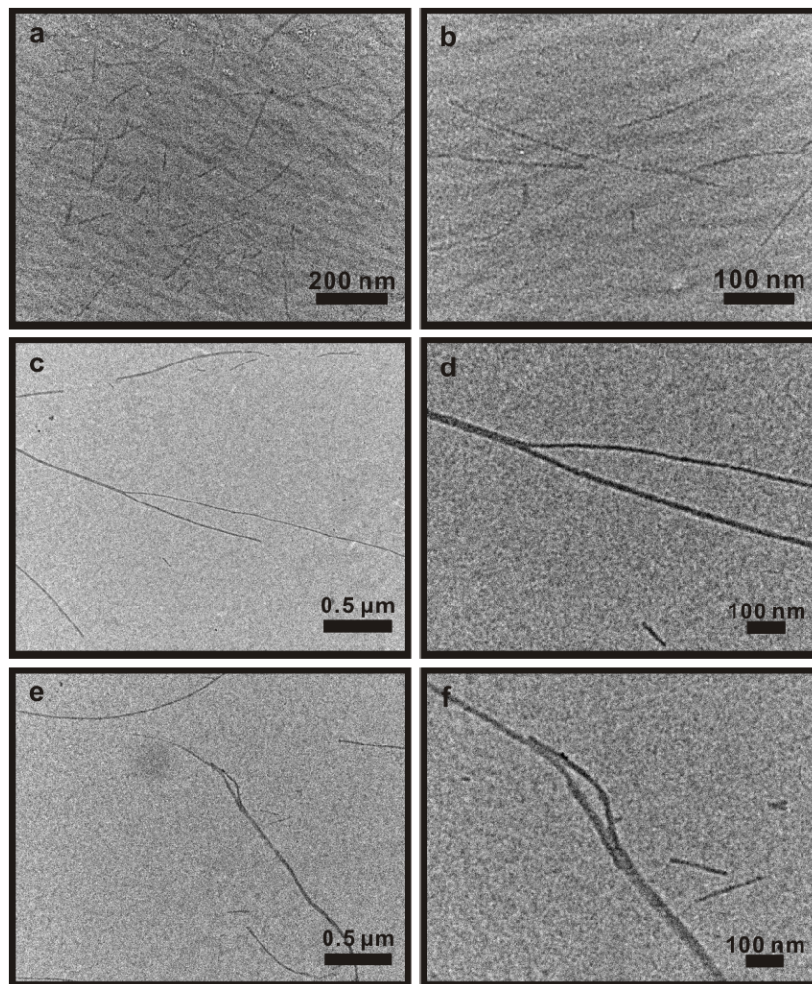
Figure 29. TEM images of BP-AYSS-PEP$_{Au}$ fibers obtained after BP-AYSS-PEP$_{Au}$ conjugates were incubated in 0.1M HEPES buffer (pH 7.3) for 30 min (a-b). STEM images of BP-AYSS-PEP$_{Au}$ fibers obtained after BP-AYSS-PEP$_{Au}$ conjugates were incubated in 0.1M HEPES buffer (pH 7.3) for 6 days (c-f). In all cases, the solution was stained with 2% phosphotungstic acid.

We suspected that gold nanoparticle superstructures prepared using BP-AYSS-PEP$_{Au}$ would form via a two step mechanism (**Figure 30**) similar to that of typical peptide-based nanoparticle assembly methods[61,109-111] rather than the one step synthesis and assembly process observed for C$_{12}$-PEP$_{Au}$.[53] We proceeded to prepare 1-D nanoparticle superstructures to determine whether a two step mechanism for BP-AYSS-PEP$_{Au}$ would impact the structural integrity and precision of organization of the gold nanoparticles. BP-AYSS-PEP$_{Au}$ fibers were incubated in HEPES buffer (30 min), and then gold nanoparticle synthesis was initiated by adding a solution of chloroauric acid (HAuCl$_4$) in TEAA buffer. The resulting mixture was allowed to stand at room temperature (30 min), after which a small sample was removed and characterized using TEM. Moreover, to investigate the scope of nanoparticle superstructures that BP-AYSS-PEP$_{Au}$ self-assembled fibers can produce, BP-AYSS-PEP$_{Au}$ fibers were incubated in HEPES buffer (6 days), and then gold nanoparticle synthesis was initiated by adding a solution of chloroauric acid (HAuCl$_4$).
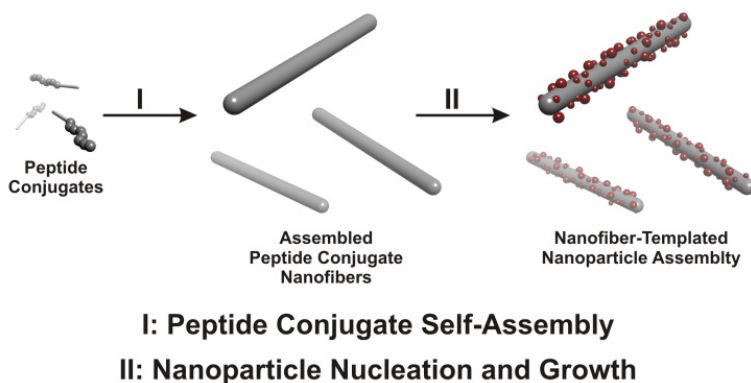
Figure 30. Illustration of nanoparticle assembly process.

Examination of multiple TEM images (**Figure 31**) revealed both 1-D gold nanoparticle superstructures, fibers, and free, non-assembled gold nanoparticles. The width of the superstructures (7.9 ± 0.7 nm, **Figure 31e**) suggests that a single BP-AYSS-PEP$_{Au}$ self-assembled fiber serves as a template for their assembly. While the superstructures possess long-range order, their local nanoparticle order is poor. The structures consist of irregularly positioned nanoparticles ranging in size from ~3 nm to ~13 nm. The structures do not exhibit the same structural regularity, precision of nanoparticle placement, and narrow nanoparticle size distribution exhibited by the nanoparticle superstructures produced using C$_{12}$-PEP$_{Au}$.[53,78] Rather, they more closely resemble structures formed using typical multi-step peptide templating methods.[61] The reaction was also sampled after 24 h, and, again, the structures exhibit excellent long range order yet poor local nanoparticle order (**Figure 32**).
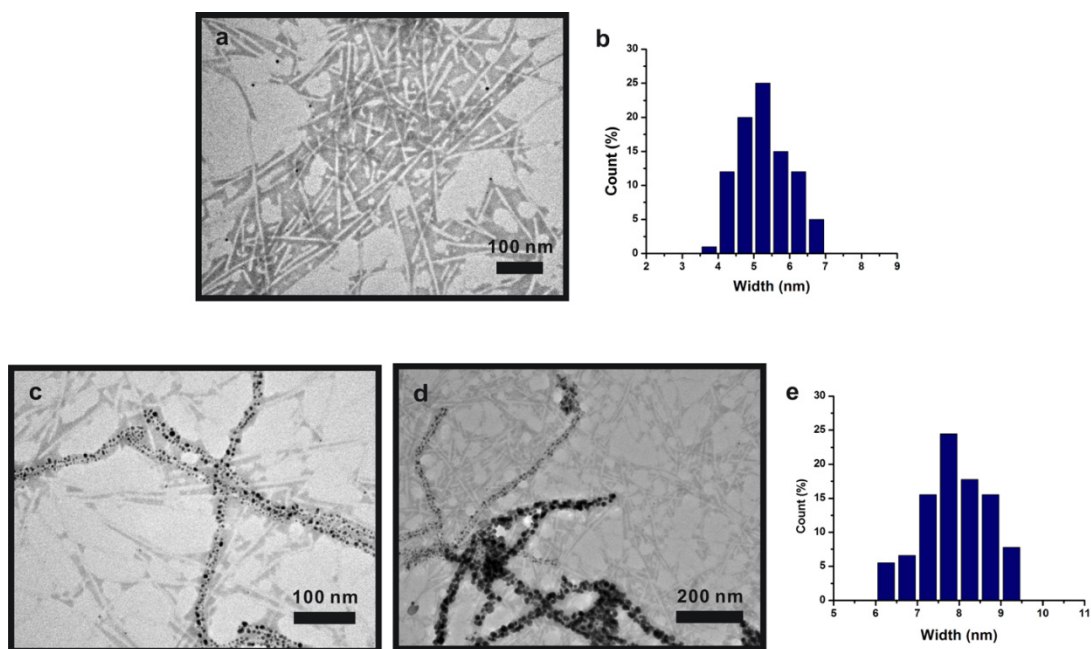
Figure 31. Negative stained TEM images of BP-AYSS-PEP$_{Au}$ fibers and 1-D gold nanoparticle superstructures (a-c) and the width distribution of the BP-AYSS-PEP$_{Au}$ fibers (d) and the gold nanoparticle superstructures (e). The samples used for these images were produced in the following way: 1) BP-AYSS-PEP$_{Au}$ was incubated for 30 min in HEPES buffer and 2) the HAuCl$_4$ solution was added to the BP-AYSS-PEP$_{Au}$ solution and the resulting mixture was allowed to incubate for 30 min. The images show that there is a mixture of fibers decorated with nanoparticles and fibers without any gold nanoparticles assembled onto them. It is clear from images b) and c) that nanoparticles of various sizes are produced. The width of the BP-AYSS-PEP$_{Au}$ fibers is 5.2 ± 0.8 nm, based on 100 counts (d). The width of the gold nanoparticle superstructures is 7.9 ± 0.7 nm, based on 90 counts (e).
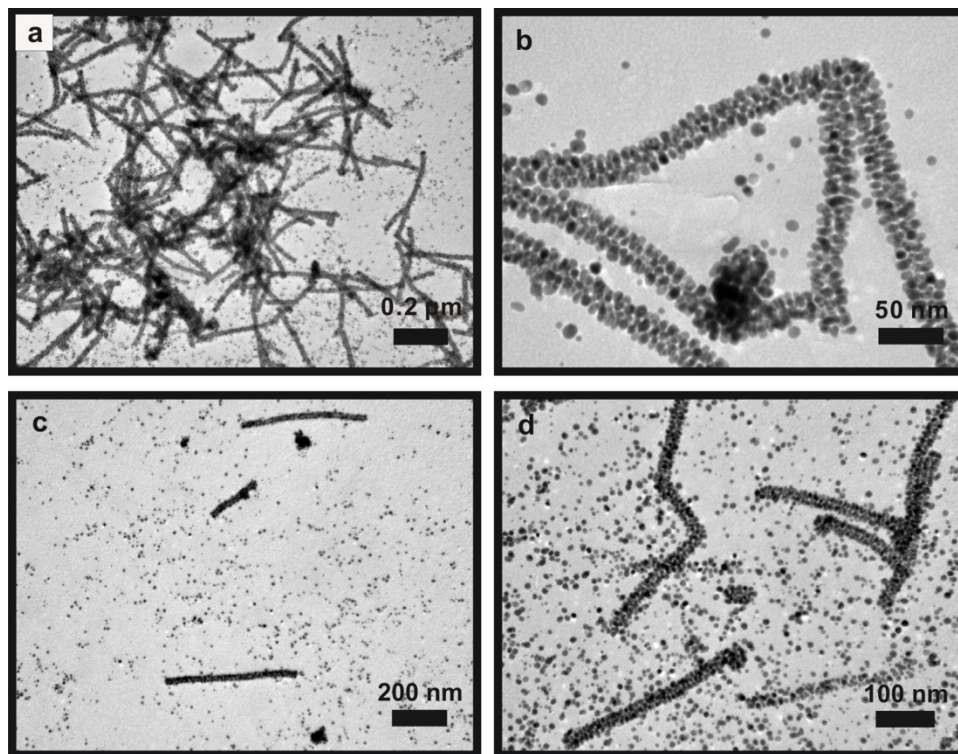
Figure 32. TEM images of 1-D gold nanoparticle superstructures formed by BP-AYSS-PEP$_{Au}$ (a-d) The samples used for these images were produced in the following way: 1) BP-AYSS-PEP$_{Au}$ was incubated for 30 min in HEPES buffer and 2) the HAuCl$_4$ solution was added to the BP-AYSS-PEP$_{Au}$ solution and the resulting mixture was allowed to incubate for 24 hrs. The images show that there is a mixture of short 1-D gold nanoparticle superstructures and free, non-assembled gold nanoparticles.

We allowed BP-AYSS-PEP$_{Au}$ to incubate for 6 days in HEPES buffer prior to adding gold salt to investigate how the stacked fibers formed after a long incubation impact the structure of nanoparticle assemply. When a solution of HAuCl$_4$ was added to this mixture of fibers, we again obseved 1-D gold nanoparticle superstructures, fibers, and free, non-assembled gold nanoparticles (as seen in **Figure 31 and 32**), as revealed in multiple TEM images. When the peptide conjugates long incubated in HEPES buffer, BP-AYSS-PEP$_{Au}$ self-assembled fibers begin to alighn and stack together in either 2 or 3 fiber bundles with width of 9.5 ± 0.8 nm or 15.5 ± 0.2 nm, repectively (**Figure 33**). A distribution of 1-D nanoparticle superstructures formed with widths of either 12.2 ± 0.5 nm or 17.6 ± 0.8 nm, suggesting that they were templated by either the 2 or 3 fiber bundles, respectively (**Figure 34**). The final structure has long fiber and width of 25.2 ± 6.8 nm (**Figure 35**).
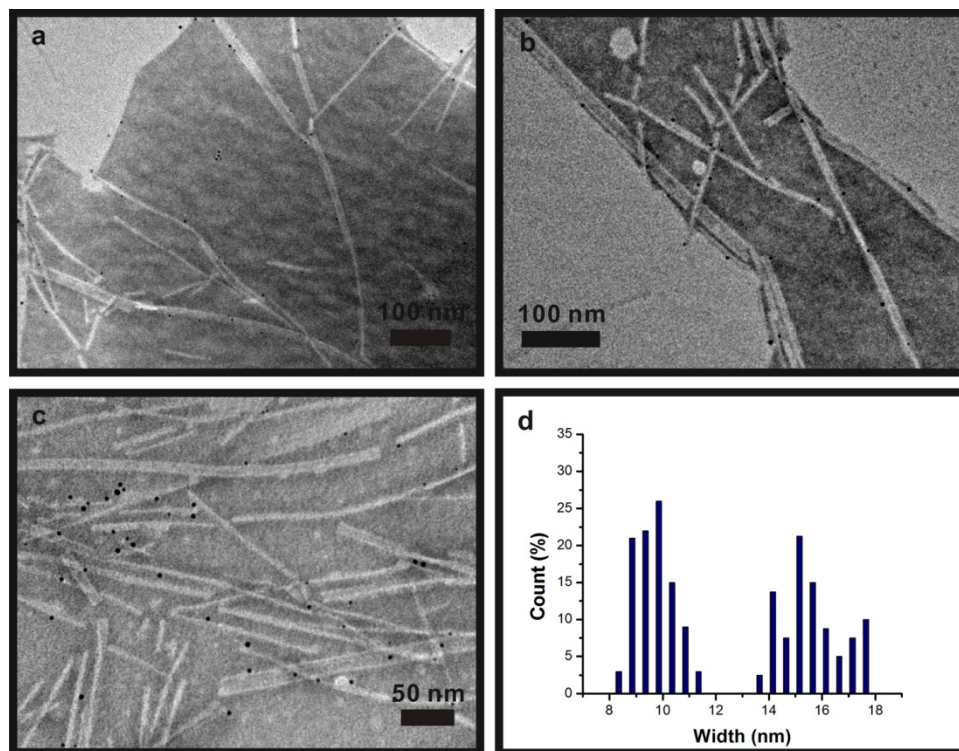
Figure 33. Negative stained TEM images (a-c) BP-AYSS-PEP$_{Au}$ fibers. The samples used for these images were produced in the following way: 1) BP-AYSS-PEP$_{Au}$ was incubated for 6 d in HEPES buffer and 2) the HAuCl$_4$ solution was added to the BP-AYSS-PEP$_{Au}$ solution and the resulting mixture was allowed to incubate for 15 min. The images (a-c) reveal that the fibers begin to stack and align along their longitudinal axes to form bundles of 2-3 fibers. The distribution of the widths of the 2-fiber bundles is 9.5 ± 0.8 nm, based on 100 counts, and the distribution of the widths of the 3-fiber bundles is 15.5 ± 0.2 nm, based on 80 counts (d).
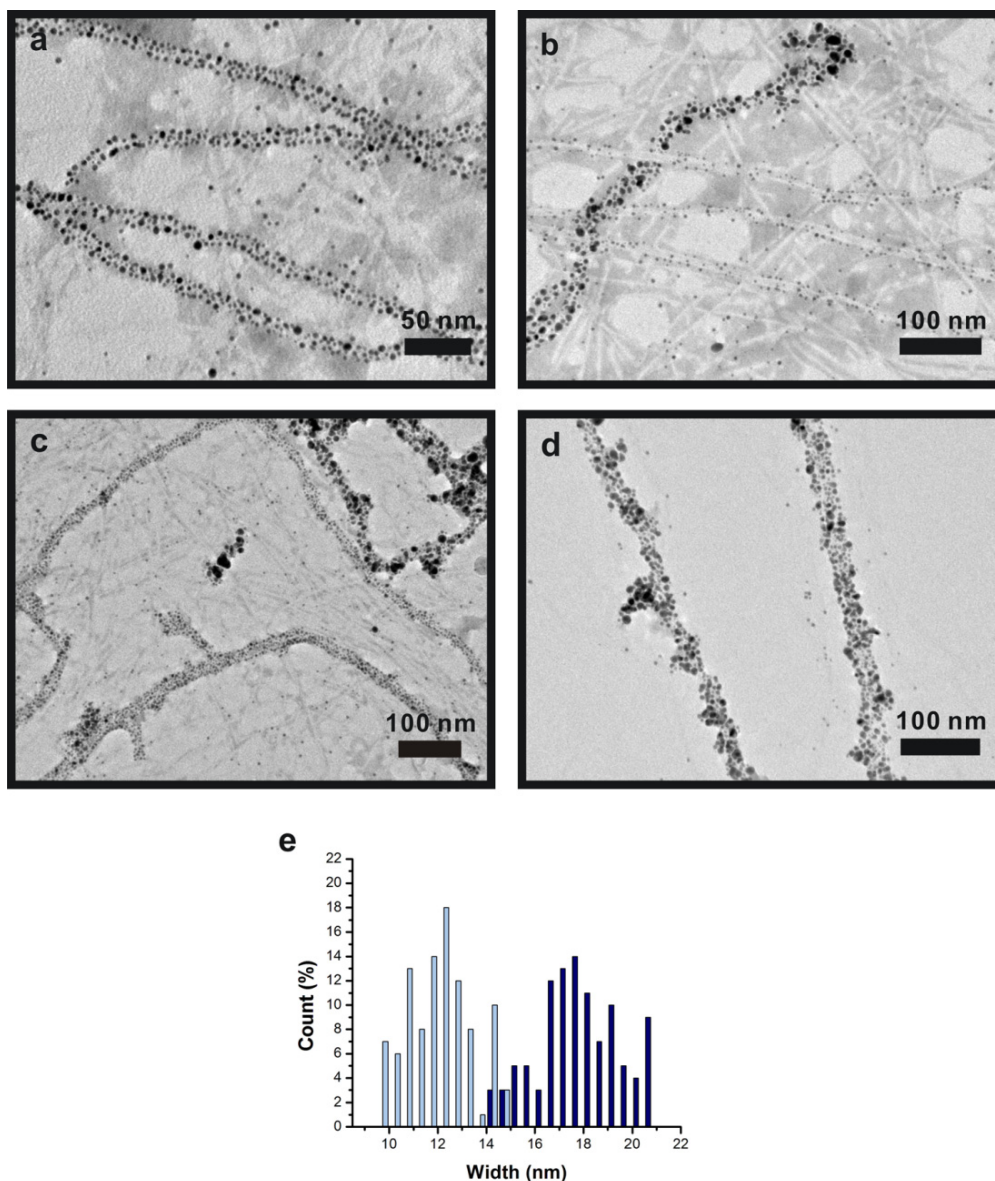
Figure 34. Negative stained TEM images of BP-AYSS-PEP$_{Au}$ fibers and 1-D gold nanoparticle superstructures (a-d) and their width distributions (e). The samples used for these images were produced in the following way: 1) BP-AYSS-PEP$_{Au}$ was incubated for 6 d in HEPES buffer and 2) the HAuCl$_4$ solution was added to the BP-AYSS-PEP$_{Au}$ solution and the resulting mixture was allowed to incubate for 15 min. The images show that there is a mixture of fibers decorated with nanoparticles and fibers without any gold nanoparticles assembled onto them. Because a mixture

of 2- and 3-fiber bundles form under this condition, gold nanoparticle superstructures of different widths are observed. Some structures had widths of 12.2 ± 0.5 nm, based on 100 counts. Other structures had widths of 17.6 ± 0.8 nm, based on 100 counts, which is consistent with templation by the 3-fiber bundles.
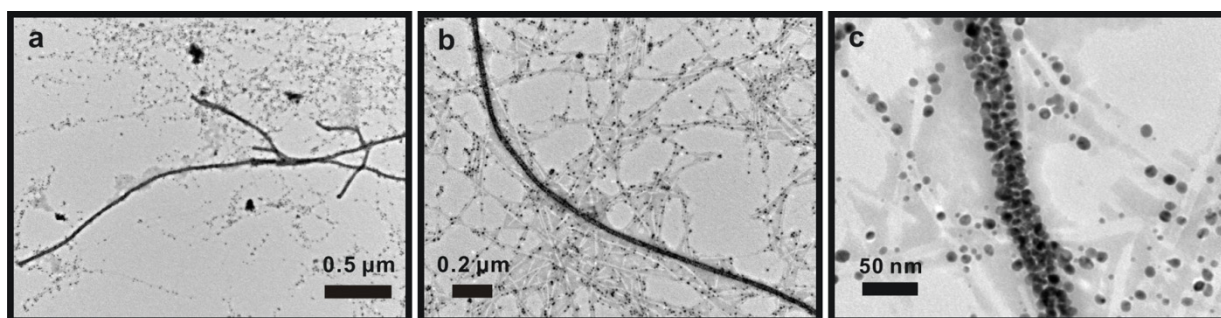
Figure 35. TEM images of BP-AYSS-PEP$_{Au}$ fibers and 1-D gold nanoparticle superstructures (a-c). The samples used for these images were produced in the following way: 1) BP-AYSS-PEP$_{Au}$ was incubated for 6 d in HEPES buffer and 2) the HAuCl$_4$ solution was added to the BP-AYSS-PEP$_{Au}$ solution and the resulting mixture was allowed to incubate for 6 hrs. The images show that thicker and longer assembled nanoparticle superstructures ultimately were produced. They exhibited good long range order, but their short range order was poor. This observation was consistent to one of nanoparticle superstructures using fiber templates that obtained by a short incubation (30min).

3.4   CONCLUSION

Collectively, BP-AYSS-PEP$_{Au}$ first assembles into a template and then nanoparticles either nucleate directly on the template or deposit onto the template from solution to yield 1-D nanoparticle superstructures having tailorable widths of either 7.9 nm, 12.2 nm, or 17.6 nm. These structures exhibit long range order, but limited local order. That is, they did not show the same structural regularity and narrow nanoparticle size distribution exhibited by the nanoparticle double helices superstructures obtained using C$_{12}$-PEP$_{Au}$. These results suggest that nanoparticle assembly directed by BP-AYSS-PEP$_{Au}$ conjugates operates by a different mechanism than C$_{12}$-PEP$_{Au}$. The results from this work suggest that, in order to produce high-quality nanoparticle superstructures using this new methodology, the peptide conjugate should not self-assemble into a template structure prior to the addition of gold salt, as this precludes a one step process in which the nanoparticles and peptide conjugates self-assemble simultaneously.

4.0   INVESTIGATIONS INTO THE MECHANISM OF FORMATION OF

GOLD NANOPARTICLE DOUBLE HELICES

This work was performed in collaboration with Chengyi Song.

4.1   INTRODUCTION

As introduced in Chapter 1, nanoparticles are widely used as functional building blocks to construct complex nanoparticle superstructures.[2-4,113] Assembled nanoparticles architectures exhibit unique ensemble physical properties due to the size, shape, composition and the spatial arrangement of the component nanoparticles within the assembly.[4,21-23,84,91,92] These properties should be controlled by methods that allow precise control of the placement of the nanoparticles or of the interparticle distances within the assembly. In the previous work, we confirmed that our new peptide-based methodology created structurally regular, complex, and multidimensional gold nanoparticle superstructures.[53,61,78-80,114] The methodology relies on peptide conjugate molecules that consist of peptides with sequences of amino acids that recognize and bind specific inorganic nanoparticles[61,63] and organic tethers that are designed to influence the self-assembly of these peptides[77]. Systematic modification of the peptide sequence or the organic tether molecules creates dramatically different nanoparticle superstructures with various shapes and different structural attributes were produced.[79,114] Careful analysis of all of the complex gold nanoparticle superstructures obtained by this new peptide based assembly approach indicated

that: 1) the self-assembly behavior of different peptide conjugates depends on experimental parameters (i.e., pH of buffer or concentration of peptide conjugates); 2) the different peptide conjugates assemble into different structures with a specific morphology; and then 3) the morphology of the assembly determines the shape of the complex gold nanoparticle superstructures. Understanding the mechanism underlying assembly of gold nanoparticles will allow us to more carefully design peptide conjugate molecules for use as building blocks and to systematically adjust particular experimental parameters. This understanding will also allow the creation of new complex nanoparticle superstructures with different structures and properties.

Among the nanoparticle superstructures that we have made, the double-helical superstructures formed by C_{12}-PEP$_{Au}$ conjugates[53] are the most unique and most structurally-regular and ordered. The gold nanoparticle double helices are left-handed twisted materials with lengths into the micrometer range. They also have an excellent local order (i.e., uniform nanoparticle size and consistent interparticle distance). The straightforward preparation of 1-D chiral nanomaterials is promising for potential applications in plasmonics and sensing. [21,22,115-118]

This chapter describes work toward understanding the fundamental mechanism by which the peptide conjugates direct the synthesis and assembly of gold nanoparticles into well-ordered double-helical superstructures. We report two important features that distinguish our peptide based methodology from typical peptide based template approaches. We show that (1) small gold nanoparticles and (2) well-dispersed peptide conjugates must be present at the outset of the reaction in order to obtain well-ordered gold nanoparticle double helices. We also present details of the postulated mechanism underlying the formation of the double helices.

4.2 EXPERIMENTAL SECTION

4.2.1 Materials

All solvents and chemicals were obtained from commercial sources and used without further purification. 0.1 M HEPES (4-(2-hydroxyethyl)-piperazineethanesulfonic acid) buffer was made with HEPES (free acid) powder (pH = 7.3 ± 0.1, pH was adjusted with NaOH; Promega) with water (NANOpure, Barnstead Diamond^{TM} System.; 18.2 MΩ). All peptides were synthesized and purified by New England Peptide (NEP).

4.2.2 Instruments

Reverse-phase high pressure liquid chromatography (HPLC) was performed at ambient temperature with an Agilent 1200 liquid chromatographic system equipped with diode array and multiple wavelength detectors using a Grace Vydac protein C4 column (214TP1010, 1.0 cm × 25 cm). Matrix-assisted laser desorption ionization time-of-flight (MALDI-TOF) mass spectra were obtained on an Applied Biosystem Voyager System 6174 MALDI-TOF mass spectrometer using an α-cyano-4-hydroxy cinnamic acid (CHCA). Transmission electron microscopy (TEM) samples were prepared by pipetting one drop of solution onto a 3-mm-diameter copper grid with carbon film; 2% aqueous phosphotungstic acid. TEM was conducted on a JEOL 200CX instrument operated at 200kV and images were collected using a Gatan CCD image system. . Samples for atomic force microscopy (AFM) were prepared on freshly peeled MICA substrates that were treated with a 1% solution of 3-aminopropyl trimethoxysilane.[95] Tapping-mode AFM

was performed on an Asylum MFP-3D. Peptide powders were mounted on a Bruker X8

Prospector Ultra diffractometer equipped with a Cu IMuS microfocus source (λ = 1.54184 Å)

operated at 45 kV, 0.65ma). The X-ray intensities were measured at 298K; the detector was

placed at a distance of 4 cm from the sample. A 360° Phi scan was collected for 60 seconds. The

Brulter Program XRD^2 Eval was used to integrate the powder pattern.

4.2.3   Preparation of peptide conjugates and gold nanoparticle superstructures

C_{12}-PEP$_{Au}$ peptide conjugate was synthesized, purified, and characterized using a previously

reported protocol (**Figure A6** and **Figure A7**).[53] Lyophilized C_{12}-PEP$_{Au}$ (~ 3.75×10^{-8} mol)

peptide conjugate was completely dissolved in 0.1M HEPES buffer (0.25 ml; pH=7.3±0.1) in a

plastic vial. This solution was allowed to incubate at room temperature (30 min). Thereafter, a

solution of 0.1M chloroauric acid (HAuCl$_4$) in 1.0 M triethylammonium acetate (TEAA; pH =

7.0) buffer was incubated for 10min at room temperature and followed by a centrifugation at 5k

rpm. 2 µl of the supernatant was added to the peptide conjugate solution. The resulting mixture

was vortexed for a few seconds as soon as the HAuCl$_4$ solution was added and then left

undisturbed at room temperature (2 h).

4.3   RESULTS AND DISCUSSION

4.3.1   Structure characterization of C_{12}-PEP_{Au} assembly prior to adding a gold salt

In the previous work, the structure of C_{12}-PEP_{Au} assembly was investigated using AFM images. The individual fibers formed by C_{12}-PEP_{Au} showed left-handed twisted ribbon structures in a left-handed direction with pitches of 84.1 ± 4.2 nm, as revealed in AFM analysis.[53] Moreover, Circular dichroism (CD) and Fourier transform infrared (FT-IR) spectroscopy suggested the existence of β-sheet structures.[53] We further probed the presence of hydrogen bonding to form the β-sheet structures and of stacks between the β-sheets by examining X-ray diffraction (XRD) of the C_{12}-PEP_{Au} assembly. A sample for the XRD study was prepared using a vapor hydration method.[119] XRD analysis of two samples revealed that fibers formed by C_{12}-PEP_{Au} peptide conjugates contained β-sheets due to the observed unique hydrogen bonding distance (~4.6 Å). Moreover, this analysis revealed that multiple β-sheet networks were stacked; the stacking distance was found to be (~9.5 Å) (**Figure 36**).[120-123] Based on AFM analysis of the fibers formed by C_{12}-PEP_{Au}[53], we were able to estimate the number of stacked β-sheets. The analysis revealed that the height of the fibers was ~ 6 nm and the height at the twisted point was ~4.7 nm (**Figure 37a**). Therefore, the estimated number of stacked β-sheets was four (~40 Å / 9.5 Å = ~4.2). This indicated that the C_{12}-PEP_{Au} fibers consisted of β-sheets and four fibers were expected to be stacked together (**Figure 37b**). The first amino acids 'AYSS' have a strong tendency to form a β-sheet[76], whereas the C-terminus, which is proline-rich, is not expected to form β-sheets. We further note that the C-terminus is somewhat sterically bulky.[53] The twisted

ribbon structure formed by C_{12}-PEP$_{Au}$ units serves as the underlying structure-directing entity for the double-helical nanoparticle superstructures.
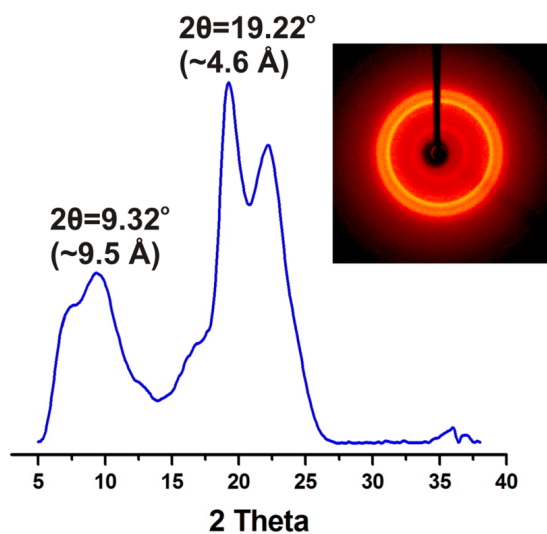
Figure 36. XRD analysis of C_{12}-PEP$_{Au}$ assembly (Note: the XRD was taken by Tao Li in Rosi group).

We confirmed that the sample used for the XRD study contained the fibers formed by C_{12}-PEP$_{Au}$ by examining them by TEM. The TEM images revealed that the peptide conjugates in water and acetonitrile assembled into fibers with the same widths that were observed in the previous report (**Figure A8**).
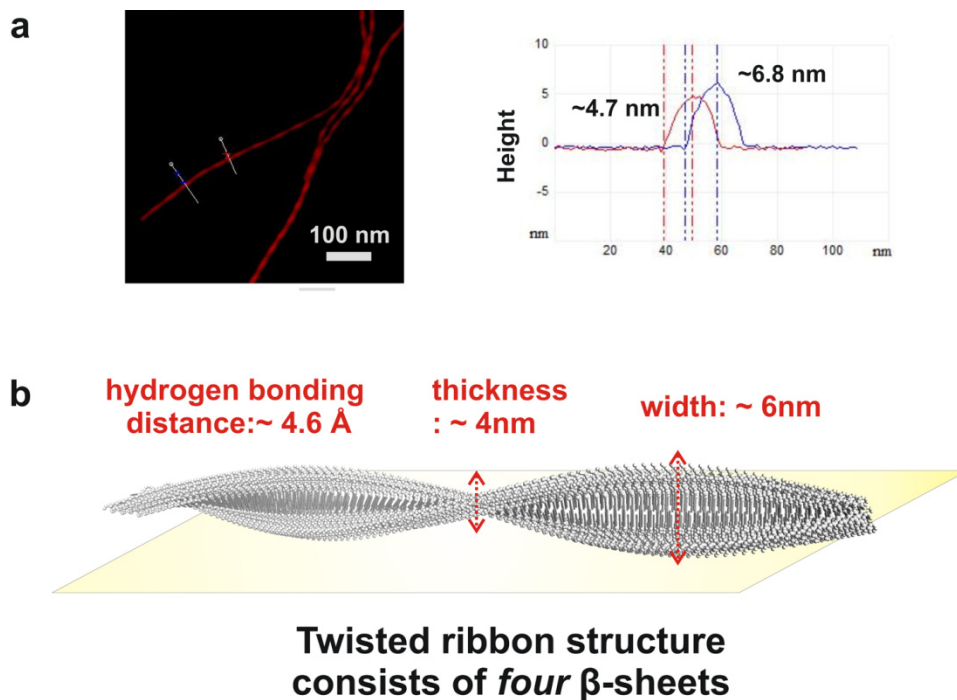
Figure 37. (a) AFM height analysis (Adapted from ref. 53); (b) schematic description of formation of C_{12}-PEP_{Au} twisted ribbon structure consists of β-sheets.

4.3.2   Self-assembly behavior of C_{12}-PEP_{Au} in HEPES buffer

The C_{12}-PEP_{Au} conjugates assemble very slowly into fibers in HEPES buffer. When the peptide conjugates were dissolved in this buffer prior to adding a gold salt, it took ~2 weeks to form a bundle of fibers with a width 6.9 ± 1.0 nm (**Figure 38**). As mentioned in Chapter 2 and 3, the overall charge of our peptide conjugates is slightly negative because the pI is 5.57 in HEPES (pH7) buffer.[105] We expected that the overall negatively charged peptide conjugates would result in electronic repulsion, which could prevent conjugate assembly. This is why the peptide

conjugates prefer being more dispersed than being assembled into fibers (**Figure 39a**). It is

important to note that the addition of a gold salt to the peptide solution significantly promoted

C_{12}-PEP$_{Au}$ assembly. We reasoned that the gold cations can shield (or created a charge balance to)

the negative charge of the peptide conjugates (**Figure 39b**).[106,124] Therefore, when the charges on

the C-termini are shielded, the peptides could aggregate, and then the hydrophobic interaction

between the C_{12} aliphatic tails would be a major driving force for their assembly (**Figure 39c**).[125]
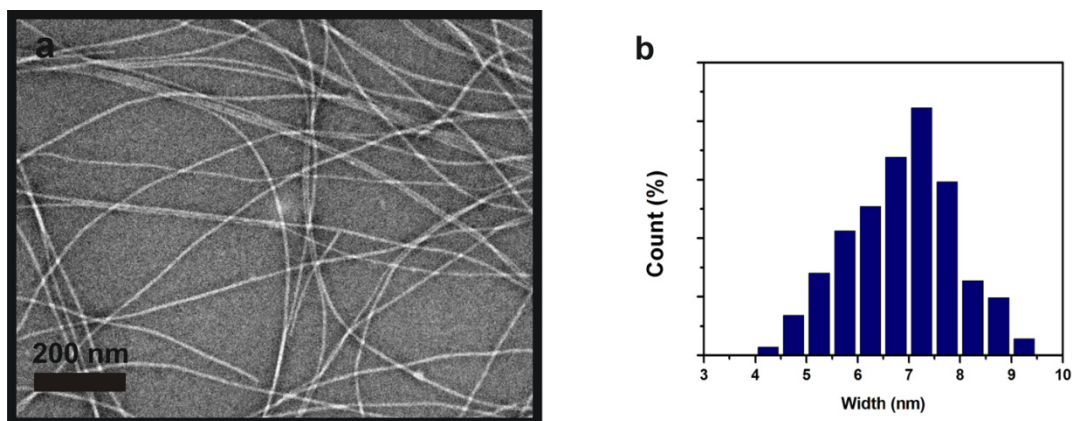
Figure 38. (a) TEM imaged of assembly of C_{12}-PEP$_{Au}$ after incubating in HEPES buffer for 2

weeks prior to adding the gold source; (b) a width distribution of 6.9 ± 1.0 nm (based on 142

counts)
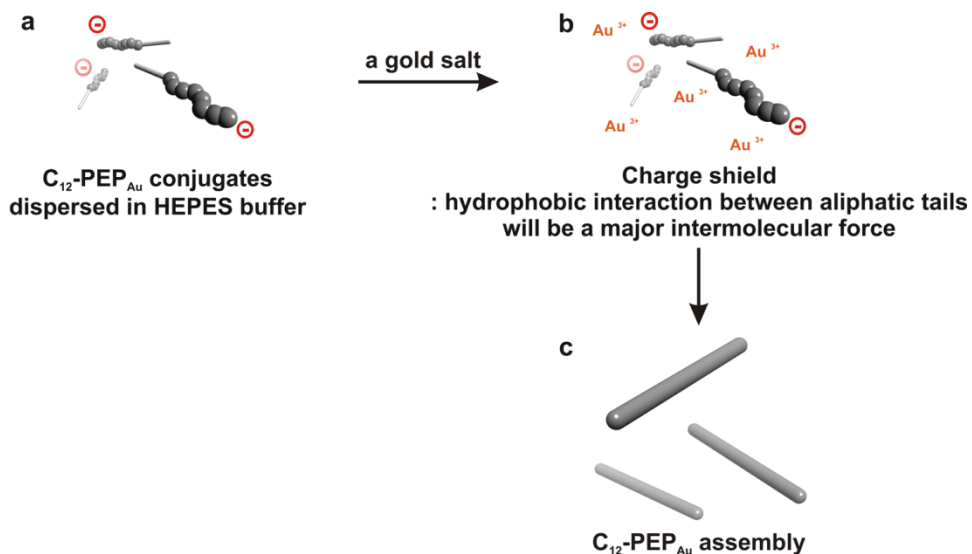
Figure 39. Schematic illustration of how to assemble rapidly into fibers in the existence of a gold salt (a) dispersed C_{12}-PEP_{Au} in the absence of the gold salt; (b) charge shielded in the presence of the gold salt; (c) assembled into fibers due to hydrophobic interaction between aliphatic tails.

4.3.3   Characteristics of gold nanoparticle double helices assembly

When an aliquot of a $HAuCl_4$/TEAA (aq.) solution is added to the HEPES solution of C_{12}-PEP_{Au} , two products result: complete gold nanoparticle double helices and assembled C_{12}-PEP_{Au} fibers (**Figure 40**). We call this a bimodal distribution of 'naked fibers' and complete double helices of gold nanoparticles (5.42 ± 0.6 nm) (**Figure 40d-e**). We also examined the reaction at an early stage of structure formation. 30min after incubation at room temperature, an

aliquot of the reaction mixture was examined by TEM. The TEM images revealed the same bimodal distribution consisting of naked fibers and 1-D nanoparticle assemblies in which gold particles with a size of 2.66 ± 0.4 nm were organized, even though several defects in the double helices structure were observed (**Figure 40b-c**).

It is important to note that the 'bimodal distribution' that results differs from the product distribution yielded by a typical peptide template approach to assembly. In typical peptide based nanoparticle assembly methods, two (or more) preparative steps are required: 1) peptide assembly into a template and (2) nucleation of nanoparticles[110] or assembly of pre-synthesized nanoparticles onto the template[109,111]. These multiple steps lead to common products consisting of the template, nanoparticle assembled superstructures, and free, non-assembled nanoparticles. In these typical template-based approaches, all of the templates should bind to nanoparticles, and one should not expect to observe a bimodal distribution of naked templates and fully-decorated templates.
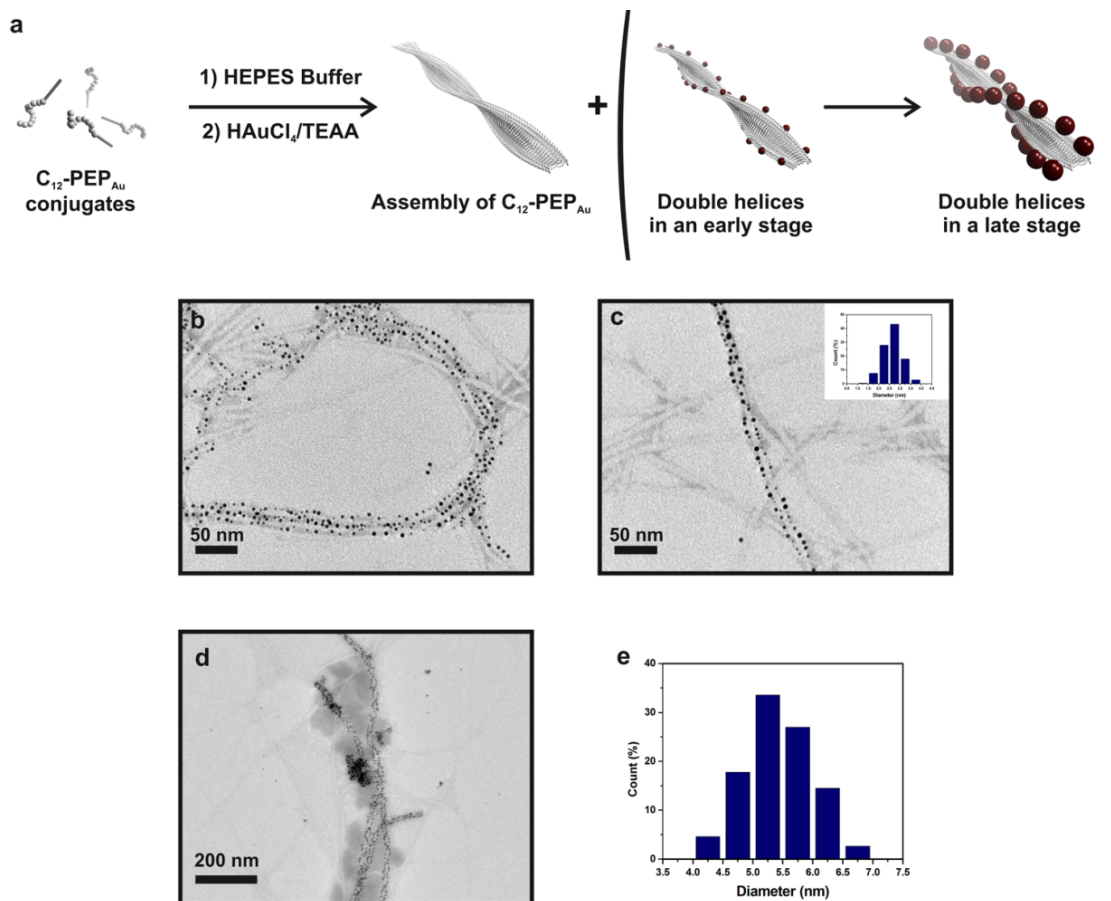
Figure 40. (a) Schematic depiction of bimodal distribution that C_{12}-PEP$_{Au}$ conjugate produce

naked fibers and 1-D double helices nanoparticle superstructures in the presence of

HAuCl$_4$/TEAA (aq.) solution (Note: schematic figures were adapted from Chengyi Song's work);

(b) and (c) TEM images of double helices formed in an early stage with a size distribution of the

comprising gold nanoparticles, 2.66 ± 0.4 nm (based on 210 counts); (d) TEM images of gold

nanoparticle double helices in a final stage; (e) a size distribution of the comprising gold

nanoparticles of the double helices, 5.42 ± 0.6 nm (based on 152 counts)

4.3.4   Comparison between two gold sources: HAuCl$_4$/H$_2$O vs. HAuCl$_4$/TEAA

In our syntheses, we use a HAuCl$_4$/TEAA (aq.) solution as a gold precursor. This differs from the HAuCl$_4$/H$_2$O (aq.) solution that is commonly used in other nanoparticle assembly methods. We decided to study whether the identity of the gold precursor played a key role in our synthesis. We started by testing the two different gold precursors, HAuCl$_4$/H$_2$O (aq.) and HAuCl$_4$/TEAA (aq.), with C$_{12}$-PEP$_{Au}$ conjugates dissolved in HEPES buffer in order to investigate whether both reactions yield well-organized gold nanoparticle double helices. HAuCl$_4$/H$_2$O (aq.) and HAuCl$_4$/TEAA (aq.) were introduced into two different sets of C$_{12}$-PEP$_{Au}$ conjugates dissolved in HEPES solution. Interestingly, the reaction with HAuCl$_4$/TEAA (aq.) produced highly ordered gold nanoparticle double helices (as seen in **Figure 40**), while the reaction with HAuCl$_4$/H$_2$O (aq.) only produced naked fibers and free nanoparticles (**Figure 41**).

These results prompted us to examine whether the two different gold solutions influenced the formation of monodisperse gold nanoparticles in the presence of PEP$_{Au}$ dissolved in HEPES buffer. We measured a UV-Vis spectrum of two PEP$_{Au}$ solutions 30 min after adding the gold solution to each vial. Both solutions showed λ_{max} at ~520 nm (**Figure 42e**). We also examined TEM images after measuring the UV-Vis spectrum and the TEM images showed that the gold nanoparticles formed from the two different sources were spherical and had a size of ~4 nm (**Figure 42a-d**). Therefore, even though HAuCl$_4$/H$_2$O and HAuCl$_4$/TEAA solution produced gold nanoparticles in the presence of PEP$_{Au}$, only HAuCl$_4$/TEAA (aq.) solution formed gold nanoparticle double helices in the presence of C$_{12}$-PEP$_{Au}$.
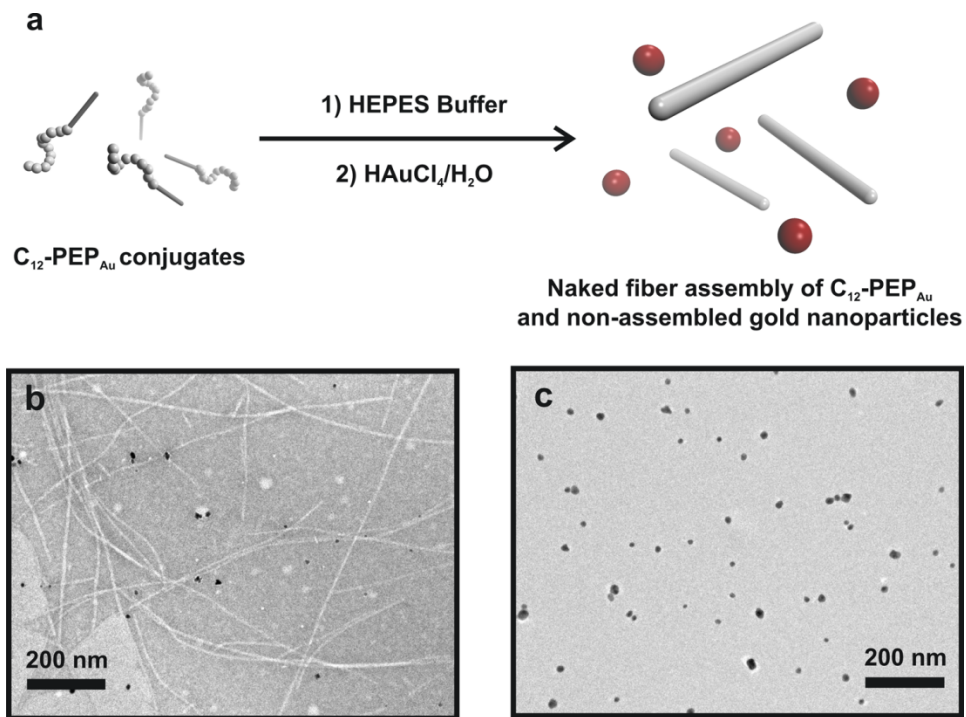
Figure 41. (a) Schematic depiction of bimodal distribution that C_{12}-PEP$_{Au}$ conjugates produce naked fibers and free nanoparticles in the presence of HAuCl$_4$/H$_2$O (aq.) solution; (b) negatively stained TEM image of fibers formed 30 min after adding the gold salt; (c) TEM image of free nanoparticles obtained 1 day after adding the gold salt.
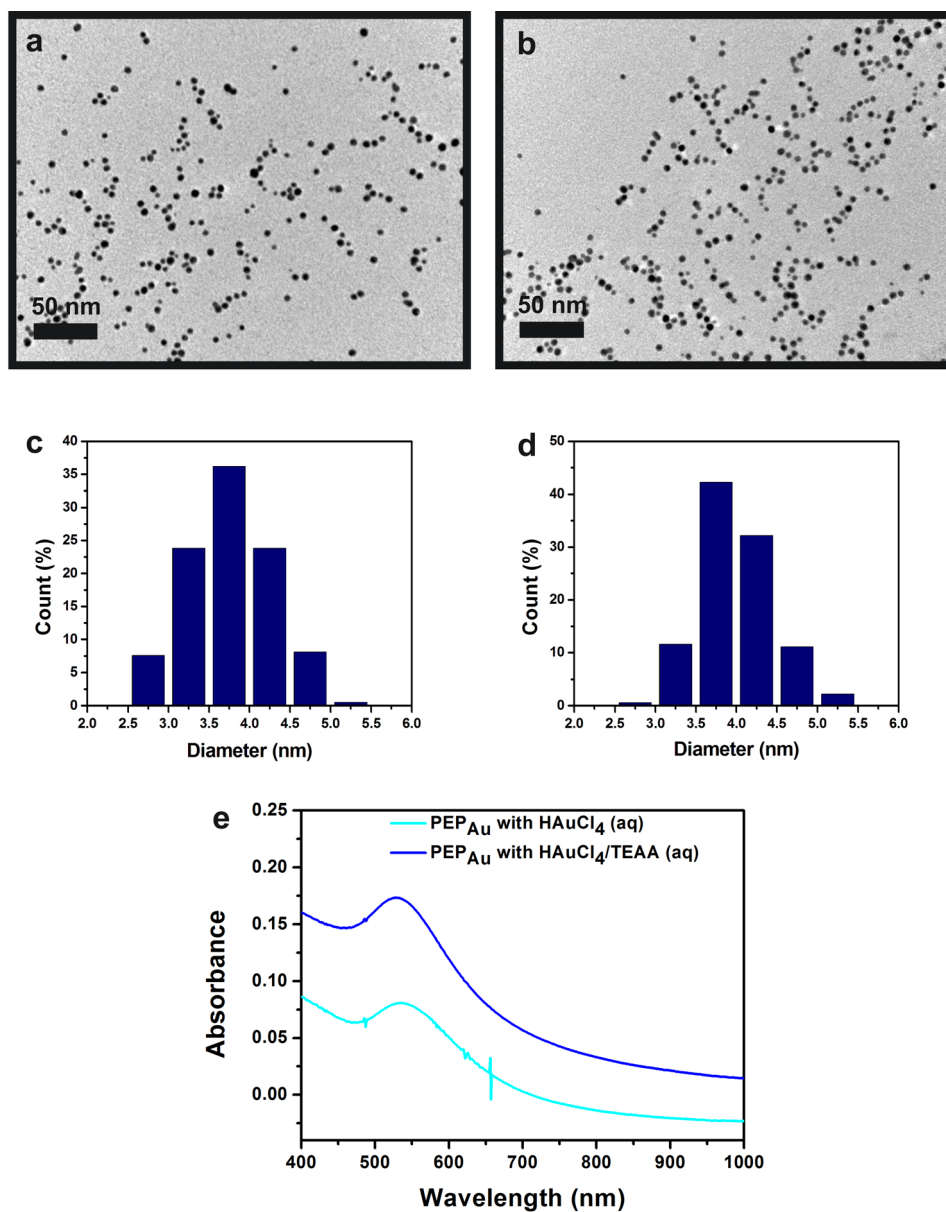
Figure 42. TEM images of PEP$_{Au}$-stabilized gold nanoparticles using (a) HAuCl$_4$/H$_2$O (aq.) and (b) HAuCl$_4$/TEAA (aq.); size distribution of gold nanoparticles (c) prepared by HAuCl$_4$/H$_2$O with a size of 3.75 ± 0.57 nm (based on 185 counts) and (d) HAuCl$_4$/TEAA (aq.) with a size of 3.93 ± 0.42 nm (based on 180 counts); (e) UV-Vis absorbance of the PEP$_{Au}$-stabilized gold nanoparticles prepared by HAuCl$_4$/H$_2$O (aq.) and HAuCl$_4$/TEAA (aq.)

4.3.5   Role of HAuCl$_4$/TEAA

According to these results, we reasoned that HAuCl$_4$/TEAA (aq.) was an important component

that leads to double helix formation. The TEAA buffer is in an equilibrium state between

triethylammonium acetate and triethylamine and acetic acid. It is known that TEA can reduce

gold cations to metallic gold.[126] Therefore, it was not surprising to observe gold nanoparticles in

the HAuCl$_4$/TEAA (aq.) solution (**Figure 43a**). The gold nanoparticles in the solution are small

with a size 3.0 ± 0.46 nm (**Figure 43b–c**); there are also some large gold nanoparticles (**Figure**

44a–c). These results indicate that the HAuCl$_4$/TEAA (aq.) solution contained small gold

nanoparticles and gold cations (Au^{3+}). AFM analysis was also performed to further confirm

whether TEAA forms small gold nanoparticles. Based on the height (2.0 ± 0.22 nm), AFM

images revealed that TEAA produced small gold nanoparticles in the presence of HAuCl$_4$

(**Figure 45**).
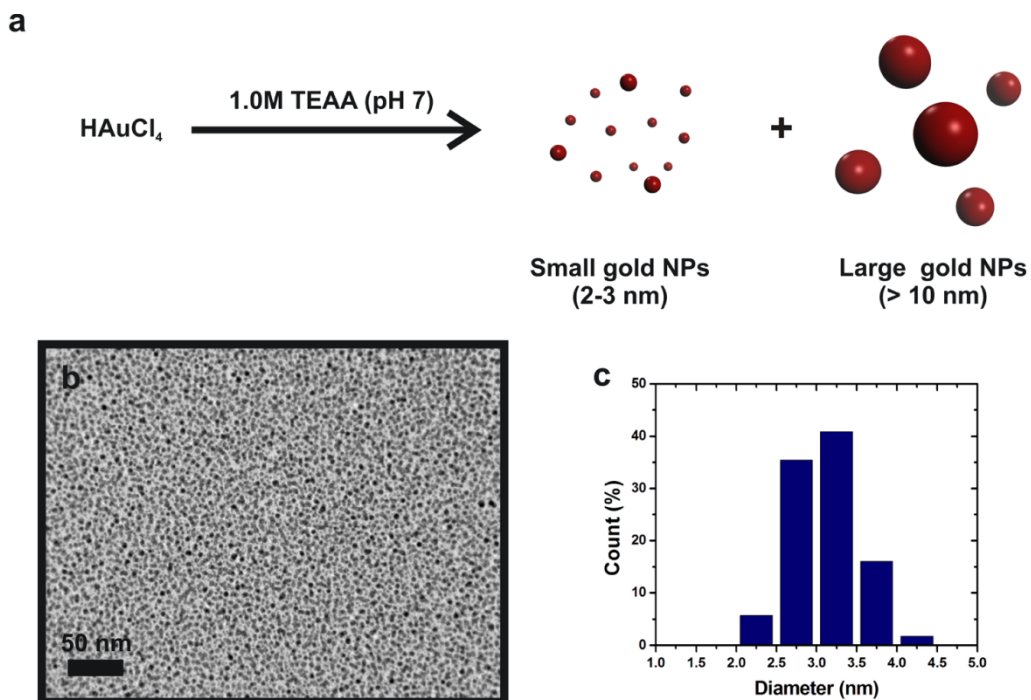
Figure 43. HAuCl$_4$/TEAA (aq.) produces small gold nanoparticles (2-3 nm) and large gold nanoparticles (see **Figure 44**). (a) schematic illustration of the formation of gold nanoparticles and large gold nanoparticles that HAuCl$_4$/TEAA (aq.) solution produced (a); TEM images of the small gold nanoparticles obtained from HAuCl$_4$/TEAA (aq.) (b); the size distribution of the gold nanoparticles show consistent size distribution of 3.0 ± 0.46 nm (based on 350 counts)
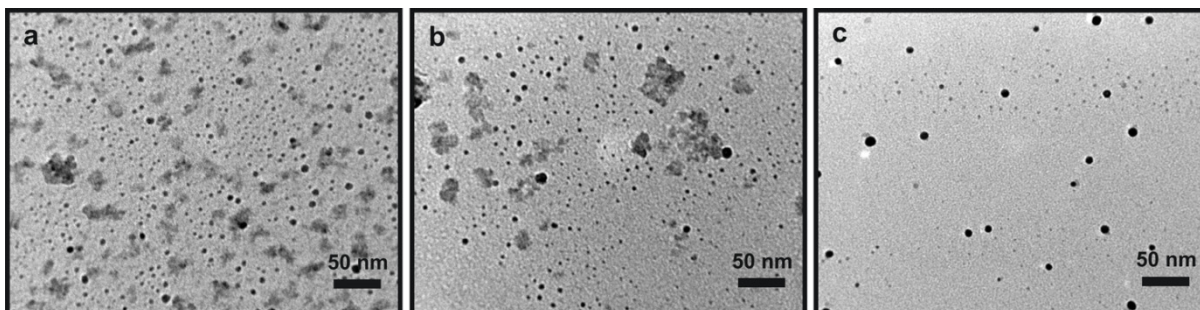
Figure 44. (a–c) additional TEM image of gold nanoparticles produced by $HAuCl_4$/TEAA solution; the $HAuCl_4$/TEAA (aq.) solution was centrifuged at 5k rpm 10min after incubating the gold solution at room temperature, and then an aliquot of the solution was examined by TEM. Three TEM images were obtained by using different fresh gold solutions.
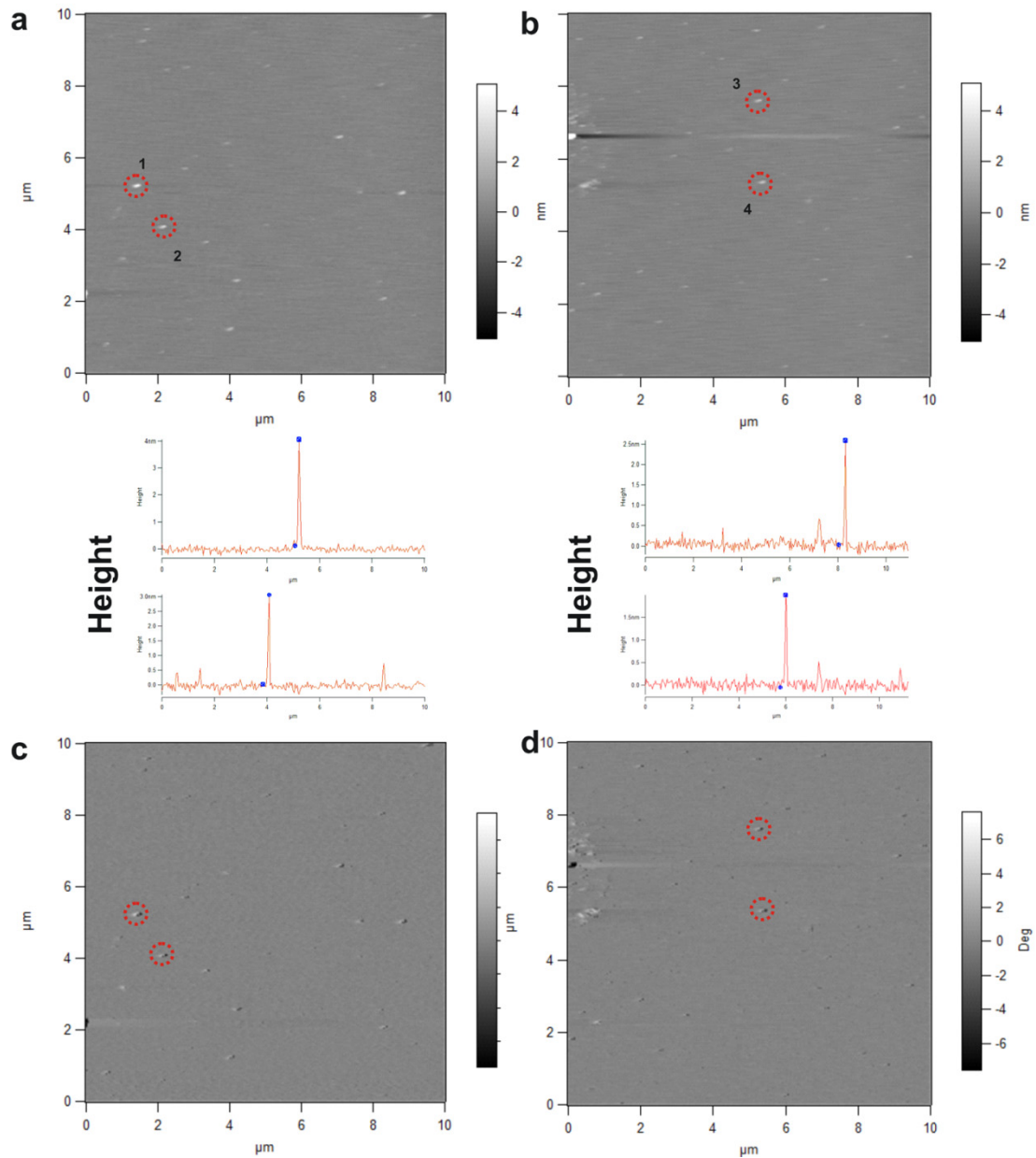
Figure 45. AFM height (a and b), phase (c and d) of gold nanoparticles formed by

HAuCl$_4$/TEAA (aq.) solution. It exhibits height distribution of gold nanoparticles (height = 2.0 ±

0.22 nm; based on 15 counts from AFM images). Height of number 1–4 was marked here as

representatives (height of 1, 2, 3, and 4 = 3.93 nm, 3.05 nm, 2.56 nm, and 2.03 nm)

Inorganic metal binding peptides can bind to the surface [111] of spherical gold nanoparticles with a certain range of diameters.[81-83] Based on our observation that HAuCl$_4$/TEAA (aq.) contains small gold nanoparticles, we speculate that C$_{12}$-PEP$_{Au}$ peptide conjugates could bind to these small gold particles and thereafter direct their assembly into 1-D gold nanoparticle double helices.

4.3.6   Role of C$_{12}$-PEP$_{Au}$ monomers

We previously found that the addition of a gold salt significantly promoted assembly of C$_{12}$-PEP$_{Au}$ conjugates into fibers (as seen in **Figure 41**). Therefore, we expected that dispersed C$_{12}$-PEP$_{Au}$ peptide conjugates in HEPES solution would assemble into fibers when we added a gold salt. The C$_{12}$-PEP$_{Au}$ conjugates can assemble into fibers following addition of the gold salt and also can be consumed as a capping agent[63] when gold nanoparticles form. We hypothesized that many of the C$_{12}$-PEP$_{Au}$ monomers would take part in the formation of either fibers or gold nanoparticles upon addition of an aliquot of HAuCl$_4$/H$_2$O (aq.). This would result in a decrease in the concentration of dispersed (non-assembled) C$_{12}$-PEP$_{Au}$ monomers in HEPES solution. When an aliquot of HAuCl$_4$/H$_2$O (aq.) was added into the HEPES/C$_{12}$-PEP$_{Au}$ solution, after 24 hr, the reaction contained naked fibers and free gold nanoparticles (**Figure 46a**).

We next decided to add a second aliquot of either HAuCl$_4$/H$_2$O (aq.) or HAuCl$_4$/TEAA (aq.) to the above solution. We hypothesized that the addition of additional gold would not lead to the formation of well-organized double helices because we believed that most of the 'free' peptide conjugates would have already been consumed in the formation of fibers or free gold nanoparticles. When we added an aliquot of HAuCl$_4$/TEAA (aq.), we observed the production of

very few 1-D gold nanoparticle assembled superstructures and large gold nanoparticle aggregates, as revealed by TEM (**Figure 46b and Figure A9a-b**). The size of the component gold nanoparticles within the structures was uniform (4.32 ± 0.8 nm, **Figure A9c**). When we added an aliquot of $HAuCl_4/H_2O$ (aq.) solution, no 1-D gold nanoparticle assembled superstructures were produced, but some free and non-assembled gold nanoparticle aggregates were found (**Figure 46c**). These observations again suggest that $HAuCl_4/TEAA$ (aq.) is needed for superstructure formation. However, they also suggested that perhaps some 'free' peptide conjugates were still present in the solution, because double helices were still formed upon the addition of $HAuCl_4/TEAA$ (aq.).
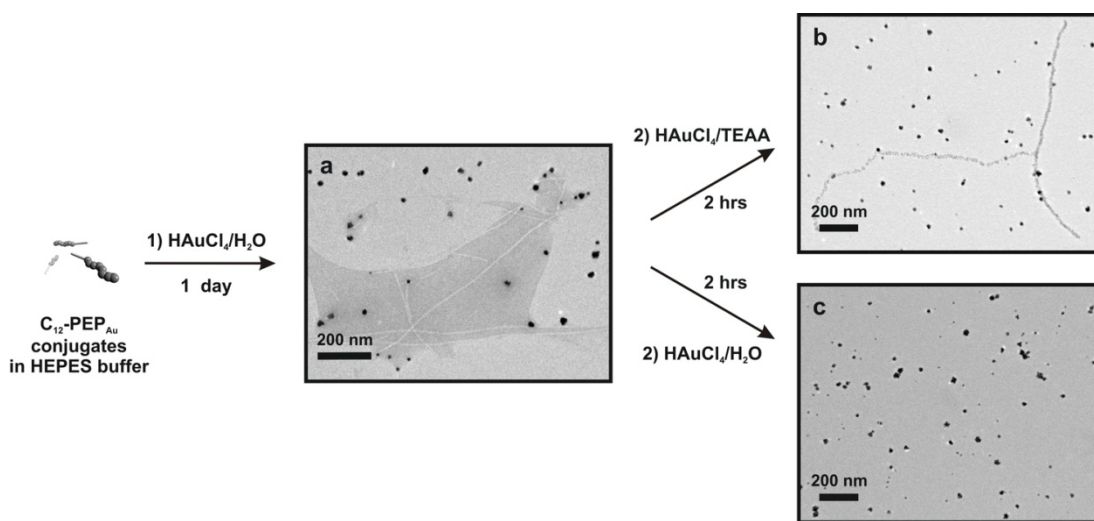
Figure 46. Schematic illustration to show the role of C_{12}-PEP$_{Au}$ monomers in HEPES buffer to direct gold nanoparticles into 1-D assembled structures. TEM Images of products (a) 1day after adding a $HAuCl_4/H_2O$; (b) 2 hrs after adding a second aliquot of $HAuCl_4/TEAA$ (aq.) into (a) solution; (c) 2 hrs after adding a second aliquot of a $HAuCl_4/H_2O$ (aq.) into (a) solution.

4.3.7 Effect of the gold nanoparticles formed by HAuCl₄/TEAA on double-helix formation

We examined how the gold particles in the TEAA solution lead to the gold nanoparticle double helices by diluting the solution to decrease the speed of the reduction of the gold salt by HEPES molecules after adding HAuCl₄/TEAA (aq.) to a C$_{12}$-PEP$_{Au}$ solution. The reaction mixture was then freeze-dried for 24 hr. We expected that lyophilizing would retard the speed of gold nanoparticle growth. Immediately after lyophilization, the dried solids were white. The lyophilized samples were placed on the bench for different time intervals (i.e. 6 hr-24 hr). During this time, they underwent a gradual color change, turning slightly purple within 15 hr (**Figure 47e**). The samples obtained at different time points were examined by TEM. The lyophilized solids incubated at room temperature for less than 15 hrs showed naked fibers as the major product. However, the lyophilized solids incubated for more than 15hrs showed the bimodal distribution consisting of naked fibers and 1-D gold nanoparticles assembled structures. The gold nanoparticles assembled structures were decorated with small gold nanoparticles (3.1 ± 0.5 nm), and the small gold nanoparticles were grew within 24 hr after the lyophilizing (6.4 ± 1.4 nm) (**Figure 47a-d**). We also ran a control experiment using a HAuCl₄/H₂O (aq.) solution instead of HAuCl₄/TEAA (aq.) solution. The samples were incubated for 1-2 days after lyophilizing at room temperature, followed by TEM examination. The major products were naked fibers and large gold nanoparticle aggregates (**Figure 48a-b**). No bimodal distribution was observed in the presence of the HAuCl₄/H₂O (aq.) solution. Collectively, these results again suggest that the HAuCl₄/TEAA (aq.) is necessary for superstructure assembly. Further, these results indicate the precursors to the gold particles are incorporated into certain fibers at the

assembly stage. The gold nanoparticles are not deposited onto the fibers after the fibers have already been assembled.
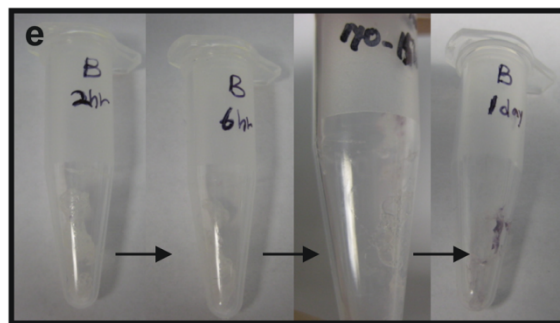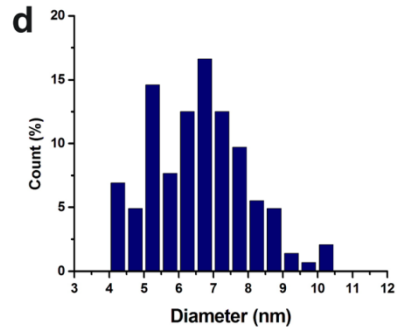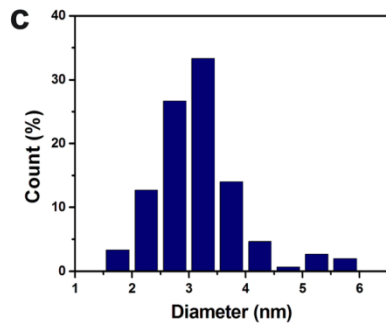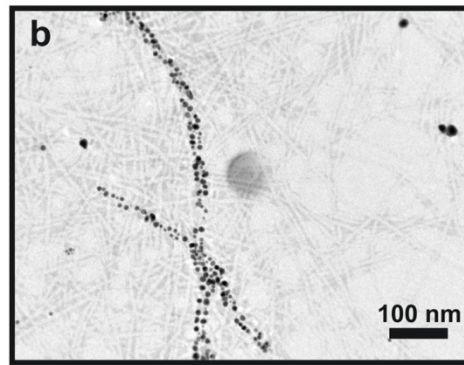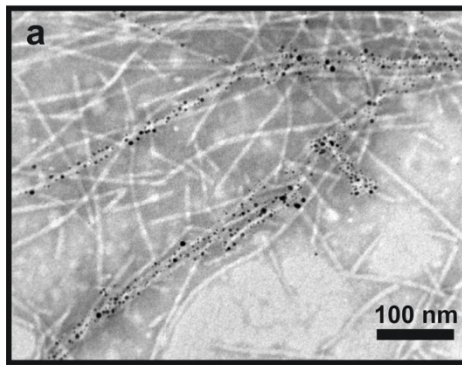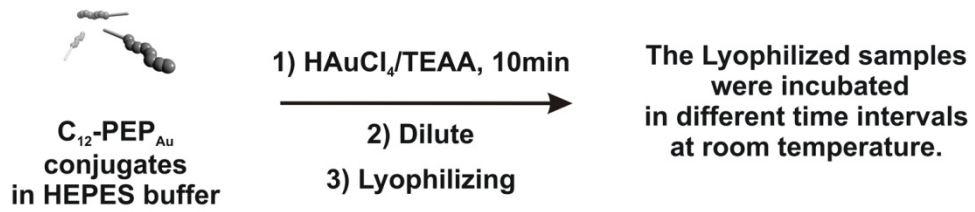
Figure 47. Negatively stained TEM images of lyophilized products using HAuCl₄/TEAA (aq.) (a) 15 hours and (b) 24 hours after incubated at room temperature; (c) size distribution of small gold nanoparticles decorated on the fibers of (a) with 3.1 ± 0.5 nm (based on 150 counts); (d) size distribution of small gold nanoparticles decorated on the fibers of (b) with 6.4 ± 1.4 nm (based on 144 counts); (e) pictures taken in different time intervals after lyophilizing.
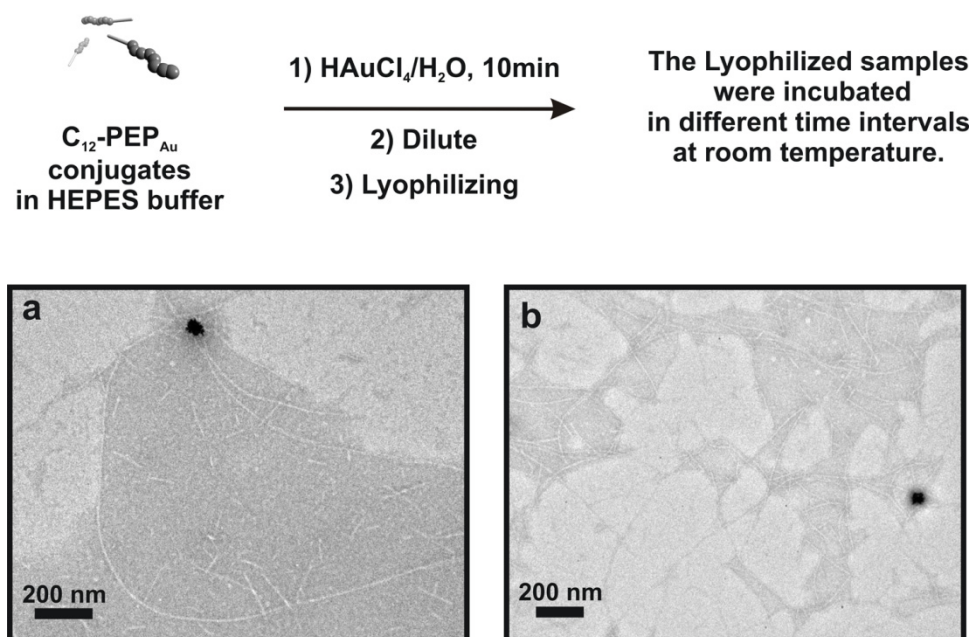
Figure 48. Negatively stained TEM images of lyophilized products using HAuCl₄/H₂O (aq.) (a) 1 day and (b) 2 days after incubated at room temperature.

We confirmed that the HAuCl₄/TEAA (aq.) solution produces gold particles with a size 3.0 ± 0.46 nm. We speculate that C_{12}-PEP$_{Au}$ conjugates recognize and bind to the small gold nanoparticles and thereafter direct their assembly into well-ordered double helices. Gold cations present in the HAuCl₄/TEAA (aq.) solution facilitate the assembly of C_{12}-PEP$_{Au}$ conjugates into

naked fibers. Based on our observation, the small gold nanoparticles must be present at the outset of reaction in order to form highly organized superstructures.

4.3.8   Proposed mechanism of formation of gold nanoparticle double helices

We showed that (1) small gold nanoparticles provided by HAuCl$_4$/TEAA (aq.) solution and (2) a high-level of dispersed (non-assembled) peptide conjugate monomers should be present at the outset of the reaction to produce well-organized gold nanoparticle double-helical superstructures using C$_{12}$-PEP$_{Au}$. Our evidence indicates that the gold nanoparticles and precursors for gold nanoparticle formation provided from HAuCl$_4$/TEAA (aq.) are incorporated into the fibers during the fiber assembly and growth process. This synthetic pathway is unique and promising. The double-helical gold nanoparticle superstructures are prepared in a single step and have excellent local order and structural regularity. Based on all of the experiments and observations reported in this chapter, we can now propose a reasonable pathway for product formation (**Figure 49**).
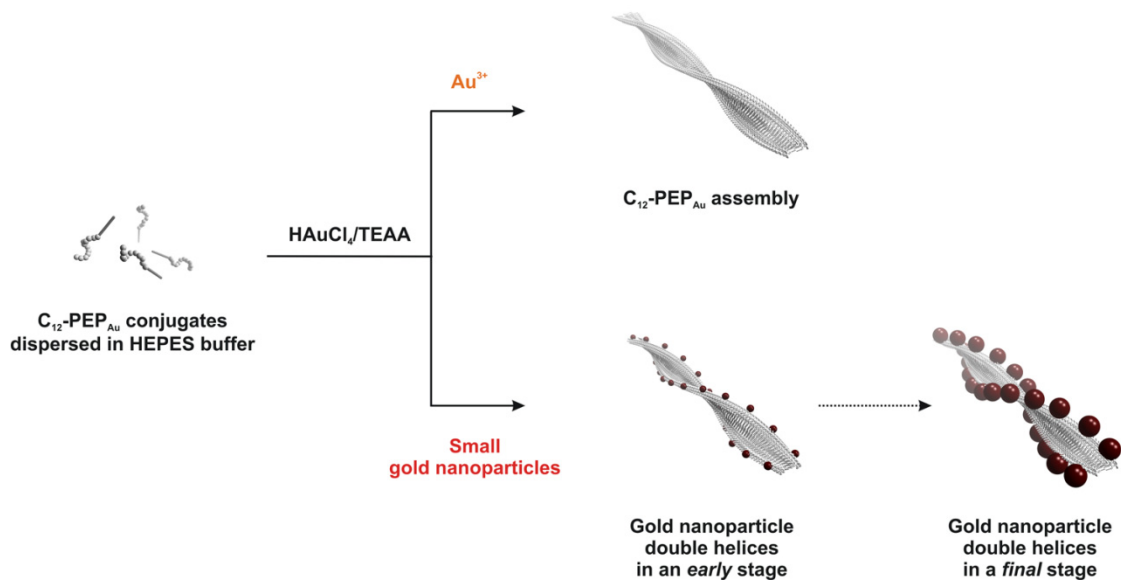
Figure 49. Proposed schematic illustration of synthetic pathway for formation of well-organized gold nanoparticle double helices.

4.4   CONCLUSION

This fundamental mechanistic insight will allow for systemic and thoughtful control over the structural attributes and for rational design of various nanoparticle superstructures. Moreover, we expect that the gold nanoparticles capped by peptide conjugate molecules can be used to construct new building blocks to assemble nanoparticle superstructures with a high degree of order and structural complexity.

5.0 PROSPECTIVE

The work presented in this thesis focused on how modifications to the peptide conjugate can impact nanoparticle assembly. Further, the key synthetic components necessary for producing well-ordered nanoparticle superstructures using our methodology were identified. Our first strategy was to modify peptide conjugate molecules in order to program substantial amounts of information that allows construction of higher-level architectures with structural regularity and topology.

The next strategy is to endow new functionality to the backbone of the peptide conjugate molecules, resulting in yielding functional materials. Similar to using the functional groups of molecules as a building unit for complex organic substances, functional moieties could be incorporated into the peptide conjugate molecules. The functional units can include (1) artificial amino acids whose secondary structures can be exchanged dynamically, and (2) target-directors such as DNA-aptamers, which can recognize and interact with a specific molecule (i.e., proteins) (**Figure 50**).

B. Endow Functionality to the Structure

C. Construction of Functional Materials

Organic group (R)

or

Organic group (R)

Artificial amino acid bearing functional groups

A. Basic Building Unit

Organic group (R)

Peptide conjugate (R-PEP_Au) Structure directing agent

Organic group (R)

Target director (DNA-aptamers)

Oxime coupling

Control of interparticle distance by a dynamic change of structures

Gold NP spherical structures as a therapeutic tool

Figure 50. Schematic strategies to endow functional moieties to the backbone of peptide conjugate structures for construction of functional materials.

First, we can change a secondary structure of a peptide sequence of the peptide conjugates by using a coupling reaction. Horne et al. recently reported that α-helical folding of medium-length peptides was promoted using oxime side chain linkage in an aqueous solution.[127] They incorporated a modified amino acid bearing an aldehyde group at the ith position and another manipulated amino acid bearing an aminooxy group at the $i+4$ position for the oxime coupling. This oxime peptide also can experience dynamic exchanges with an aminooxy-functionalized small molecules.[127] This indicates that the $i \rightarrow i+4$ spacing of the peptide can be controlled by isomerization of the oxime linkage.

By taking advantage of this concept, the modified amino acids bearing aldehyde and aminooxy groups into the i and $i + 4$ positions, respectively, can be incorporated into our peptide conjugate structure (**Figure 50B**). This incorporation will result in a change of the secondary structure of the peptide conjugates and production of different resulting nanoparticle assembled

structures. At this point, it is important to note that an organic tether group should be tuned at the same time. Based on our fundamental studies, we realized that the balance between hydrophobic interactions (from the organic groups and a few hydrophobic amino acids) and hydrogen bonding (or hydrophilic parts) from the peptide sequence is important in determining its assembly structures. Therefore, when we add more amino acids that are especially hydrophilic, this indicates that we should choose organic groups that exhibit stronger hydrophobic interactions (i.e., that have longer aliphatic chains).

For example, we can construct a dynamic spherical structure using a building unit, C_6-A_2-PEP_{Au} that provided hollow spherical structures of -100nm. We can program the peptide conjugate to have a longer aliphatic tail, when the artificial amino acids are incorporated into the peptide sequence. The appropriate position for incorporation of the artificial amino acids will be before the segment of amino acid sequences that recognize and bind gold nanoparticles. Prior to oxime linkage, the newly designed C_{6+X}-A_{2+Y}-PEP_{Au} (bearing modified amino acids at $i \rightarrow i+4$) can provide spherical structures. After oxime coupling, the size of the spherical structures will be smaller due to the shorter spacing due to α-helix formation. Addition of aminooxy-functionalized small molecules for dynamic exchange will produce spherical structures with an original size (**Figure 50C**). It is worth to control the distance of the comprising nanoparticle within the assembled superstructures by exchanging the secondary structure of peptide sequence of the peptide conjugate molecules.

Second, the structure of peptide conjugates can be modified to a functional unit such as cell-targeting peptides or DNA-aptamers. The DNA-aptamers, in particular, have become attracted recently as target specific directors.[128-131] Therefore, we can create designs where the DNA-aptamer is incorporated into the C-terminus of the peptide sequence (**Figure 50B**).

Therefore, when we have a good control over the charge-balance of the peptide-DNA aptamer structure, we expect that the functional unit will be exposed to the outside of the assembled nanoparticle superstructures. The DNA aptamers as a functional unit will be used to interact with a specific cell type (i.e., cancer cells).[124] For example, spherical gold nanoparticle bearing DNA-aptamers at the exterior of the spheres can be used as a therapeutic tool (**Figure 50C**). Gold nanoparticles with a certain diameter are well known to absorb near-IR radiation.[132] The absorption of near IR by gold nanoparticles generates heat, which is a great tool to kill cancer cells. Spherical gold nanoparticle superstructures bearing DNA-aptamers on the surface of the spheres will direct the structures to a specific cancer cell. Subsequent irradiation with near IR would then kill cancer cells. It is also worth note that the resulting new building blocks with their new functionality will be useful for assembly of nanomaterials that can be used for therapeutic purposes.

The next strategy is to design a new nanoparticle building block. Throughout our fundamental mechanistic studies, small gold nanoparticles that bind to peptide conjugate molecules assemble into well-ordered double helical superstructures (**Figure 51A**). It is well known that specific peptide sequences can recognize and bind to the surface of gold nanoparticles. [63,83] Therefore, we can prepare nanoparticles with different sizes bearing modified peptide conjugate molecules in order to design new building blocks for preparing nanoparticle superstructures.

The strategy is here: 1) our peptide conjugate molecules consist of a peptide sequence (PEP$_{Au}$) that binds to gold nanoparticles and an organic tether (i.e., aliphatic tails) as a structure directing part; 2) gold nanoparticles with different sizes are prepared; 3) the number of 'PEP$_{Au}$' segments or (and) the length of the aliphatic tails can be tuned based on the size of gold

nanoparticles; and 4) the pre-synthesized nanoparticles and modified peptide conjugate

molecules are mixed to create new building blocks for forming nanoparticle superstructures

(**Figure 51B**). This new approach will allow one to readily modify the size of nanoparticles by

manipulating peptide sequence molecules (i.e., C_{12+X}-PEP_{Au}).
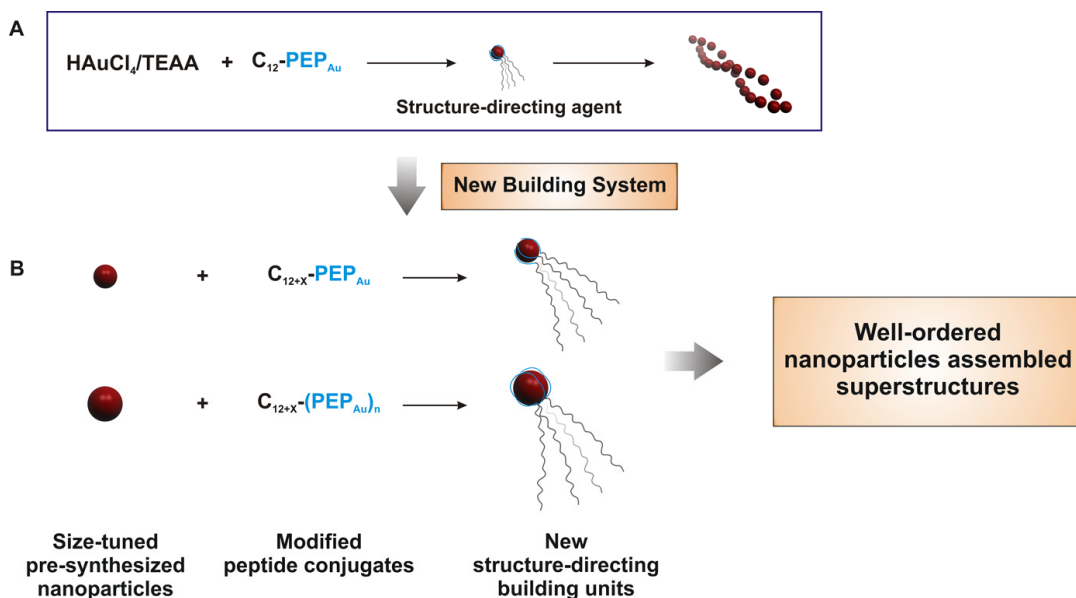
Figure 51. Proposed synthetic scheme to design new nanoparticle building blocks for

construction of well-ordered nanoparticle assembled superstructures.

Appendix
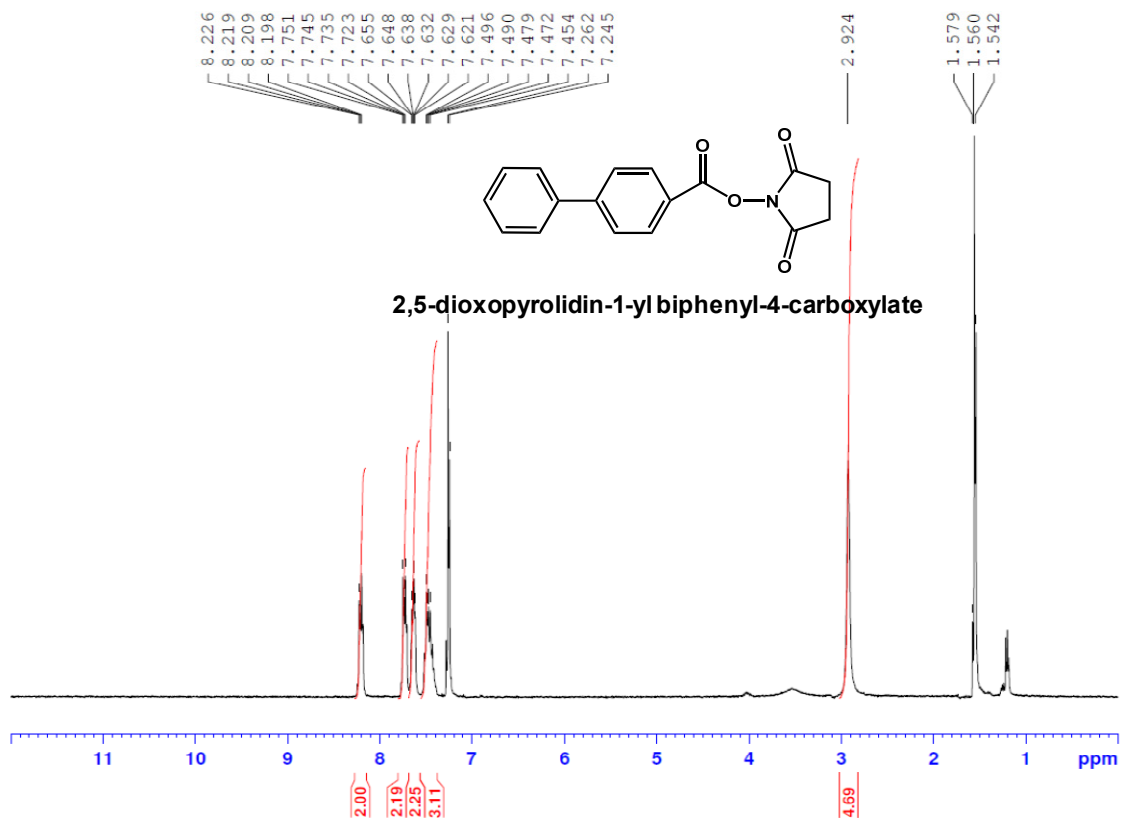
Figure A1. NMR analysis of NHS-activated biphenyl.
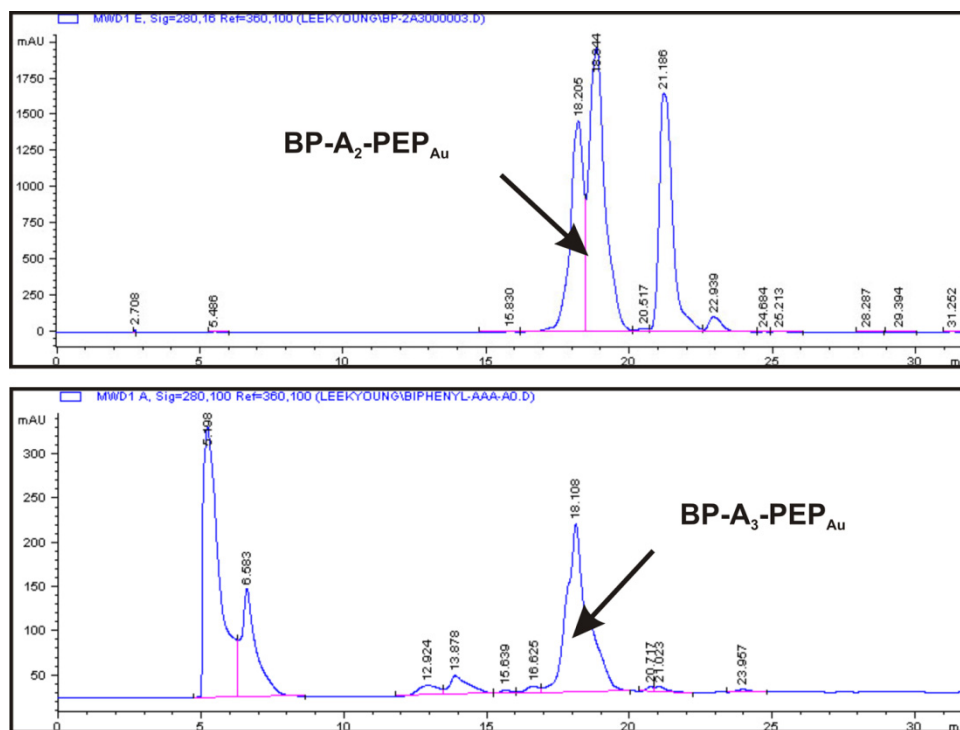
Figure A2. Reverse-phase HPLC charts for product of the coupling reaction between A_2-PEP$_{Au}$ (AAAYSSGAPPMPPF) or A_3-PEP$_{Au}$ (AAAAYSSGAPPMPPF) with biphenyl N-hydroxyl-succinimide ester, respectively.

Note: BP-A-PEP$_{Au}$ were prepared, purified and characterized in a similar fashion.
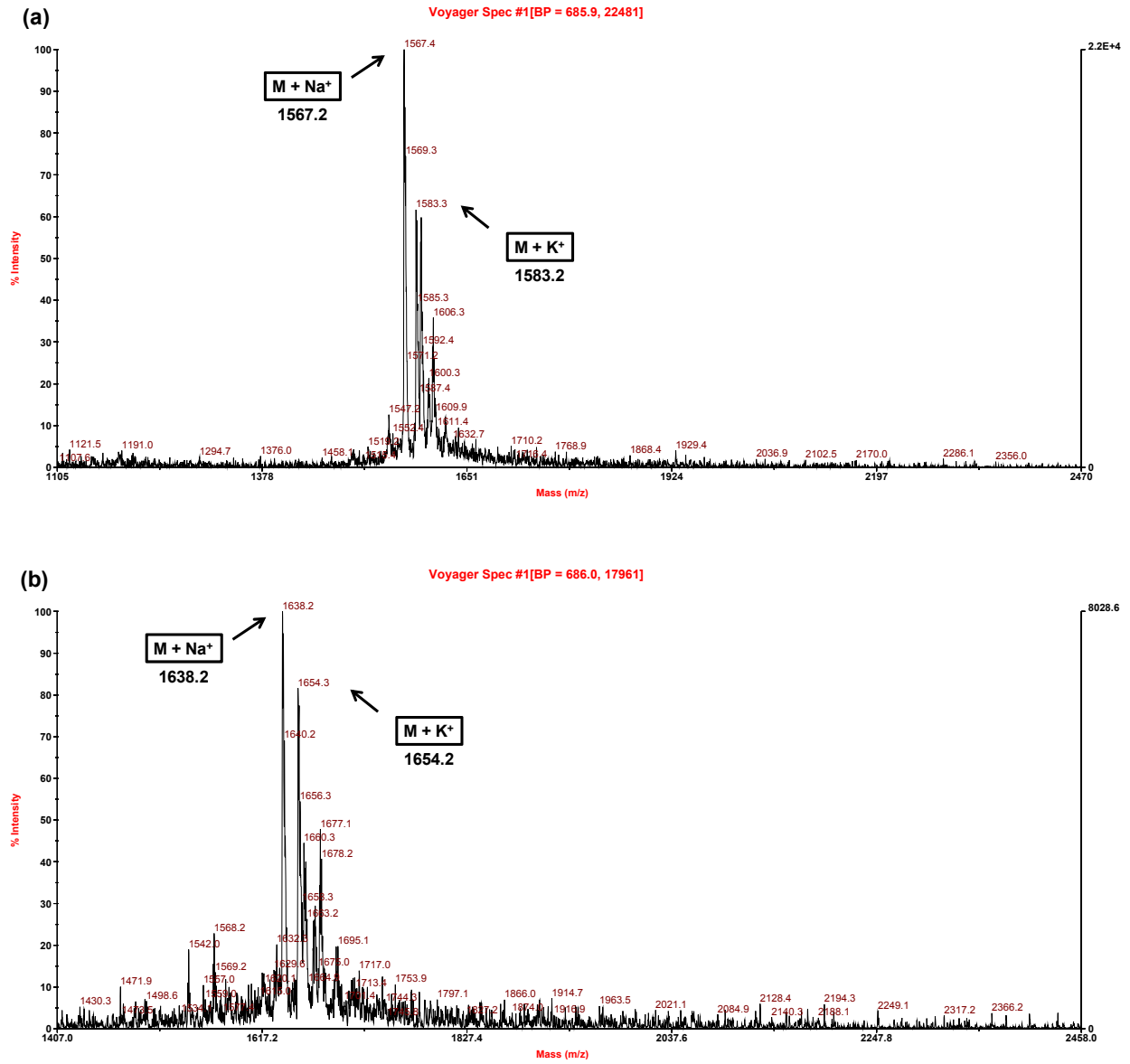
Figure A3. MALDI-TOF mass spectra of purified (a) BP-A$_2$-PEP$_{Au}$ (Calcd. Mw. = 1544.2) and (b) BP-A$_3$-PEP$_{Au}$ (Calcd. Mw. = 1615.2).
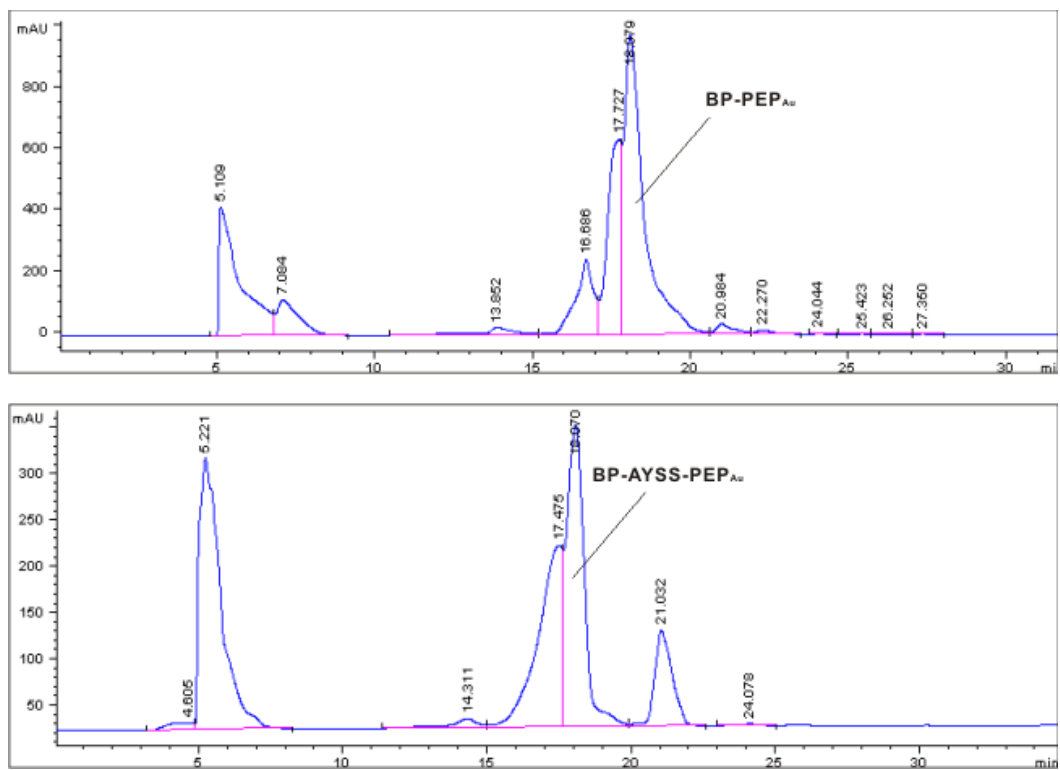
Figure A4. Reverse-phase HPLC chart for the coupling reaction between either PEP_{Au} or AYSS-PEP_{Au} with biphenyl N-hydroxyl-succinimide ester.
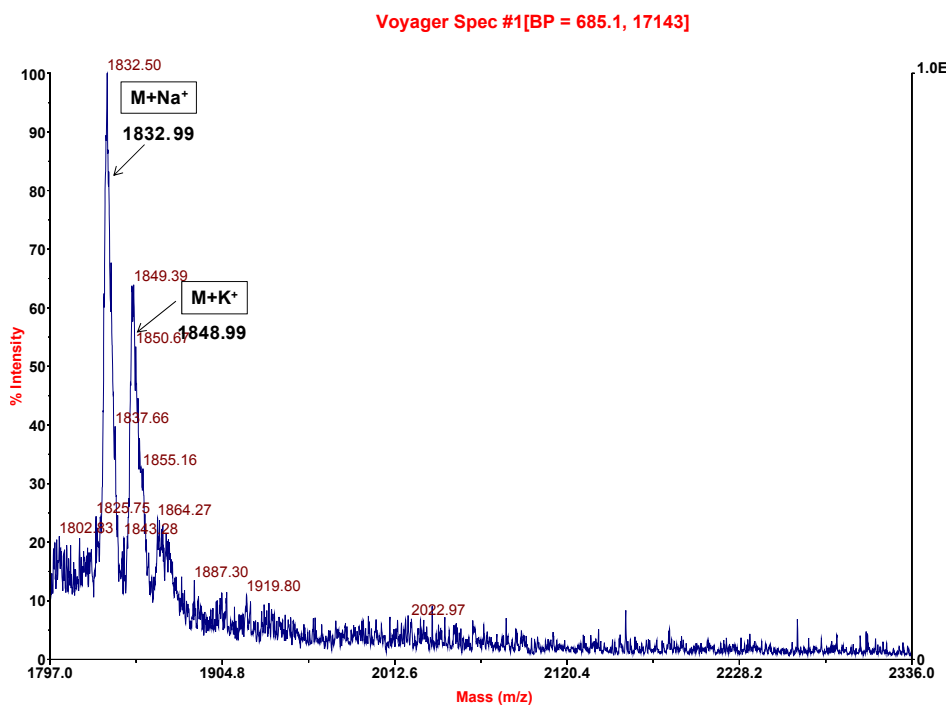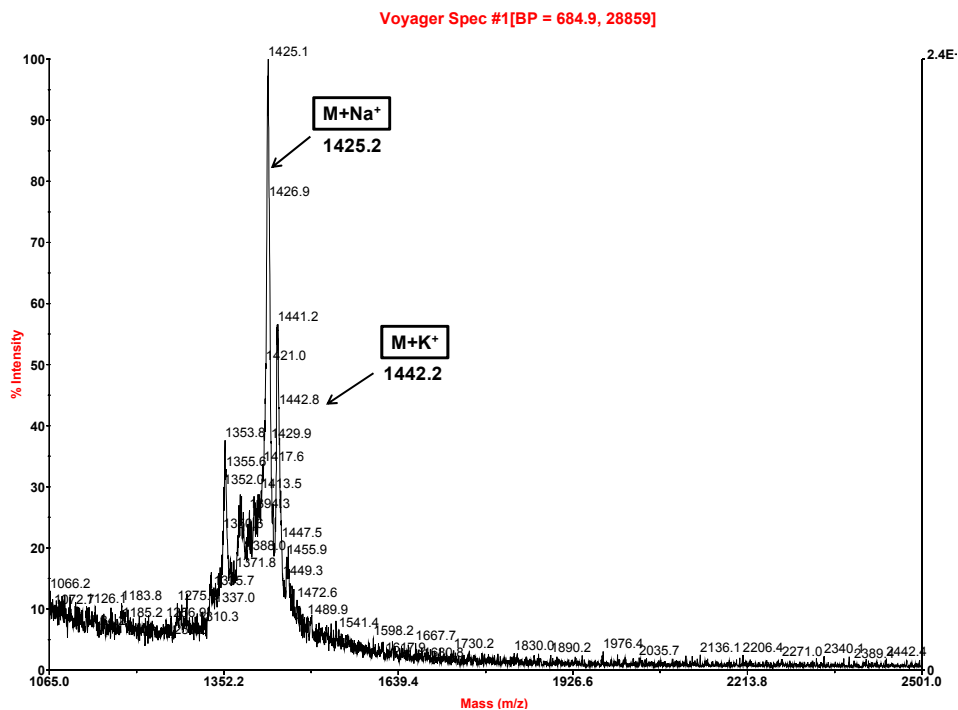
Figure A5. MALDI-TOF mass spectrum of purified BP-PEP$_{Au}$ (Calcd. Mw. = 1402.2) (a) and BP-AYSS-PEP$_{Au}$ (Calcd. Mw. = 1810.2) (b).
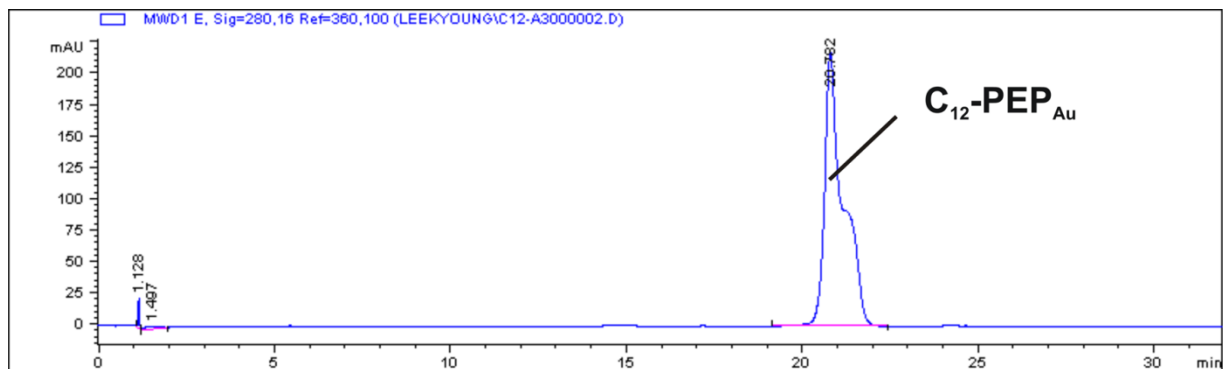
Figure A6. Reverse-phase HPLC chart for the coupling reaction between either PEP_{Au} with C_{12}-N-hydroxyl-succinimide ester.
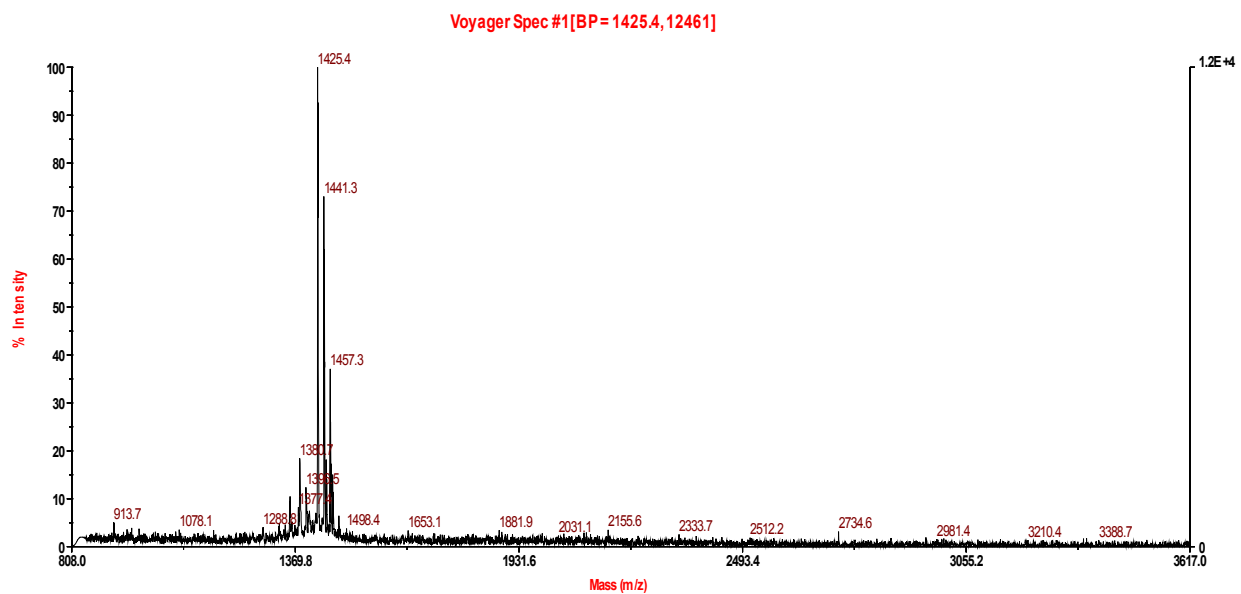
Figure A7. MALDI-TOF mass spectrum of purified C_{12}-PEP_{Au} (Calcd. Mw. = 1404.3).
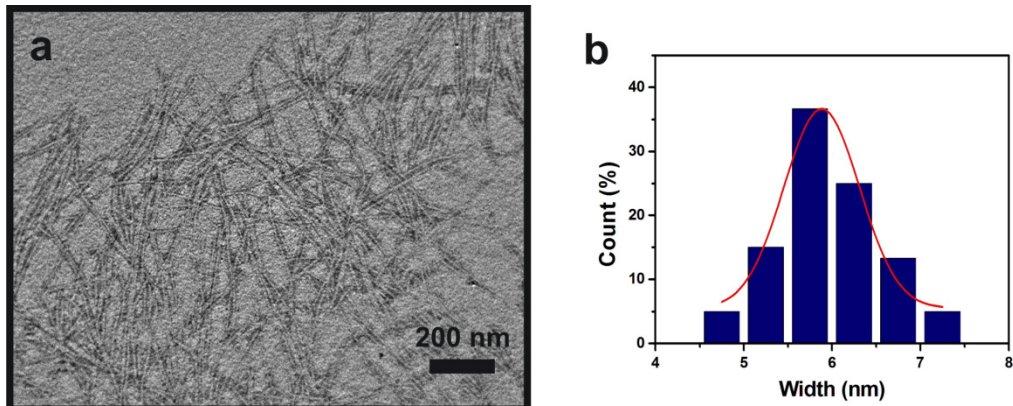
Figure A8. Sample used for the XRD study contained the fibers formed by C_{12}-PEP$_{Au}$ by examining them by TEM. (a) Schematic description of C_{12}-PEP assembly (b) TEM images of the fibers (c) size distribution of width of the fibers (5.88± 0.43 nm; based on 60 counts).
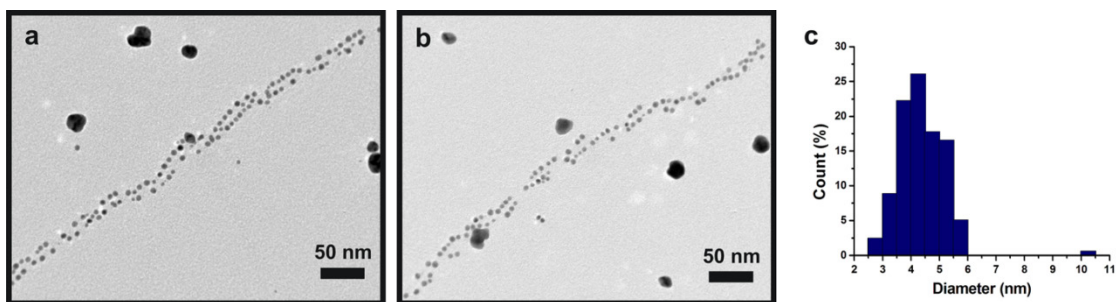
Figure A9. (a) and (b) Zoom-in TEM images of 1-D gold nanoparticle assembled superstructures after adding the second aliquot of HAuCl$_4$/TEAA (aq.) into the solution that contained naked fibers and free gold nanoparticles, which were produced by the first aliquot of HAuCl$_4$/H$_2$O (aq.); (c) a size distribution of the comprising nanoparticles in the 1-D assembly, 4.32 ± 0.8 nm (based on 157 counts).

BIBLIOGRAPHY

(1)   Niemeyer, C. M. *Angewandte Chemie International Edition* **2001**, *40*, 4128.

(2)   Kotov, N. A.; Stellacci, F. *Advanced Materials* **2008**, *20*, 4221.

(3)   Grzelczak, M.; Vermant, J.; Furst, E. M.; Liz-Marzán, L. M. *ACS Nano* **2010**, *4*, 3591.

(4)   Nie, Z.; Petukhova, A.; Kumacheva, E. *Nature Nanotechnology* **2010**, *5*, 15.

(5)   Whitesides, G. M.; Grzybowski, B. *Science* **2002**, *295*, 2418.

(6)   Ulijn, R. V.; Smith, A. M. *Chemical Society Reviews* **2008**, *37*, 664.

(7)   An, J.; Fiorella, R. P.; Geib, S. J.; Rosi, N. L. *Journal of the American Chemical Society* **2009**, *131*, 8401.

(8)   An, J.; Geib, S. J.; Rosi, N. L. *Journal of the American Chemical Society* **2009**, *132*, 38.

(9)   An, J.; Geib, S. J.; Rosi, N. L. *Journal of the American Chemical Society* **2009**, *131*, 8376.

(10) Eustis, S.; El-Sayed, M. A. *Chemical Society Reviews* **2006**, *35*, 209.

(11) Daniel, M.-C.; Astruc, D. *Chemical Reviews* **2003**, *104*, 293.

(12) Stark, W. J. *Angewandte Chemie International Edition* **2011**, *50*, 1242.

(13) Burda, C.; Chen, X.; Narayanan, R.; El-Sayed, M. A. *Chemical Reviews* **2005**, *105*, 1025.

(14) Kim, B.; Tripp, S. L.; Wei, A. *Journal of the American Chemical Society* **2001**, *123*, 7955.

(15) Dickerson, M. B.; Sandhage, K. H.; Naik, R. R. *Chemical Reviews* **2008**, *108*, 4935.

(16) Katz, E.; Willner, I. *Angewandte Chemie International Edition* **2004**, *43*, 6042.

(17) Ofir, Y.; Samanta, B.; Rotello, V. M. *Chemical Society Reviews* **2008**, *37*, 1814.

(18) Shenton, W.; Davis, S. A.; Mann, S. *Advanced Materials* **1999**, *11*, 449.

(19) Maye, M. M.; Luo, J.; Lim, I. I. S.; Han, L.; Kariuki, N. N.; Rabinovich, D.; Liu; Zhong, C.-J. *Journal of the American Chemical Society* **2003**, *125*, 9906.

(20)   Boal, A. K.; Ilhan, F.; DeRouchey, J. E.; Thurn-Albrecht, T.; Russell, T. P.; Rotello, V. M. *Nature* **2000**, *404*, 746.

(21)   Chang, W.-S.; Slaughter, L. S.; Khanal, B. P.; Manna, P.; Zubarev, E. R.; Link, S. *Nano Letters* **2009**, *9*, 1152.

(22)   Hentschel, M.; Saliba, M.; Vogelgesang, R.; Giessen, H.; Alivisatos, A. P.; Liu, N. *Nano Letters* **2010**, *10*, 2721.

(23) Euliss, L. E.; Grancharov, S. G.; O'Brien, S.; Deming, T. J.; Stucky, G. D.; Murray, C. B.; Held, G. A. *Nano Letters* **2003**, *3*, 1489.

(24)   Wang, L.; Xu, L.; Kuang, H.; Xu, C.; Kotov, N. A. *Accounts of Chemical Research* **2012**. ASAP

(25)   Ohara, P. C.; Leff, D. V.; Heath, J. R.; Gelbart, W. M. *Physical Review Letters* **1995**, *75*, 3466.

(26) Collier, C. P.; Vossmeyer, T.; Heath, J. R. *Annual Review of Physical Chemistry* **1998**, *49*, 371.

(27)   Kiely, C. J.; Fink, J.; Brust, M.; Bethell, D.; Schiffrin, D. J. *Nature* **1998**, *396*, 444.

(28)   Kalsin, A. M.; Fialkowski, M.; Paszewski, M.; Smoukov, S. K.; Bishop, K. J. M.; Grzybowski, B. A. *Science* **2006**, *312*, 420.

(29) Shevchenko, E. V.; Talapin, D. V.; Kotov, N. A.; O'Brien, S.; Murray, C. B. *Nature* **2006**, *439*, 55.

(30)   Nykypanchuk, D.; Maye, M. M.; van der Lelie, D.; Gang, O. *Nature* **2008**, *451*, 549.

(31)   Shevchenko, E. V.; Talapin, D. V.; O'Brien, S.; Murray, C. B. *Journal of the American Chemical Society* **2005**, *127*, 8741.

(32)   Katz, E.; Willner, I. *Angewandte Chemie International Edition* **2004**, *43*, 6042.

(33) McMillan, R. A.; Paavola, C. D.; Howard, J.; Chan, S. L.; Zaluzec, N. J.; Trent, J. D. *Nature Materials* **2002**, *1*, 247.

(34) Rosi, N. L.; Thaxton, C. S.; Mirkin, C. A. *Angewandte Chemie International Edition* **2004**, *43*, 5500.

(35) Blum, A. S.; Soto, C. M.; Wilson, C. D.; Cole, J. D.; Kim, M.; Gnade, B.; Chatterji, A.; Ochoa, W. F.; Lin, T.; Johnson, J. E.; Ratna, B. R. *Nano Letters* **2004**, *4*, 867.

(36) Blum, A.; Soto, C.; Wilson, C.; Brower, T.; Pollack, S.; Schull, T.; Chatterji, A.; Lin, T.; Johnson, J.; Amsinck, C.; Franzon, P.; Shashidhar, R.; Ratna, B. *Small* **2005**, *1*, 702.

(37) Lim, S. I.; Zhong, C.-J. *Accounts of Chemical Research* **2009**, *42*, 798.

(38) Shimizu, T.; Masuda, M.; Minamikawa, H. *Chemical Reviews* **2005**, *105*, 1401.

(39) Frankamp, B. L.; Uzun, O.; Ilhan, F.; Boal, A. K.; Rotello, V. M. *Journal of the American Chemical Society* **2002**, *124*, 892.

(40) Mucic, R. C.; Storhoff, J. J.; Mirkin, C. A.; Letsinger, R. L. *Journal of the American Chemical Society* **1998**, *120*, 12674.

(41) Alivisatos, A. P.; Johnsson, K. P.; Peng, X.; Wilson, T. E.; Loweth, C. J.; Bruchez, M. P.; Schultz, P. G. *Nature* **1996**, *382*, 609.

(42) Aldaye, F. A.; Sleiman, H. F. *Angewandte Chemie International Edition* **2006**, *45*, 2204.

(43) Aldaye, F. A.; Sleiman, H. F. *Journal of the American Chemical Society* **2007**, *129*, 4130.

(44) Le, J. D.; Pinto, Y.; Seeman, N. C.; Musier-Forsyth, K.; Taton, T. A.; Kiehl, R. A. *Nano Letters* **2004**, *4*, 2343.

(45) Deng, Z.; Tian, Y.; Lee, S.-H.; Ribbe, A. E.; Mao, C. *Angewandte Chemie International Edition* **2005**, *44*, 3582.

(46) Zhang, J.; Liu, Y.; Ke, Y.; Yan, H. *Nano Letters* **2006**, *6*, 248.

(47) Yan, H.; Park, S. H.; Finkelstein, G.; Reif, J. H.; LaBean, T. H. *Science* **2003**, *301*, 1882.

(48) Nakao, H.; Shiigi, H.; Yamamoto, Y.; Tokonami, S.; Nagaoka, T.; Sugiyama, S.; Ohtani, T. *Nano Letters* **2003**, *3*, 1391.

(49) Wang, G.; Murray, R. W. *Nano Letters* **2003**, *4*, 95.

(50) Beyer, S.; Nickels, P.; Simmel, F. C. *Nano Letters* **2005**, *5*, 719.

(51) Palmer, L. C.; Stupp, S. I. *Accounts of Chemical Research* **2008**, *41*, 1674.

(52) Naik, R. R.; Jones, S. E.; Murray, C. J.; McAuliffe, J. C.; Vaia, R. A.; Stone, M. O. *Advanced Functional Materials* **2004**, *14*, 25.

(53) Chen, C.-L.; Zhang, P.; Rosi, N. L. *Journal of the American Chemical Society* **2008**, *130*, 13555.

(54) Ulijn, R. V.; Woolfson, D. N. *Chemical Society Reviews* **2010**, *39*, 3349.

(55) König, H. M.; Kilbinger, A. F. *Angewandte Chemie International Edition* **2007**, *46*, 8334.

(56) Hentschel, J.; Krause, E.; Borner, H. G. *Journal of the American Chemical Society* **2006**, *128*, 7722.

(57) Couet, J.; Samuel, J. D. J. S.; Kopyshev, A.; Santer, S.; Biesalski, M. *Angewandte Chemie International Edition* **2005**, *44*, 3297.

(58) Hartgerink, J. D.; Beniash, E.; Stupp, S. I. *Science* **2001**, *294*, 1684.

(59) Djalali, R.; Chen, Y.-f.; Matsui, H. *Journal of the American Chemical Society* **2002**, *124*, 13660.

(60) Naik, R. R.; Jones, S. E.; Murray, C. J.; McAuliffe, J. C.; Vaia, R. A.; Stone, M. O. *Advanced Functional Materials* **2004**, *14*, 25.

(61) Chen, C.-L.; Rosi, N. L. *Angewandte Chemie International Edition* **2010**, *49*, 1924.

(62) Sarikaya, M.; Tamerler, C.; Jen, A. K. Y.; Schulten, K.; Baneyx, F. *Nature Materials* **2003**, *2*, 577.

(63) Slocik, J. M.; Stone, M. O.; Naik, R. R. *Small* **2005**, *1*, 1048.

(64) Slocik, J. M.; Naik, R. R. *Advanced Materials* **2006**, *18*, 1988.

(65) Dujardin, E.; Peet, C.; Stubbs, G.; Culver, J. N.; Mann, S. *Nano Letters* **2003**, *3*, 413.

(66) Fu, X.; Wang, Y.; Huang, L.; Sha, Y.; Gui, L.; Lai, L.; Tang, Y. *Advanced Materials* **2003**, *15*, 902.

(67) Li, L.-s.; Stupp, S. I. *Angewandte Chemie International Edition* **2005**, *44*, 1833.

(68) Djalali, R.; Chen, Y.-f.; Matsui, H. *Journal of the American Chemical Society* **2003**, *125*, 5873.

(69) Sone, E. D.; Stupp, S. I. *Journal of the American Chemical Society* **2004**, *126*, 12756.

(70) Aili, D.; Enander, K.; Rydberg, J.; Nesterenko, I.; Björefors, F.; Baltzer, L.; Liedberg, B. *Journal of the American Chemical Society* **2008**, *130*, 5780.

(71) DeVries, G. A.; Brunnbauer, M.; Hu, Y.; Jackson, A. M.; Long, B.; Neltner, B. T.; Uzun, O.; Wunsch, B. H.; Stellacci, F. *Science* **2007**, *315*, 358.

(72) Xu, X.; Rosi, N. L.; Wang, Y.; Huo, F.; Mirkin, C. A. *Journal of the American Chemical Society* **2006**, *128*, 9286.

(73) Claridge, S. A.; Goh, S. L.; Frechet, J. M. J.; Williams, S. C.; Micheel, C. M.; Alivisatos, A. P. *Chemistry of Materials* **2005**, *17*, 1628.

(74) Mastroianni, A. J.; Claridge, S. A.; Alivisatos, A. P. *Journal of the American Chemical Society* **2009**, *131*, 8455.

(75) Zubarev, E. R.; Xu, J.; Sayyad, A.; Gibson, J. D. *Journal of the American Chemical Society* **2006**, *128*, 15098.

(76) Minor, D. L.; Kim, P. S. *Nature* **1994**, *367*, 660.

(77) Zelzer, M.; Ulijn, R. V. *Chemical Society Reviews* **2010**, *39*, 3351.

(78) Chen, C.-L.; Rosi, N. L. *Journal of the American Chemical Society* **2010**, *132*, 6902.

(79) Song, C.; Zhao, G.; Zhang, P.; Rosi, N. L. *Journal of the American Chemical Society* **2010**, *132*, 14033.

(80) Hwang, L.; Chen, C.-L.; Rosi, N. L. *Chemical Communications* **2011**, *47*, 185.

(81) Pandey, R. B.; Heinz, H.; Feng, J.; Farmer, B. L.; Slocik, J. M.; Drummy, L. F.; Naik, R. R. *Physical Chemistry Chemical Physics* **2009**, *11*, 1989.

(82) Heinz, H.; Farmer, B. L.; Pandey, R. B.; Slocik, J. M.; Patnaik, S. S.; Pachter, R.; Naik, R. R. *Journal of the American Chemical Society* **2009**, *131*, 9704.

(83) Yu, J.; Becker, M. L.; Carri, G. A. *Small* **2010**, *6*, 2242.

(84) Lal, S.; Link, S.; Halas, N. J. *Nature Photonics* **2007**, *1*, 641.

(85) Caruso, F.; Caruso, R. A.; Möhwald, H. *Science* **1998**, *282*, 1111.

(86) Wong, M. S.; Cha, J. N.; Choi, K.-S.; Deming, T. J.; Stucky, G. D. *Nano Letters* **2002**, *2*, 583.

(87) Park, S.; Lim, J.-H.; Chung, S.-W.; Mirkin, C. A. *Science* **2004**, *303*, 348.

(88) Liu, B.; Zeng, H. C. *Journal of the American Chemical Society* **2004**, *126*, 8124.

(89) Rana, R. K.; Murthy, V. S.; Yu, J.; Wong, M. S. *Advanced Materials* **2005**, *17*, 1145.

(90) Hickey, R. J.; Haynes, A. S.; Kikkawa, J. M.; Park, S.-J. *Journal of the American Chemical Society* **2011**, *133*, 1517.

(91) Vasquez, Y.; Sra, A. K.; Schaak, R. E. *Journal of the American Chemical Society* **2005**, *127*, 12504.

(92) Coppage, R.; Slocik, J. M.; Sethi, M.; Pacardo, D. B.; Naik, R. R.; Knecht, M. R. *Angewandte Chemie International Edition* **2010**, *49*, 3767.

(93) Jin, Y.; Gao, X. *Journal of the American Chemical Society* **2009**, *131*, 17774.

(94) Wu, G.; Mikhailovsky, A.; Khant, H. A.; Fu, C.; Chiu, W.; Zasadzinski, J. A. *Journal of the American Chemical Society* **2008**, *130*, 8175.

(95) Hu, J.; Wang, M.; Weier, H. U. G.; Frantz, P.; Kolbe, W.; Ogletree, D. F.; Salmeron, M. *Langmuir* **1996**, *12*, 1697.

(96) Kremer, J. R.; Mastronarde, D. N.; McIntosh, J. R. *Journal of Structural Biology* **1996**, *116*, 71.

(97) Pettersen, E. F.; Goddard, T. D.; Huang, C. C.; Couch, G. S.; Greenblatt, D. M.; Meng, E. C.; Ferrin, T. E. *Journal of Computational Chemistry* **2004**, *25*, 1605.

(98) Habib, A.; Tabata, M.; Wu, Y. G. *Bulletin of the Chemical Society of Japan* **2005**, *78*, 262.

(99) Xie, J. P.; Lee, J. Y.; Wang, D. I. C. *Chemistry of Materials* **2007**, *19*, 2823.

(100) Kim, B.-S.; Taton, T. A. *Langmuir* **2006**, *23*, 2198.

(101) Li, Z.; Sai, H.; Warren, S. C.; Kamperman, M.; Arora, H.; Gruner, S. M.; Wiesner, U. *Chemistry of Materials* **2009**, *21*, 5578.

(102) Voet, D.; Voet, J. G. *Biochemistry*; 2 ed.; John Wiley & Sons: New York, 1995.

(103) Link, S.; El-Sayed, M. A. *The Jounral of Physcial Chemistry B* **1999**, *103*, 8410.

(104) Yeechi Chen, K. M. a. D. S. G. *MRS Bulletin* **2008**, *33*, 536.

(105) Zhang, X.; Chen, J.; Yang, P.; Yang, W. *Journal of Inorganic Biochemistry* **2005**, *99*, 1692.

(106) Velichko, Y. S.; Stupp, S. I.; de la Cruz, M. O. *The Journal of Physical Chemistry B* **2008**, *112*, 2326.

(107) Chien, M.-P.; Rush, A. M.; Thompson, M. P.; Gianneschi, N. C. *Angewandte Chemie International Edition* **2010**, *49*, 5076.

(108) Pileni, M. P. *The Journal of Physical Chemistry B* **2001**, *105*, 3358.

(109) Li, L.-s.; Stupp, S. I. *Angewandte Chemie International Edition* **2005**, *44*, 1833.

(110) Gao, X.; Matsui, H. *Advanced Materials* **2005**, *17*, 2037.

(111) Ostrov, N.; Gazit, E. *Angewandte Chemie International Edition* **2010**, *49*, 3018.

(112) Jahnke, E.; Severin, N.; Kreutzkamp, P.; Rabe, J. P.; Frauenrath, H. *Advanced Materials* **2008**, *20*, 409.

(113) Cutler, J. I.; Auyeung, E.; Mirkin, C. A. *Journal of the American Chemical Society* **2012**, *134*, 1376.

(114) Hwang, L.; Zhao, G.; Zhang, P.; Rosi, N. L. *Small* **2011**, *7*, 1939.

(115) Oh, H. S.; Liu, S.; Jee, H.; Baev, A.; Swihart, M. T.; Prasad, P. N. *Journal of the American Chemical Society* **2010**, *132*, 17346.

(116) Shemer, G.; Krichevski, O.; Markovich, G.; Molotsky, T.; Lubitz, I.; Kotlyar, A. B. *Journal of the American Chemical Society* **2006**, *128*, 11006.

(117) Shen, X.; Song, C.; Wang, J.; Shi, D.; Wang, Z.; Liu, N.; Ding, B. *Journal of the American Chemical Society* **2011**, *134*, 146.

(118) Slocik, J. M.; Govorov, A. O.; Naik, R. R. *Nano Letters* **2011**, *11*, 701.

(119) Bond, J. P.; Deverin, S. P.; Inouye, H.; El-Agnaf, O. M. A.; Teeter, M. M.; Kirschner, D. A. *Journal of Structural Biology* **2003**, *141*, 156.

(120) Jarvis, J. A.; Craik, D. J.; Wilce, M. C. J. *Biochemical and Biophysical Research Communications* **1993**, *192*, 991.

(121) Castelletto, V.; Hamley, I. W.; Harris, P. J. F.; Olsson, U.; Spencer, N. *The Journal of Physical Chemistry B* **2009**, *113*, 9978.

(122) Blake, C.; Serpell, L. *Structure* **1996**, *4*, 989.

(123) Squires, A. M.; Devlin, G. L.; Gras, S. L.; Tickler, A. K.; MacPhee, C. E.; Dobson, C. M. *Journal of the American Chemical Society* **2006**, *128*, 11738.

(124) Tong, G. J.; Hsiao, S. C.; Carrico, Z. M.; Francis, M. B. *Journal of the American Chemical Society* **2009**, *131*, 11174.

(125) Reboul, J.; Nugay, T.; Anik, N.; Cottet, H.; Ponsinet, V.; In, M.; Lacroix-Desmazes, P.; Gerardin, C. *Soft Matter* **2011**, *7*, 5836.

(126) Kuo, P.-L.; Chen, C.-C. *Langmuir* **2006**, *22*, 7902.

(127) Haney, C. M.; Loch, M. T.; Horne, W. S. *Chemical Communications* **2011**, *47*, 10915.

(128) Famulok, M.; Mayer, G. *Accounts of Chemical Research* **2011**, *44*, 1349.

(129) Willner, I.; Willner, B. *Nano Letters* **2010**, *10*, 3805.

(130) Cho, H.; Baker, B. R.; Wachsmann-Hogiu, S.; Pagba, C. V.; Laurence, T. A.; Lane, S. M.; Lee, L. P.; Tok, J. B. H. *Nano Letters* **2008**, *8*, 4386.

(131) Kim, N. H.; Lee, S. J.; Moskovits, M. *Advanced Materials* **2011**, *23*, 4152.

(132) Lal, S.; Clare, S. E.; Halas, N. J. *Accounts of Chemical Research* **2008**, *41*, 1842.